Open file - Andros Inc.

DEVELOPMENT OF A PERSONAL CO_2 DETECTOR AND A CH_4 DETECTOR

Prepared for

UNITED STATES DEPARTMENT OF THE INTERIOR
BUREAU OF MINES

by

ANDROS INCORPORATED
2332 Fourth Street
Berkeley, California 94710

FINAL REPORT

Contract No. H0377096
Development of a Personal CO_2 Detector and a CH_4 Detector

August 1979

DISCLAIMER NOTICE

The views and conclusions contained in this document are those of the author and should not be interpreted as necessarily representing the official policies or recommendations of the Interior Department's Bureau of Mines or of the U.S. Government.

1. Report No.	2.	3. Recipient's Accession No.

4. Title and Subtitle	5. Report Date
DEVELOPMENT OF A PERSONAL CO_2 DETECTOR AND A CH_4 DETECTOR	Issued August 1979
	6.

7. Author(s)	8. Performing Organization Report No.
Irvin G. Burough	ARFR-115

9. Performing Organization Name and Address	10. Project/Task/Work Unit No.
ANDROS INCORPORATED 2332 Fourth Street Berkeley, California 94710	11. Contract or Grant No. H0377096

12. Sponsoring Organization Name and Address	13. Type of Report
OFFICE OF THE ASSISTANT DIRECTOR - MINING Bureau of Mines Department of the Interior Washington, D.C. 20241	FINAL REPORT
	14.

15. Supplementary Notes

This activity was a continuation of the effort started under USBM Contract H0230050, "A Portable, Low-cost NO_2, CO and CH_4 Gas Analyzer for In-mine Personnel Safety Monitoring".

16. Abstract

ANDROS INCORPORATED has designed, manufactured and delivered four handheld CO_2 DETECTORS and three handheld CH_4 DETECTORS. These instruments are for in-mine safety use.

The DETECTORS incorporated an NDIR optical/electronic analyzer design in which exceptional zero stability is achieved by pressure modulation of the sample gas. This eliminates the need for daily calibration. This stability and the miniature design (2.5" x 4.5" x 4.5"; 4.5 lbs) of the CO_2/CH_4 DETECTORS provide practical instruments suitable for routine safety inspections.

This report includes the theory and design of the instruments as well as studies of gas-pressure modulation by a piezoceramic-driven Helmholtz resonator.

17. Originator's Key Words	18. Availability Statement
CO_2 DETECTOR CH_4 DETECTOR HANDHELD GAS DETECTOR NDIR GAS DETECTOR HELMHOLTZ RESONATOR PRESSURE MODULATION	Availability Unlimited

19. U. S. Security Classif. of the Report	20. U. S. Security Classif. of This Page	21. No. of Pages	22. Price
Unclassified	Unclassified	123	

FOREWORD

This report was prepared by Andros Incorporated, 2332 Fourth Street, Berkeley, California 94710, under U.S. Bureau of Mines Contract No. H0377096. The contract was initiated under the Coal Mine Health and Safety Research Program. It was administered under the technical direction of the Pittsburgh Mining and Safety Research Center with Dr. G.H. Schnakenberg acting as the Technical Project Officer. Mr. Alan G. Bolton, Jr., was the Contract Administrator for the Bureau of Mines.

This report is a summary of the work recently completed as part of this contract during the period of September 1977 to May 1979. This report was submitted by the author in August 1979.

No patentable features were developed in the course of this contract.

TABLE OF CONTENTS

TABLE OF FIGURES

INTRODUCTION

There has been increasing concern during the last two decades over health and safety in industry, particularly in the mining industry. This concern is becoming more acute with the expectation of greater mining activity to supply coal as a petroleum substitute. A practical, convenient and reliable means of detecting toxic gases is one aspect of present-day mine safety requirements. A portable CO_2 DETECTOR is a safety-related need of both the Bureau of Mines and the mining industry because of the growing use of diesel-powered vehicles in underground mining. An equally urgent requirement is for a portable CH_4 DETECTOR, capable of reading up to 20% CH_4, for routine safety monitoring and in post-disaster situations.

This final report summarizes the work done by Andros Incorporated under U.S. Bureau of Mines Contract Number H0277096. This contract called for..."Development of a Personal CO_2 Detector and a CH_4 Detector."

Specifically, Andros Incorporated was to design, develop, fabricate, test and deliver four intermittent-duty portable lightweight direct-indicating carbon dioxide detectors and three similar methane detectors for use in the underground coal and hard-rock mining environment.

This work was started in September of 1977. In May of 1979 Andros Incorporated shipped four CO_2 DETECTORS and three CH_4 DETECTORS (each with leather case, calibration kit and two copies of an INSTRUCTION MANUAL). Drawings of the instruments shipped are shown in Figures 1 and 2. Electronic circuit diagrams appear in Appendix A of this report.

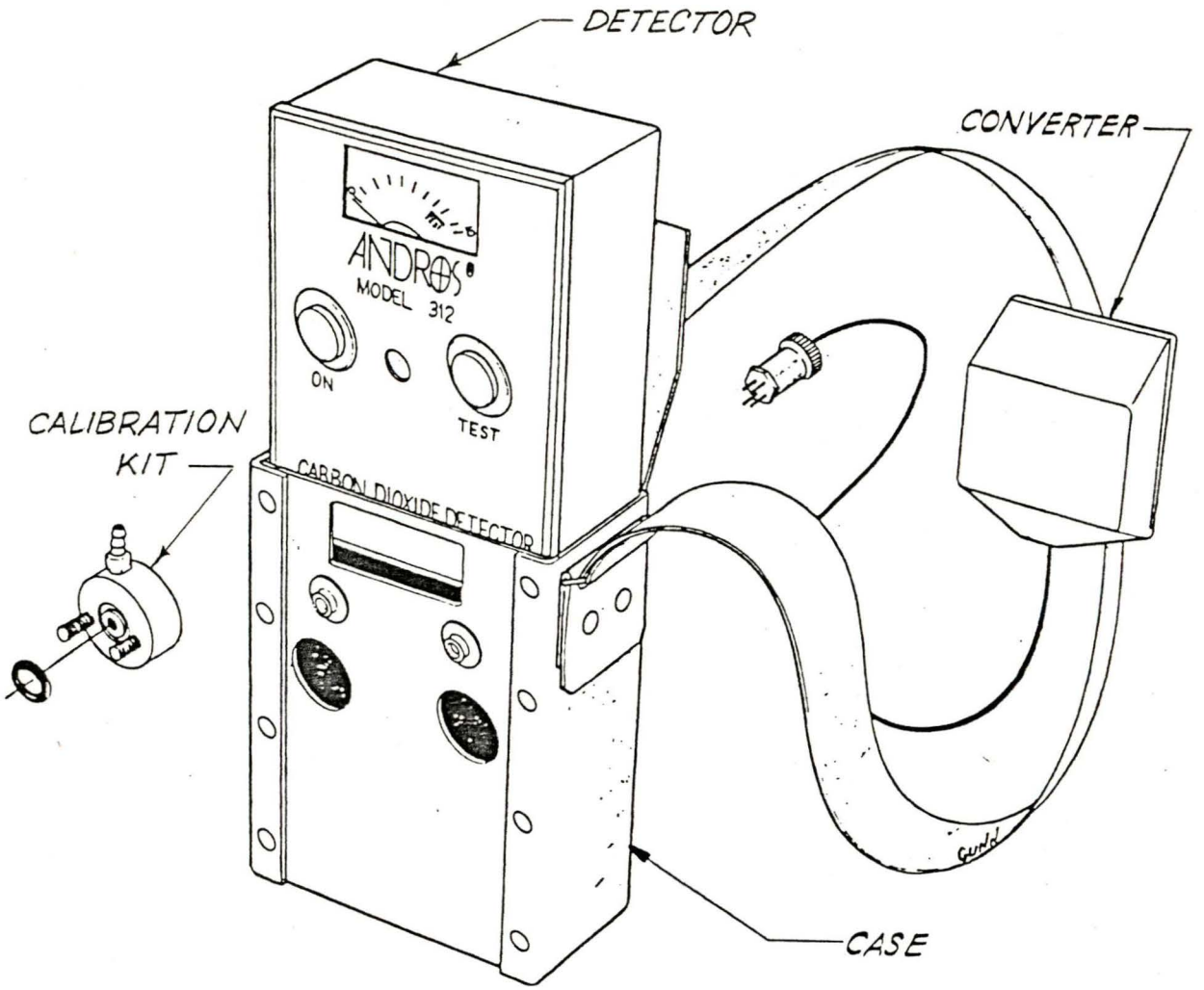

FIGURE 1. COMPONENTS OF THE MINIATURE CO_2 DETECTOR.

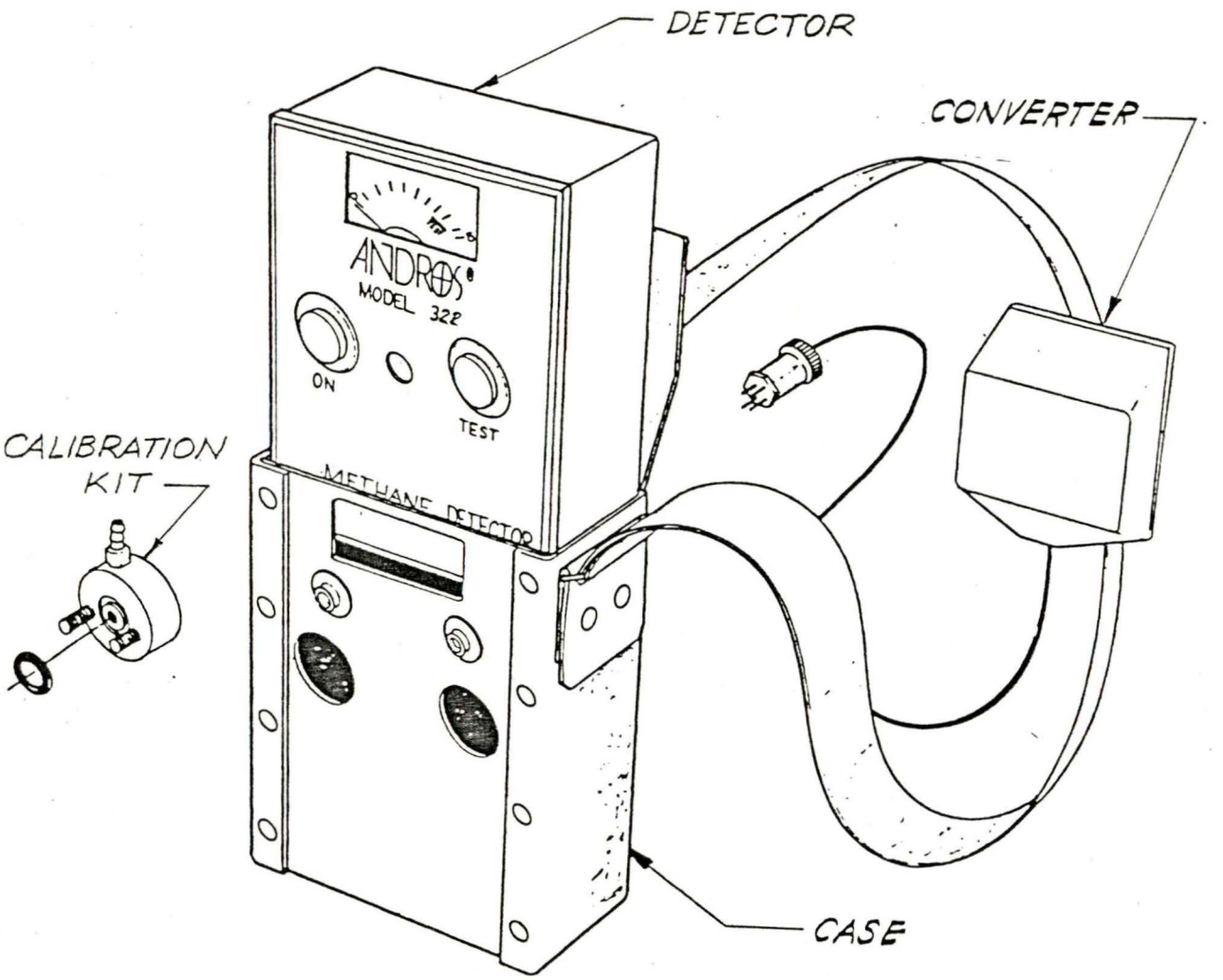

FIGURE 2. COMPONENTS OF THE MINIATURE CH_4 DETECTOR.

PROJECT OBJECTIVES

The Andros CO_2/CH_4 DETECTOR proposal was formulated in the summer of 1977. In the preceeding four years Andros Incorporated had developed a new type of nondispersive electro-optical gas analyzer. This was the result of self-funded research and a subsequent contract from the U.S. Bureau of Mines (No. H0230050) to develop a prototype.* By the autumn of 1976 this device had been built in breadboard form for the measurement of various gases (CH_4, CO, NO_2). In the spring of 1976 the CH_4 channel of this device was modified to measure CO_2. For a number of reasons, this design appeared to be most promising for CO_2 and CH_4 detection by a hand-held instrument.

Andros Incorporated proposed to apply this technology to building a pressure-modulated CO_2 DETECTOR and a pressure-modulated CH_4 DETECTOR. The project objectives described below were formulated.

- To design, fabricate and test a miniature optical bench consisting of a low-power infrared source, a Helmholtz resonator cavity driven by a piezoelectric diaphragm, a lead-selenide detector operated at room temperature, and an interference filter to select either the 4.25μm absorption band of CO_2 or the 3.31μm absorption band of CH_4.**

- To design, fabricate and test a miniature electronic processor.

- To design, fabricate and test a power supply utilizing rechargeable batteries as a power source.

---

* A "Portable Compact Low-Cost NO_2, CO and CH_4 Gas Analyzer for In-Mine Personnel Safety Monitoring". Final Report on Contract No. H0230050. July 1977. Andros Incorporated, Berkeley, California.

** "Development of a Portable Carbon Dioxide Monitor for Use in a Mining Environment". A Proposal. ARP-115; July 1977. Andros Incorporated, Berkeley, California.

- To integrate these components into an overall package design for the CO_2 and CH_4 DETECTORS weighing about 2 lbs and of dimensions 4" W x 2" D x 6" H.

The specifications of the delivered instruments are shown in Figures 3 and 4. The target specifications for range, accuracy, specificity, time response, warmup time, calibration, power, readout and applicable design specification were met.* As will be explained in detail in the sections that follow, research during development made it apparent that some of the other design objectives could not be met in this project. Problems with the Helmholtz resonator design led to the production decision to construct a pump-modulated DETECTOR. This decision was incorporated in the development contract in June of 1978.
This design increased the DETECTOR size and weight from a target of 2 lbs at dimensions 4" W x 2" D x 6" H to 4 lbs at dimensions 4.5" W x 2.5" D x 6.5" H. This increase was, for the most part, the result of increased battery capacity required to power the pump-modulation mechanism.

---

* "Development of a Portable Carbon Dioxide Monitor for Use in a Mining Environment". A Proposal. ARP-115; July 1977. Andros Incorporated, Berkeley, California.

Range:	0-1% Carbon Dioxide (CO_2)
Accuracy:	$\pm$ 10% of CO_2 reading $\pm$ 2% of full scale.
Specificity:	Less than 0.01% CO_2 equivalent response from other gaseous species commonly found in a mining atmosphere.
Time Response:	Less than 10 sec to 90% of reading.
Warmup Time:	Less than 20 seconds.
Operating Humidity:	0-90% RH.
Operating Temperature:	50° F - 100° F.
Operating Altitude Range:	0 - 8000 feet.
Calibration:	Monitor should be calibrated monthly, using a known standard CO_2 in N_2 mixture. Calibration should be performed within 25° F of operating temperature.
Test:	Built-in test function can be used to check proper instrument operation.
Power:	Rechargeable battery provides a total of fifty minutes of continuous operation or 100 individual CO_2 readings between charges.
Readout:	Meter with 0-1% CO_2 scale in increments of 0.02 CO_2.
Size:	4.5" W x 2.5" D x 6.5" H.
Applicable Design Specification:	Detector shall be designed to comply with 30 CFR 18.

FIGURE 3. SPECIFICATIONS OF THE CO_2 DETECTOR.

Range:	0-5% and 0-20% Methane (CH_4).
Accuracy:	$\pm$ 10% of CH_4 reading $\pm$ 2% of full scale.
Specificity:	Less than 0.01% CH_4 equivalent response from other gaseous species commonly found in a mining atmosphere.
Time Response:	Less than 10 sec to 90% of reading.
Warmup Time:	Less than 20 seconds.
Operating Humidity:	0-90% RH.
Operating Temperature:	50° F - 100° F.
Operating Altitude Range:	0 - 8000 feet.
Calibration:	Monitor should be calibrated monthly, using a known standard CH_4 in N_2 mixture. Calibration should be performed within 25° F of operating temperature.
Test:	Build-in test function can be used to check proper instrument operation.
Power:	Rechargeable battery provides a total of fifty minutes of continuous operation or 100 individual CH_4 readings between charges.
Readout:	Meter with 0-5% and 0-20.0% CH_4 concentrations.
Size:	4.5" W x 2.5" D x 6.5" H.
Applicable Design Specification:	Detector shall be designed to comply with 30 CFR 18, 30 CFR 27.

FIGURE 4. SPECIFICATIONS OF THE CH_4 DETECTOR.

BRIEF THEORY OF OPERATION

Technical details of the theory of operation of the CO_2/CH_4 DETECTORS are explained in a later section. A brief overview, however, may help understanding of the discussions in the sections of this report that follow.

Consider the imaginary gas analyzer shown in Figure 5. Infrared light from the SOURCE passes through a bandpass FILTER to the SAMPLE CELL. The FILTER is designed to pass only those wavelengths of light which are absorbed by the gas of interest. Carbon dioxide has an absorption peak centered on 4.25μm in the infrared region, so a CO_2 DETECTOR would have a bandpass filter transmitting only in a narrow band around this wavelength. Methane has an absorption peak of 3.31μm, so a CH_4 DETECTOR would have a bandpass filter centering on 3.31μm.

The SAMPLE CELL contains the gas sample. Here light is absorbed by the gas and the unabsorbed light passes on to the DETECTOR. The amount of light absorbed is a function of the *gas concentration*, as well as other gas variables and instrument parameters. The DETECTOR converts the transmitted light into an electrical signal and the PROCESSOR translates this signal into gas-concentration values.

The problem with the simple instrument diagrammed in Figure 5 is stability. Every component may be expected to drift away from calibration settings. There are a variety of ways to solve this problem of instability. Any solution, however, must involve generation of at least two channels of information: One to carry information about the stability of the instrument and the other to carry information about the sample-gas concentration. This may be accomplished through separate, but identical light paths (split-beam instruments), or through sequential measurements over the same light path (one measurement against a reference and the other against the unknown sample).

Research at Andros Incorporated has indicated that for the purposes of miniaturization, one of the most efficient ways of generating two channels of information is to modulate

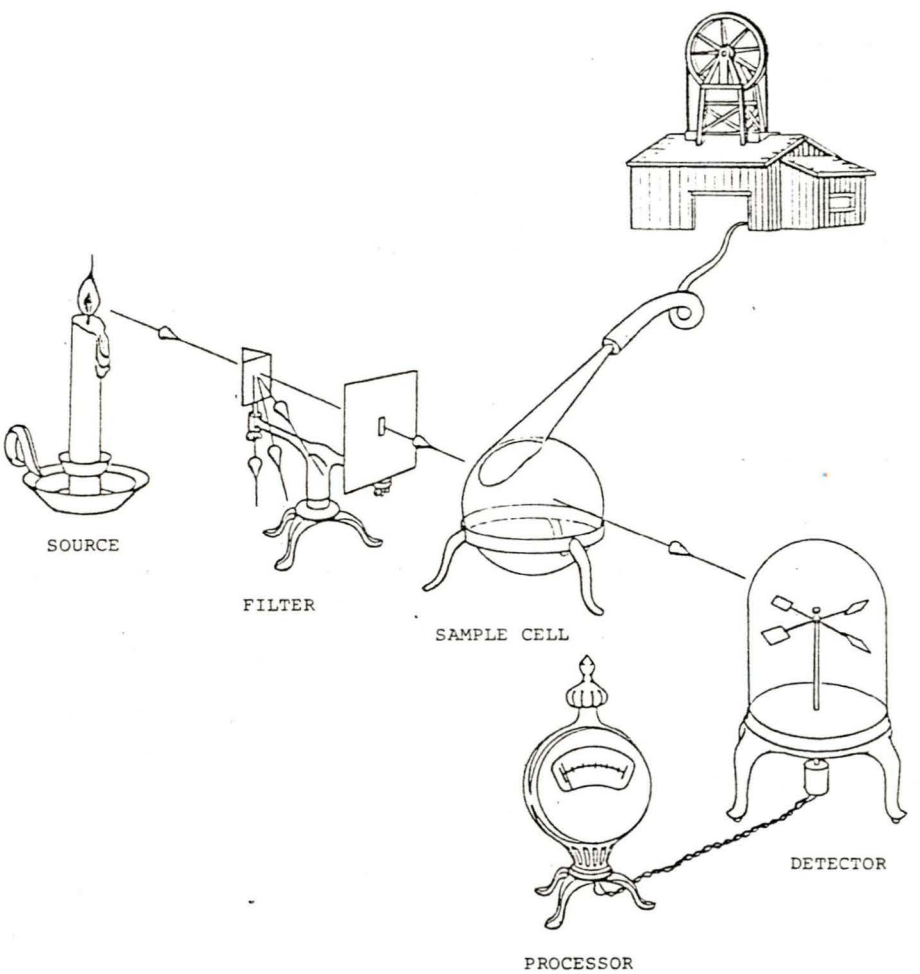

FIGURE 5. AN IMAGINARY GAS ANALYZER

the SOURCE output and the SAMPLE CELL-gas pressure at different frequencies. This modulation creates two channels of information along the single path from SOURCE to DETECTOR-signal output. The gas pressure is modulated at frequency f_1 and carries information about the SAMPLE CELL gas concentration. The SOURCE is modulated at frequency f_2 and this AC signal carries information about the instrument stability.

First consider the AC signal at frequency f_2 (see Figure 6). An OSCILLATOR operating at frequency f_2 drives the SOURCE. The infrared light output of the SOURCE will fluctuate at frequency f_2 and, ultimately, the electrical signal output of the DETECTOR will alternate at frequency f_2. This signal is amplified and enters the INPUT of an AUTOMATIC GAIN CONTROL AMPLIFIER. The OUTPUT signal from the AGC AMPLIFIER is gated by an FET SWITCH controlled by the OSCILLATOR. The gate is "closed" at the maximum excursion of the OSCILLATOR signal. The output of the FET SWITCH is a DC voltage equal to the maximum signal from the AGC AMPLIFIER. This voltage enters a COMPARATOR where it is compared to a preset REFERENCE voltage. The DC signal from the COMPARATOR is applied to the GAIN CONTROL of the AGC AMPLIFIER. This "loop" serves to constantly adjust the gain of the AGC AMPLIFIER according to the frequency f_2 channel and the REFERENCE voltage.

The major sources of instability are the SOURCE output and the DETECTOR response. Both vary with temperature and the DETECTOR response drifts with age. The REFERENCE voltage, however, remains remarkably stable once set. As the SOURCE output and DETECTOR response change, the signal going into the AGC AMPLIFIER will change. This will result in a change in the output of the COMPARATOR and the AGC AMPLIFIER gain will be readjusted against the REFERENCE voltage to make the AGC AMPLIFIER output the same as when the REFERENCE was set.

Now consider the AC signal at frequency f_1 (see Figure 7). A pressure variation at frequency f_1 is induced in the gas of the SAMPLE CELL by the PRESSURE MODULATOR. Since the light absorption of a gas is a function of gas concentration, it is a function of gas pressure. The variation in gas pressure will be transmitted to the DETECTOR, *provided* there is an absorbing gas in the SAMPLE CELL. "Zero gas" will result in zero variation in the DETECTOR output. The amplitude of the AC DETECTOR signal output will be a function of the *concentration* of absorbing gas in the SAMPLE CELL. This frequency-f_1 signal is detected (demodulated) by

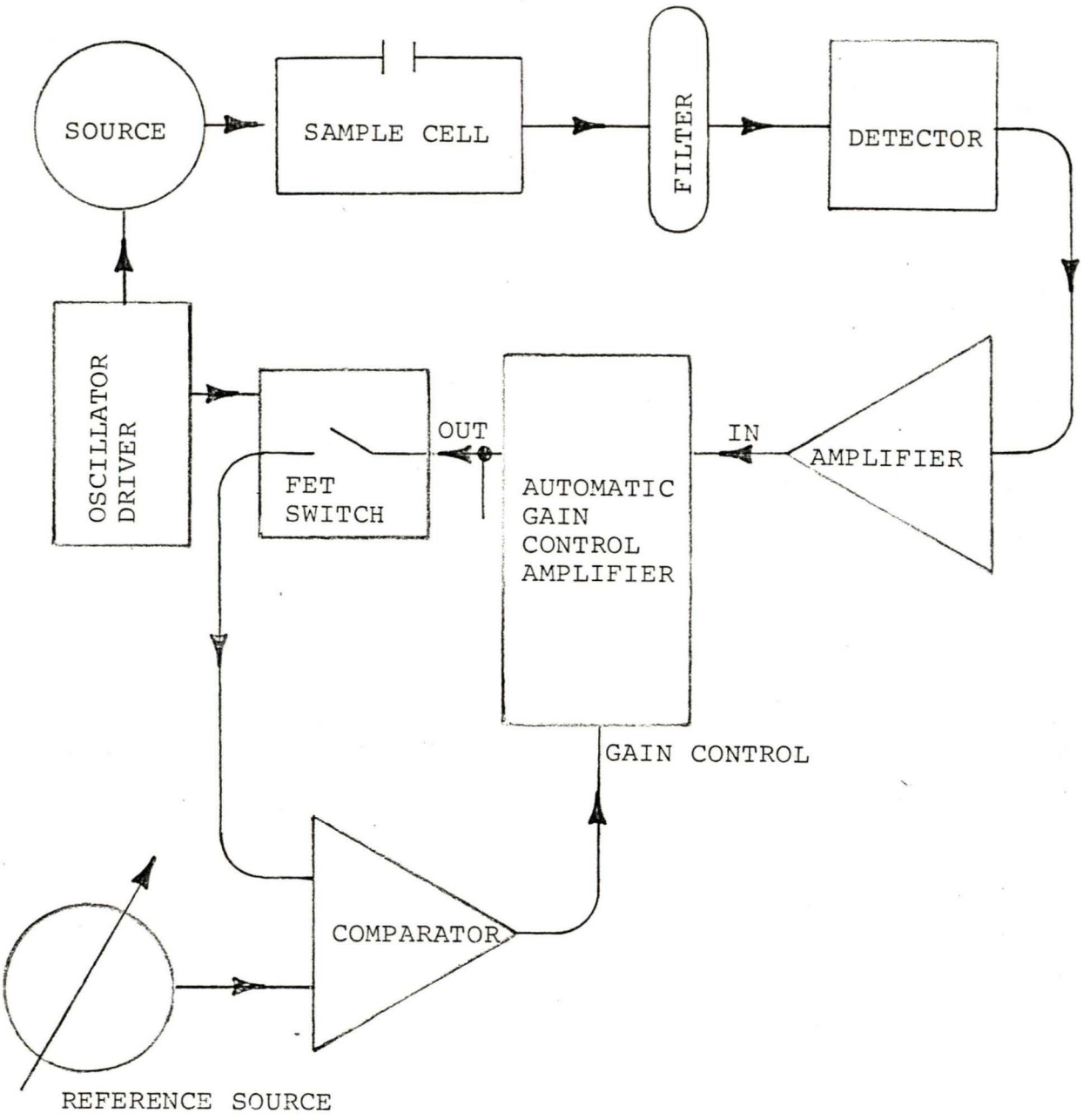

FIGURE 6. BLOCK DIAGRAM OF FREQUENCY-f_2 CHANNEL.

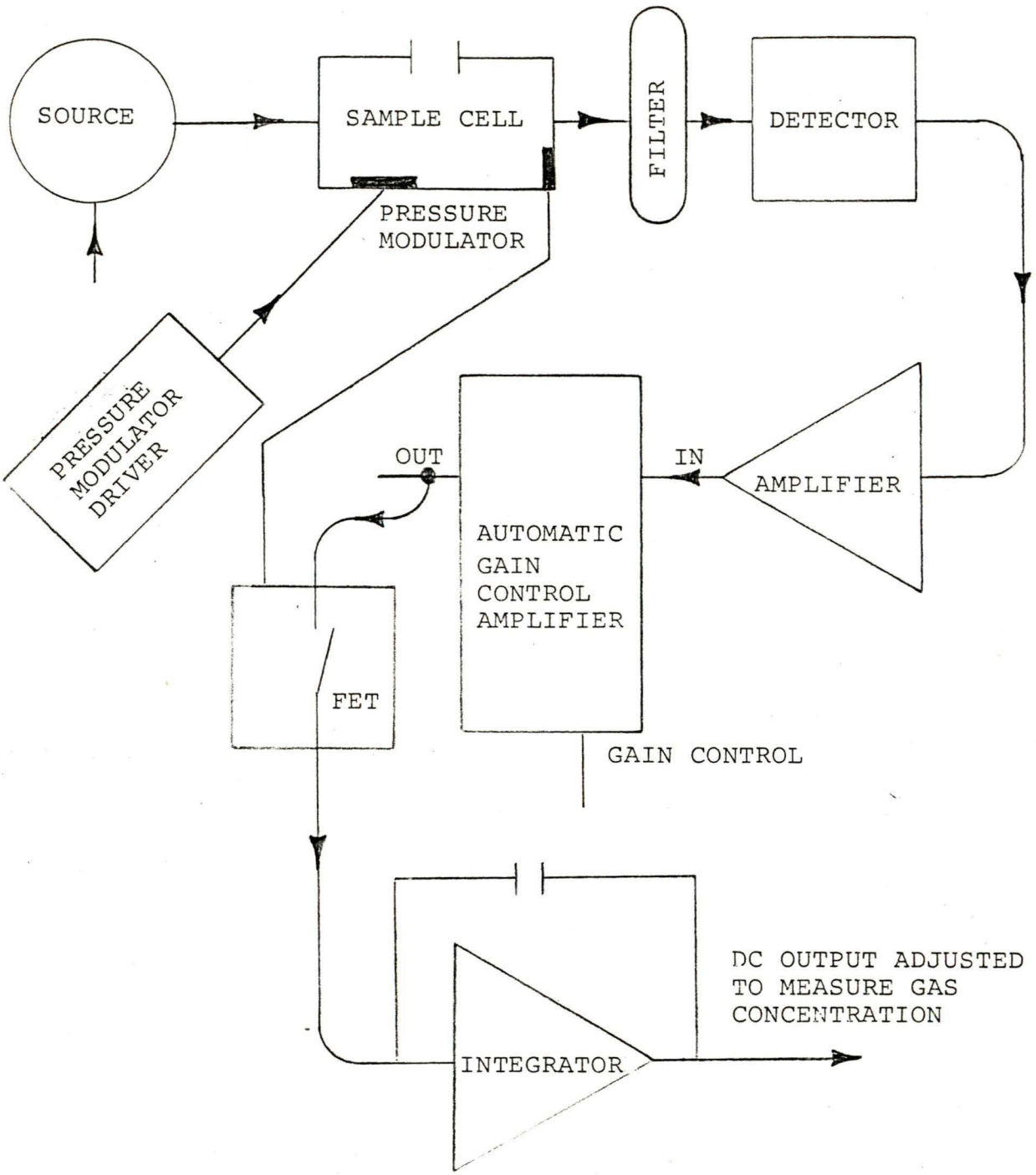

FIGURE 7. BLOCK DIAGRAM OF FREQUENCY-f_1 CHANNEL.

the FET SWITCH controlled by the PRESSURE TRANSDUCER. Before detection, it is amplified by the AGC AMPLIFIER according to the setting of the AGC AMPLIFIER GAIN CONTROL. This amplification compensates for any drift in the components of the instrument. The value of the demodulated frequency-f_1 signal is calibrated (zero and span) to measure the concentration of absorbing gas in the SAMPLE CELL.

This design has two clear benefits. Firstly, the method of compensation for drift provides for stability over both time and reasonable mechanical shock. Secondly, the instrument is capable of miniaturization to produce a hand-held gas detector.

PRIMARY RESEARCH/DEVELOPMENT DECISION

Prior to this project, Andros Incorporated has explored two methods by which the CO_2/CH_4 DETECTOR SAMPLE CELL gas-pressure modulation could be achieved.

- Pressure modulation by means of a motor-driven reciprocating pump connected to the sample cell and operating with a stroke frequency of f_1.

- Pressure modulation by designing the SAMPLE CELL as a Helmholtz resonator driven at resonant frequency $f_o = f_p$ by a piezoceramic acoustic transducer.

In this project the primary design decision was to choose between these two methods. It was clear from the beginning of the project that the modulation mechanism chosen would largely determine the remaining design parameters. The design concept of the pump-modulated SAMPLE CELL is shown in Figure 8. A simple reciprocating-pump mechanism is driven by a miniature DC motor. The SAMPLE CELL is valved so that there is an "intake stroke" in which gas is drawn into the CELL and an "exhaust stroke" in which the gas is first compressed, then exhausted from the CELL.

This design has several advantages. The theory of operation is simple and the design fundamentals of the method are straightforward. The peak-to-peak pressure excursion is more than sufficient for the PROCESSOR operation. Further, this design had, at the time of the beginnning of this project, been tested in a prototype (Figure 9) hand-held CO_2 DETECTOR whose performance was within the target specificatons.

The disadvantages of the pump-modulation design, however, had stimulated exploration of the Helmholtz resonator system. One of the problems with the pump-modulator was that of maintaining a constant pressure excursion (the amplitude of signal f_1). In the prototype this problem had been carefully examined. Attempts to eliminate the variation in pressure excursion were not found to be practical and attention was focused on compensating for the variation. This problem will be discussed further in the section entitled "Designing the Pump-modulated Detector".

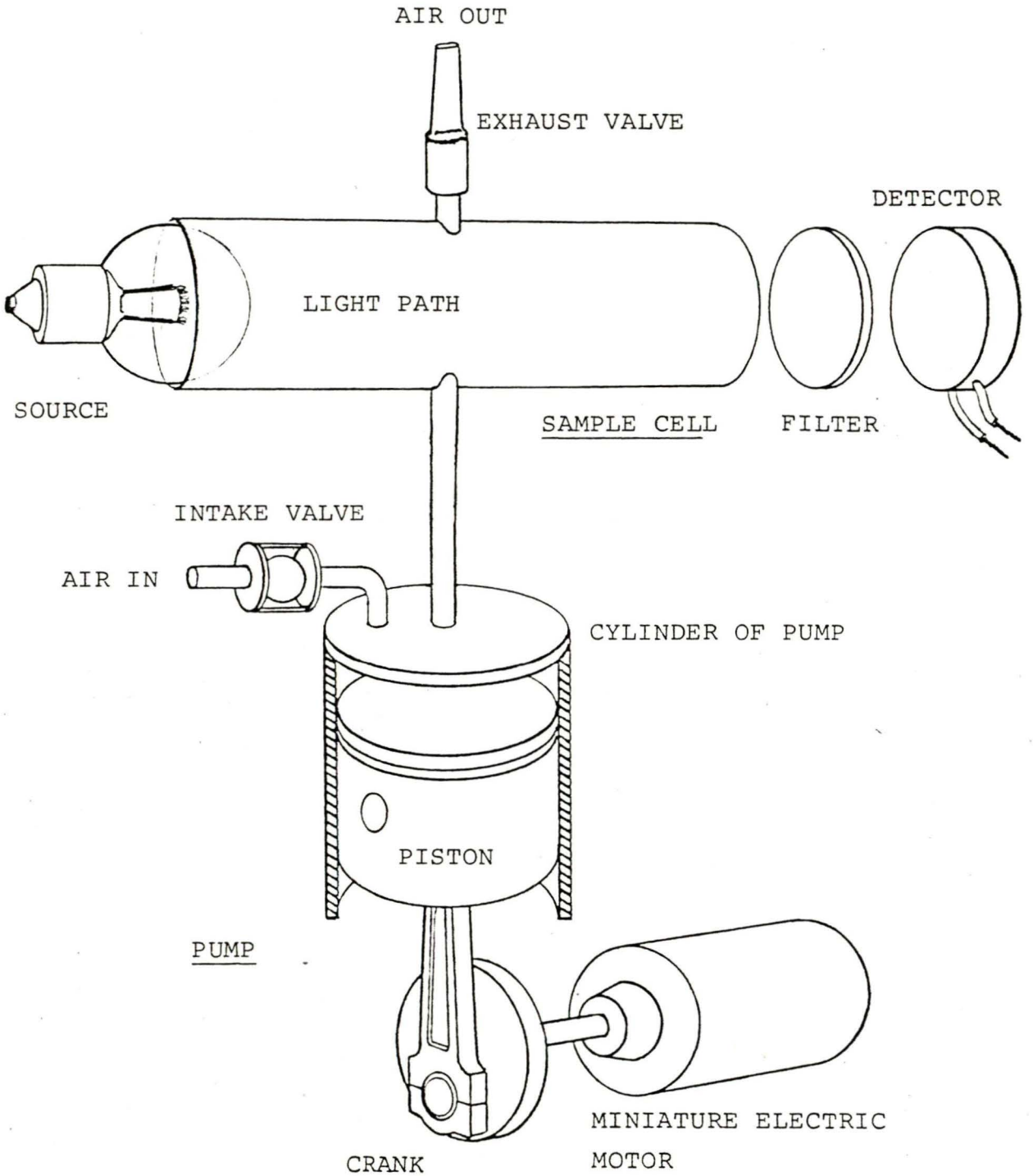

FIGURE 8. THE PUMP-MODULATED SAMPLE-CELL DESIGN.

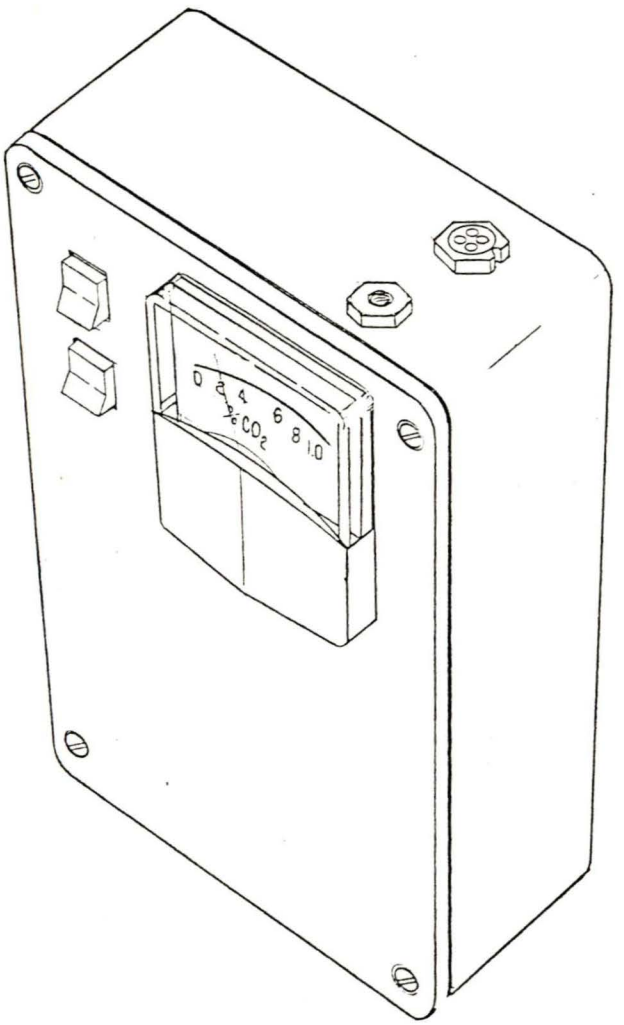

FIGURE 9. DRAWING OF THE PROTOTYPE HANDHELD CO_2 DETECTOR.

Another problem with pump-modulation is design limiting. The upper limit of possible pump-modulated pressure frequency f_1 is about 80 Hz. The signal-to-noise ratio in the system is frequency-dependent and improves greatly with higher f_1 frequencies. The lower f_1 frequency limit for an acceptable signal-to-noise ratio is about 50 Hz. Further, lower f_1 frequencies mean greater component size. For these two reasons, the limit to modulation frequency with the pump-modulated system is regarded as an inherent design limitation.

A third problem is the power requirement of the pump motor. This is the critical power requirement of the design and is, approximately, 0.5 watts. Power requirement directly influences instrument weight through battery size.

The fourth major problem of the pump-modulation design is vibration-induced microphonics. This problem will be discussed further in the sections entitled DESIGNING THE PUMP-MODULATED DETECTOR and CONCLUSIONS.

It appeared that the major problems of the pump-modulation system might be solved by using a Helmholtz resonator for a SAMPLE CELL.

Here is the reader is reminded that a soft-drink bottle is a form of Helmholtz resonator. Blow across the opening and the bottle will "hum" at its resonant frequency. Partially fill the bottle and the hum goes up in pitch: A smaller volume means a higher resonant frequency. In general, the resonant frequency of a simple Helmholtz resonator is related to its geometry by the formula:

$$f_o = \frac{c}{2\pi}\sqrt{\frac{A}{LV}}$$

Where... f_o = resonant frequency (Hz);

c = sound velocity (cm/sec)'

A = neck cross-sectional area (cm^2);

L = neck length (cm);

V = chamber volume (cm^3).

The Helmholtz-resonator SAMPLE CELL design concept is shown in Figure 10. The resonator has two chambers, one which contains the sample gas and optics, the other of which contains the piezoceramic driver and pressure transducer. The driver is a piezoceramic acoustic transducer with a natural resonant frequency $f_p = f_o$. This ensures the maximum pressure excursion.

The Helmholtz-resonator design possesses some clear advantages. Firstly, the resonant frequency and pressure amplitude at resonance are stable since they are a function of physical dimensions and parameters which are expected to undergo little variation over operating conditions.

Secondly, it is possible to obtain relatively high resonant frequencies (in the order of 1000 to 1500 Hz). This greatly improves the signal-to-noise ratio and helps reduce component size.

Thirdly, less power is required to drive the Helmholtz resonator. An adequate peak-to-peak pressure excursion of up to 0.8 psi can be obtained with a 100 mW driver. This enables the battery size to be reduced.

The major design limitation of the Helmholtz resonator is that the resonant frequency f_o and the piezoceramic-driver frequency f_p must be closely matched for optimum pressure excursion. The problem may be seen in Figure 11, where frequency versus pressure is shown for a Helmholtz resonator driven by an acoustic speaker. The pressure excursion falls off quite sharply on either side of the resonant frequency. To achieve precise matching requires detailed understanding of the relationship between frequency, pressure and geometry of dual-chambered Helmholtz resonators. Since this information was not available, the first research priority was to examine the parameters of Helmholtz resonators.

This research had three objectives.

- To experimentally examine the relationship between the resonant frequency f_o and the geometry of the dual-chamber Helmholtz resonator.
- To derive a formula relating design geometry to pressure and frequency.
- To examine the resonant frequency and pressure variation in a Helmholtz resonator driven by a piezoceramic acoustic transducer.

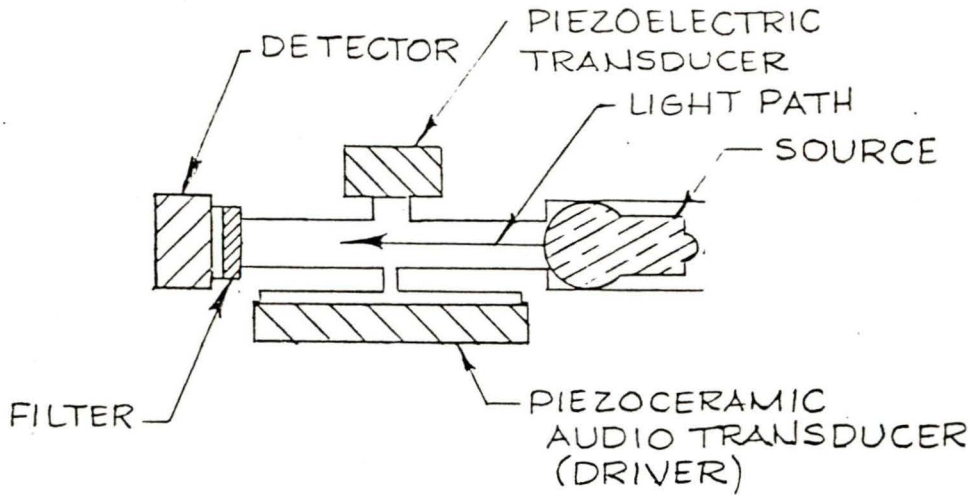

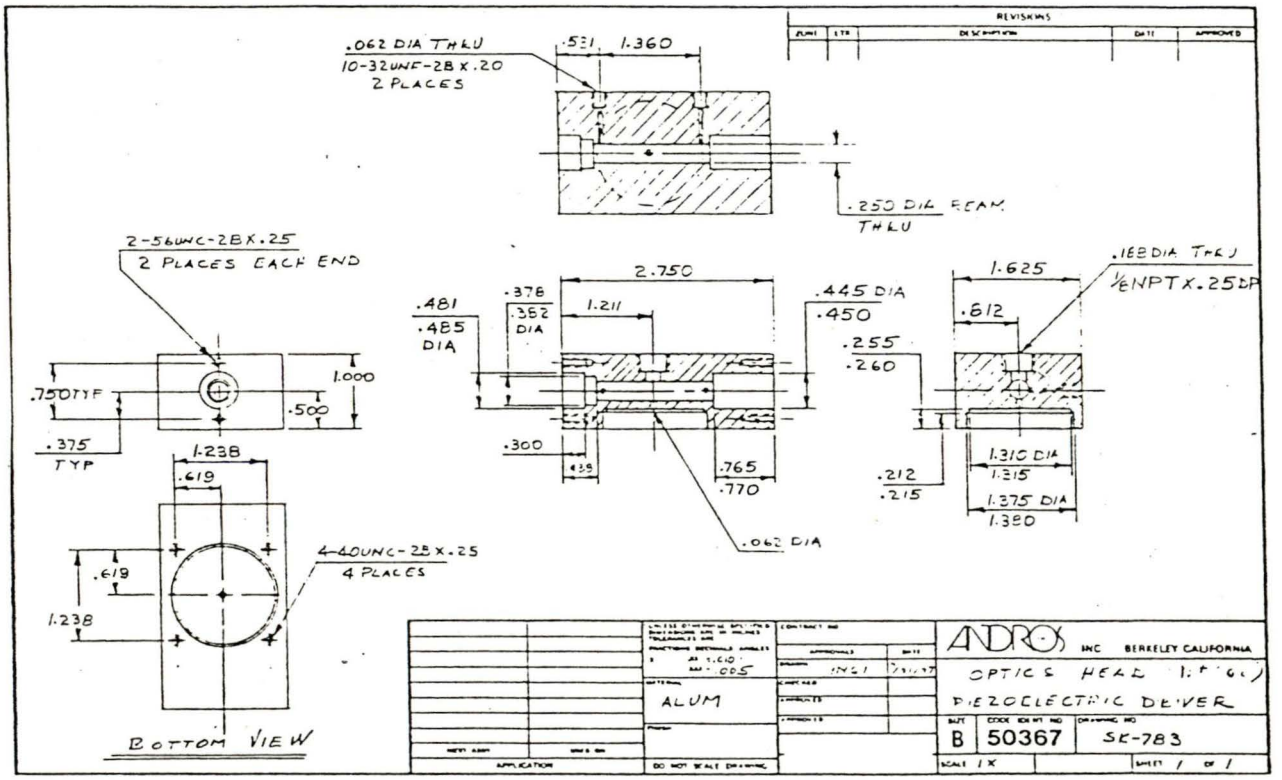

FIGURE 10. HEMLHOLTZ-RESONATOR SAMPLE CELL DESIGN FOR THE MINIATURE CO_2/CH_4 DETECTORS.

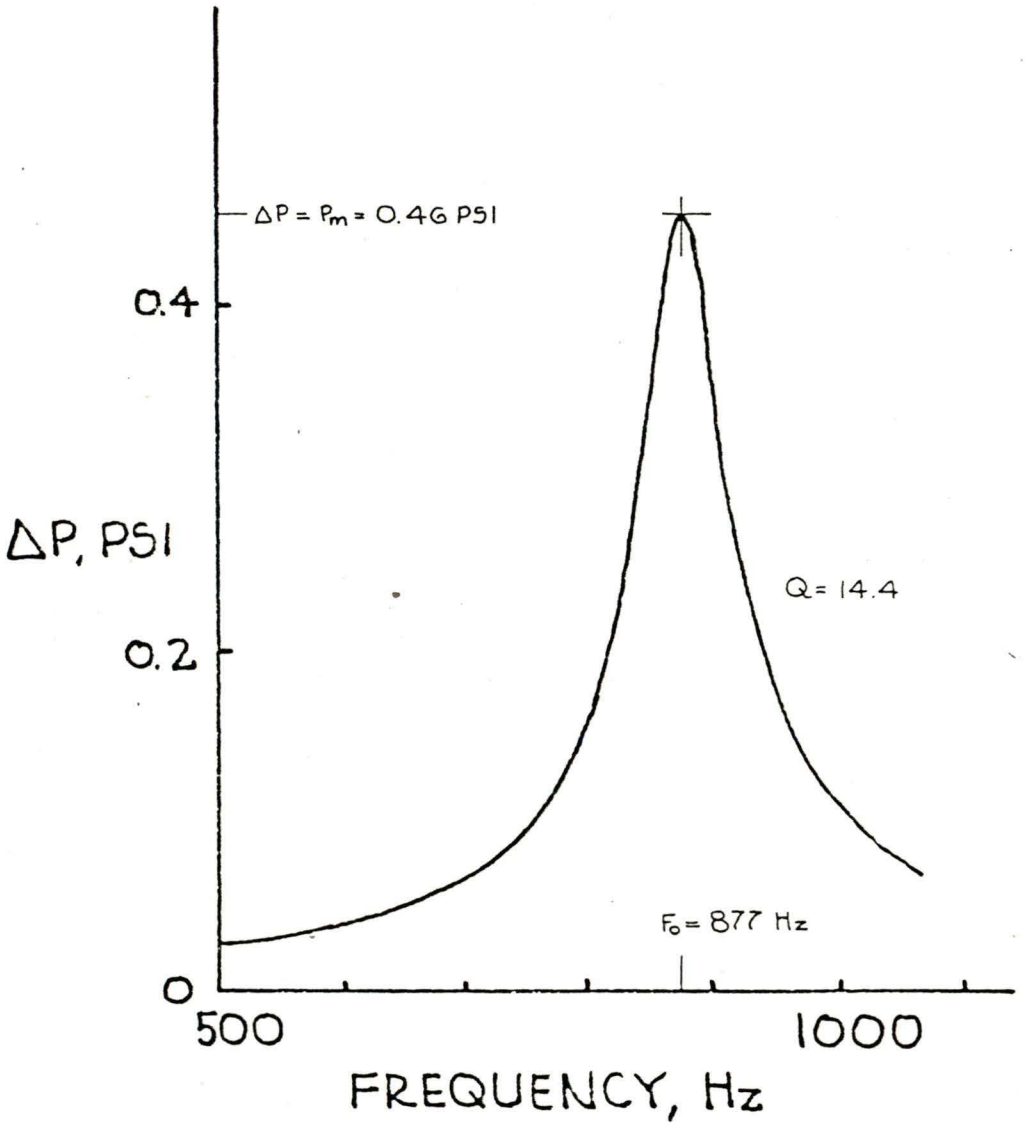

FIGURE 11. FREQUENCY VERSUS PRESSURE EXCURSION IN A HELMHOLTZ RESONATOR.

HELMHOLTZ RESONATOR STUDIES

A classical Helmholtz resonator consists of a single chamber from which the only opening to the exterior is through a narrow neck (see Figure 12). In this simple system, resonant frequency and geometry are related by the expression $f_o = (c/2\pi)\sqrt{A/LV}$. This expression may be easily derived from analogy with a resonant RLC-electrical circuit.*

The classical Helmholtz analysis assumes an input of acoustical energy directed through the neck of the resonator. At the resonant frequency this energy will induce the maximum pressure excursion (P_m = max ΔP) within the resonator chamber.

In practice, the energy source is usually part of a double-chamber (see Figure 12). An acoustical driver, either a speaker or a piezoceramic acoustical transducer, is mounted in the first chamber (W). The sound energy generated by the driver is directed through the connecting neck into the second chamber (V), which reacts as a Helmholtz resonator.

An expression for the behavior of the double-chamber system may be derived from analogy with a resonant RLC-electrical circuit in which two capacitors are in parallel (see Figure 12).

$$f_o = \frac{c}{2\pi}\sqrt{\frac{A}{L}\left(\frac{1}{W} + \frac{1}{V}\right)}$$

Since the design parameters of a miniature Helmholtz-resonator SAMPLE CELL for the CO_2/CH_4 DETECTOR depended upon understanding the geometry of this double-chamber system, the initial experiments in this study were directed toward testing the equation given above for various ranges of the variables (A, W, V, L). The test equipment shown in Figures 13 and 14 was assembled for that purpose.

---

* Morse, P.M. and Ingard, K.U. (1968) Theoretical Acoustics. McGraw-Hill Book Company, New York.

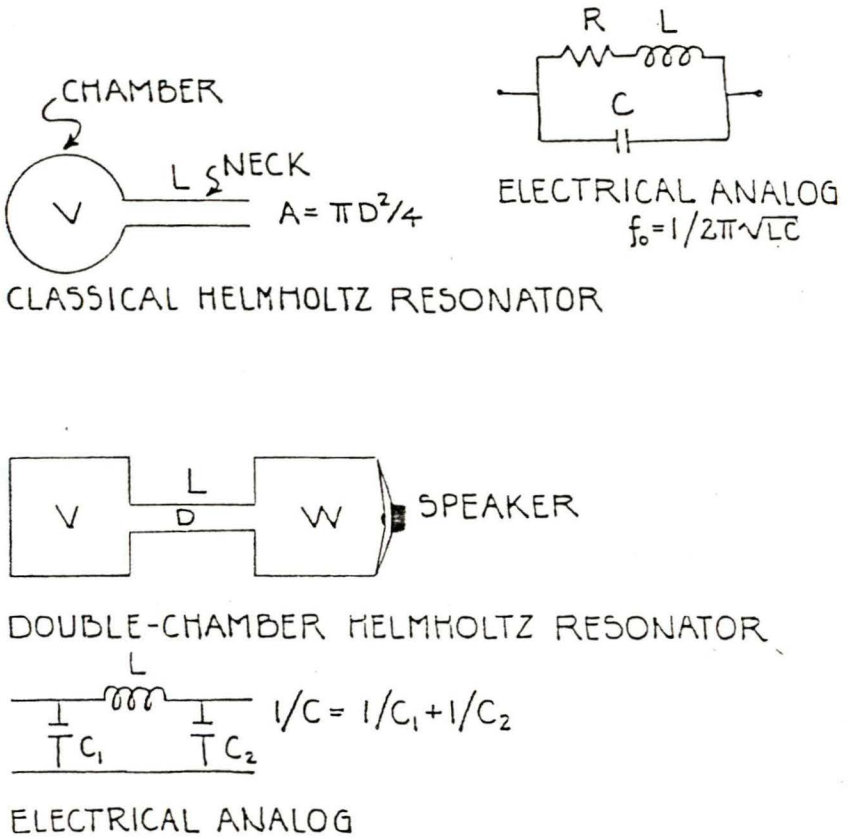

FIGURE 12. A CLASSICAL HELMHOLTZ RESONATOR AND A DOUBLE-CHAMBER HELMHOLTZ RESONATOR EXCITED BY AN ACOUSTICAL SPEAKER.

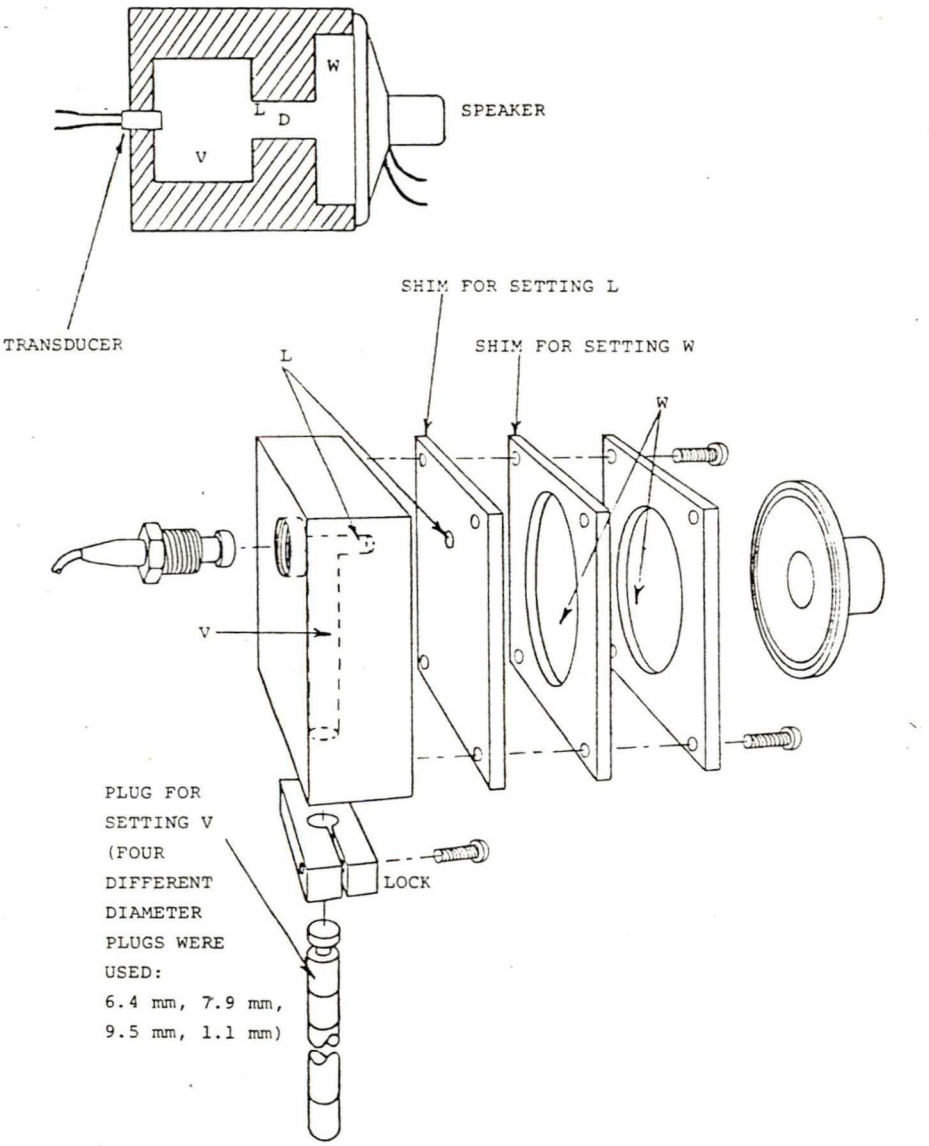

FIGURE I3. DOUBLE-CHAMBER RESONATOR DESIGNED FOR TESTING THE RELATIONSHIP BETWEEN F_o AND THE RESONATOR GEOMETRY.

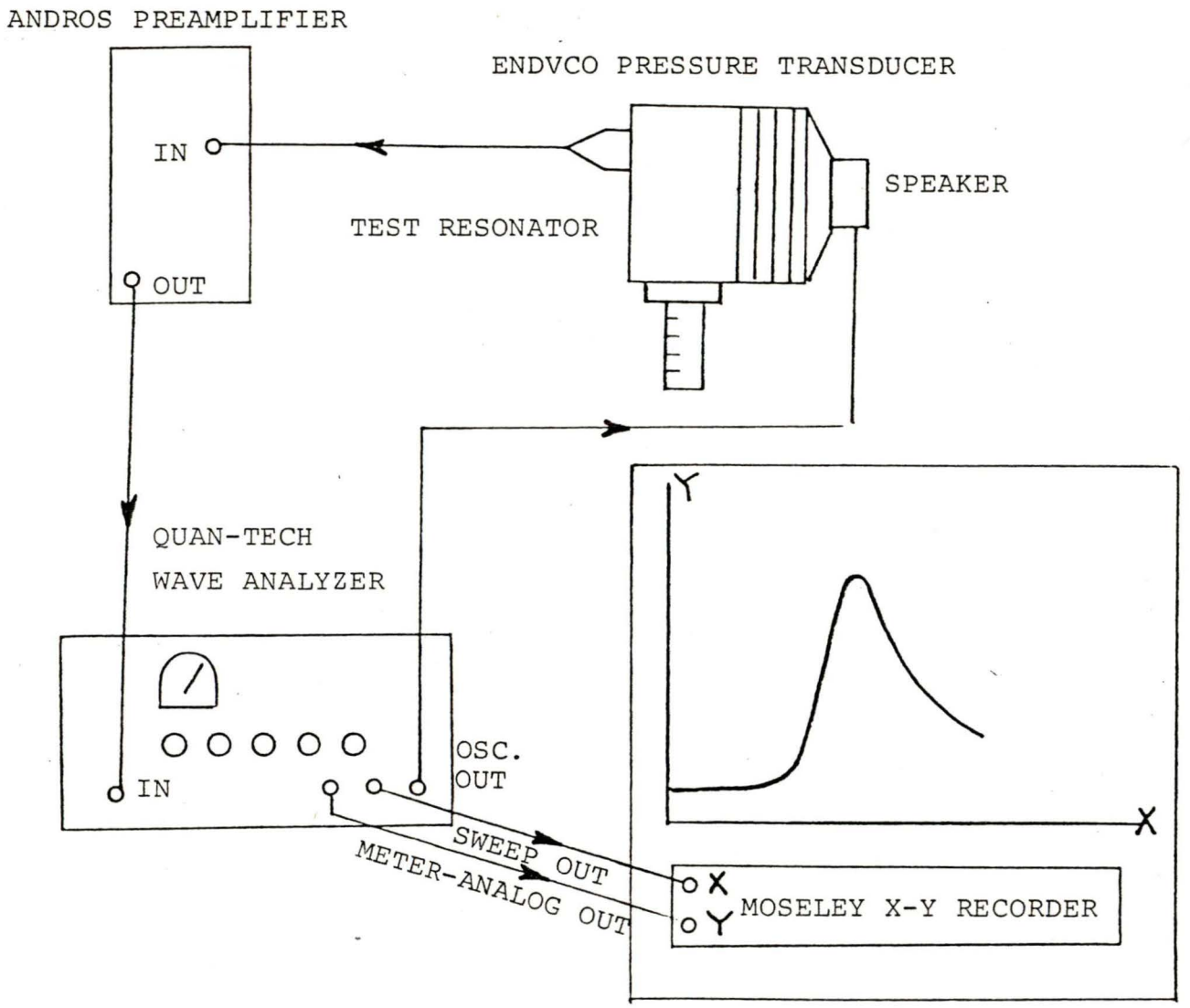

FIGURE 14. EXPERIMENTAL APPARATUS FOR STUDYING THE DOUBLE-CHAMBER HELMHOLTZ RESONATOR.

The double-chamber resonator shown in Figure 13 was designed by the engineering staff at Andros and fabricated by the Andros machine shop. The system was designed to enable the experimental resonant frequency F_o to be measured for various combinations of W, V, L and D. The ranges over which these variables could be tested are given in the short table below.

Chamber Volume	W = 4.20 cm^3 to 41.27 cm^3
Chamber Volume	V = 0.402 cm^3 to 5.85 cm^3
Neck Length	L = 1.27 cm to 3.81 cm
Neck Diameter	D = 0.45 cm to 0.64 cm.

The pressure excursion within the chamber V, was measured by an ENDVCO* Model 8503-4 pressure transducer mounted in the wall of the chamber V. The output of the pressure transducer was scaled to a nominal 1V/psi sensitivity by an Andros-designed preamplifier. The output of this preamplifier was connected to the input of a Quan-Tech Laboratories Model 304 wave analyzer. The meter-analog output of the wave analyzer was connected to the Y-axis input of a MOSELEY 7004-A X-Y recorder. The sweep-analog output of the wave analyzer was connected to the X-axis input of the recorder (see Figure 14). The pressure-range measured was from 0 psi to 0.7 psi (4.826×10^4 dynes/cm^2).

The resonant chamber was excited by various 2", 2¼" and 1.75" 0.2W 45-Ohm speakers. The speakers were driven at 100 mW by an Andros-designed power amplifier connected to the oscillator output of the Quan-Tech wave analyzer. Thus, as the oscillator frequency was varied in a sweep over the frequency range of the wave analyzer, the speaker was driven at a continuum of frequencies and the X-axis of the recorder was traversed.

---

* Reference to specific brands, equipment, or trade names in this report is made to facilitate understanding and does not imply endorsement by the Bureau of Mines.

The result of this instrumentation was a series of curves of ΔP versus frequency. At the resonance frequency F_o of the Helmholtz resonator the sound energy (pressure vibrations) was much more efficiently communicated through the resonator neck, into the resonator chamber and to the pressure transducer. Thus max ΔP = Pm defined F_o.

In each TEST four of the parameters, W, L and "plug diameter" were fixed (see Figure 13). The neck diameter remained constant throughout all tests at 0.45 cm. In each EXPERIMENT the plug was set to one of the 6 volume stops and the Quan-Tech oscillator was allowed to sweep through a frequency interval. There were 6 EXPERIMENTS per TEST and 60 TESTS.

A typical TEST is shown in Figure 15. The volume W = 8.64 cm^3; the length L = 2.54 cm; and the plug size was 0.635 cm. The six plug stops corresponded to: V = 0.40 cm^3, 0.70 cm^3, 1.01 cm^3, 1.31 cm^3, 1.61 cm^3, 1.91 cm^3.

The values of F_o were plotted against V (TEST 1) in Figure 16. The experimental curve obtained conformed in shape to the expectation that resonant frequency varied with the reciprocal square root of the chamber volume V. The predicted values of f_o, however, consistently exceeded the experimental values by about 430 Hz. This was found to be typical of all TESTS and EXPERIMENTS (Figure 17) and will be analyzed in detail in the discussion that follows.

The causes of this discrepancy between experimental and theoretical values became apparent upon a linear analysis of these data. The object of a linear analysis is to transform the variables in such a way that the relationship between any pair of transformed variables is expected to be linear. Discrepancies between expected and experimentally determined values then show up as either non-linear behavior or as differences in the parameters of linear equations.

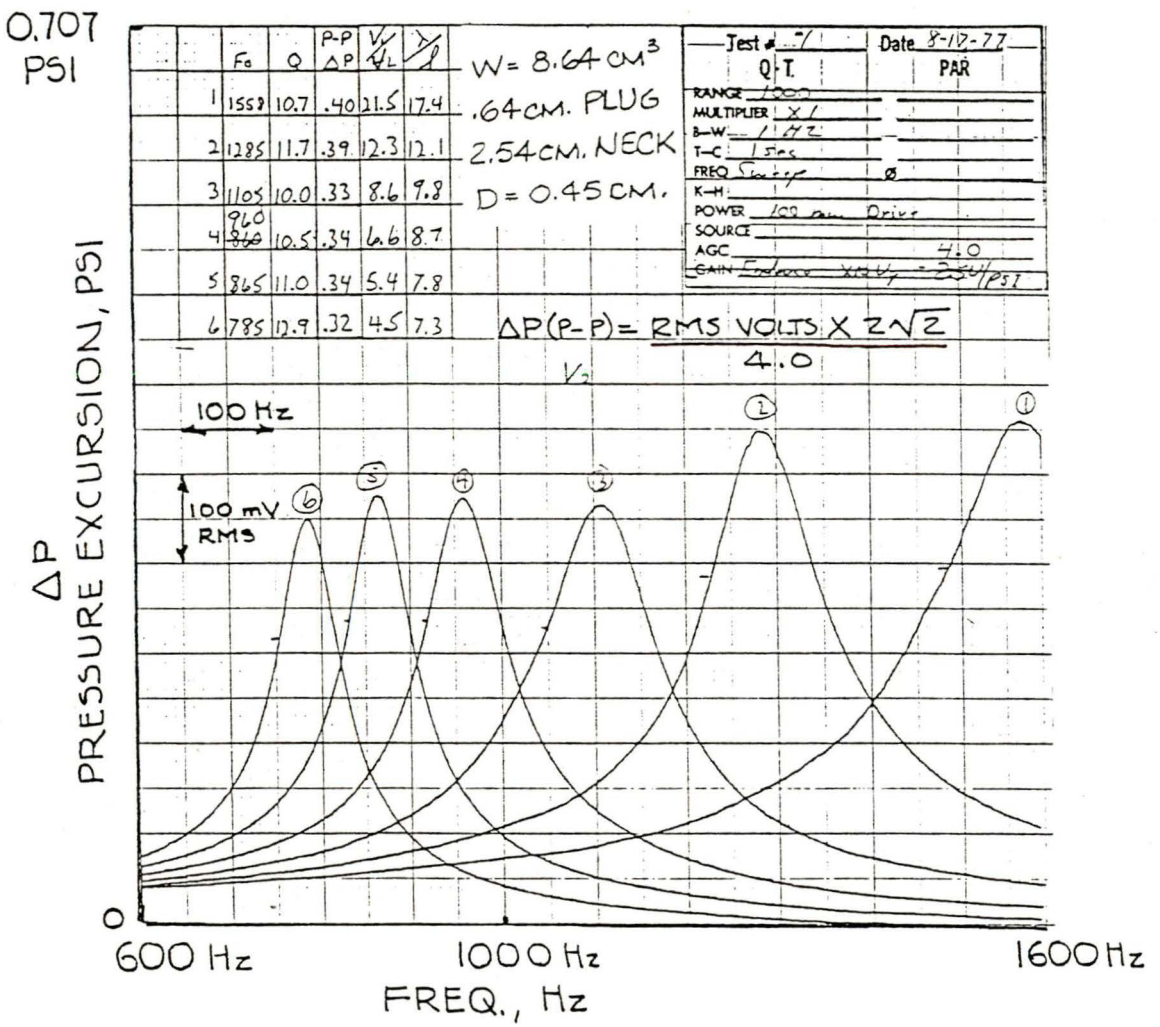

FIGURE 15. A TYPICAL TEST WITH SERIES OF EXPERIMENTS.

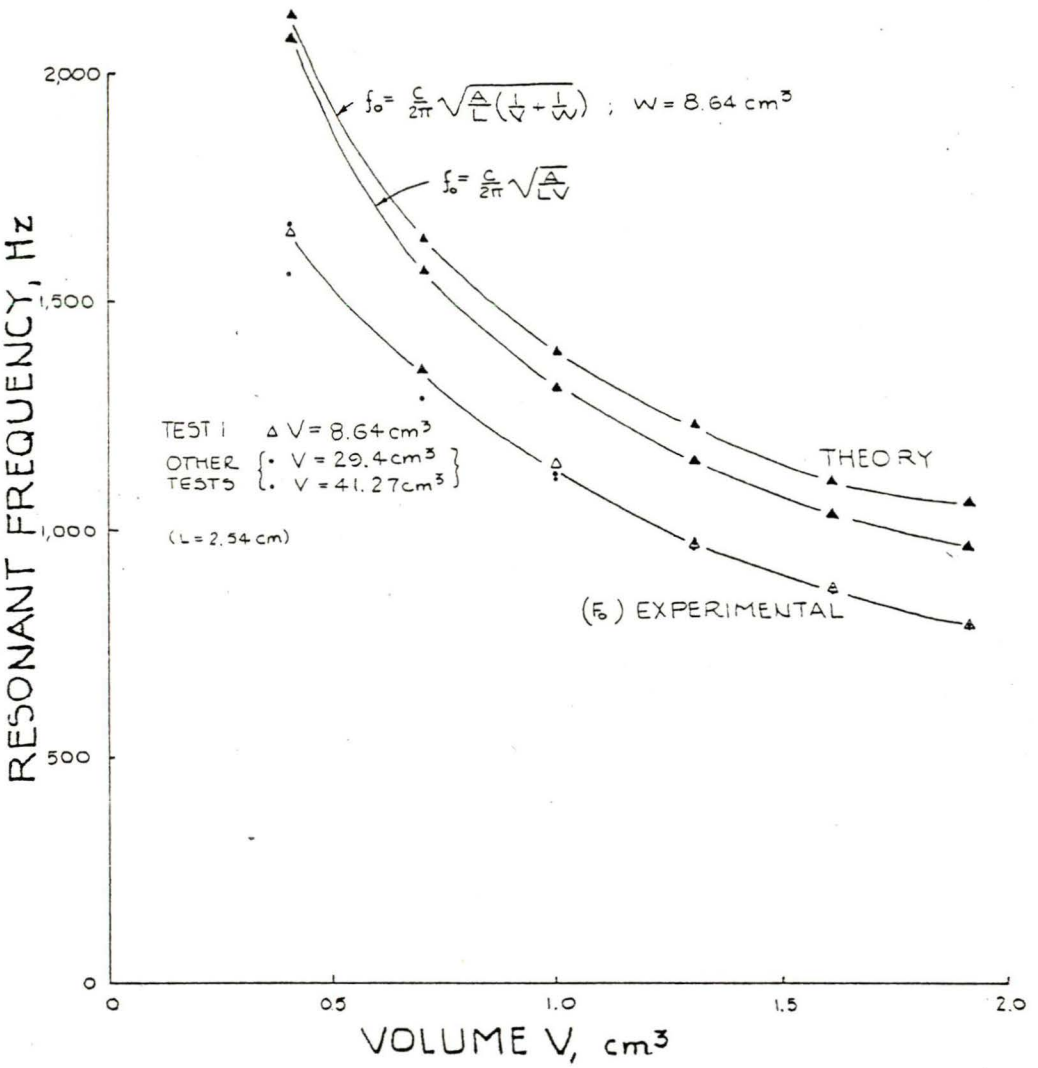

FIGURE 16. EXPERIMENTAL AND THEORETICAL RESONANCE CURVES FROM TEST 1.

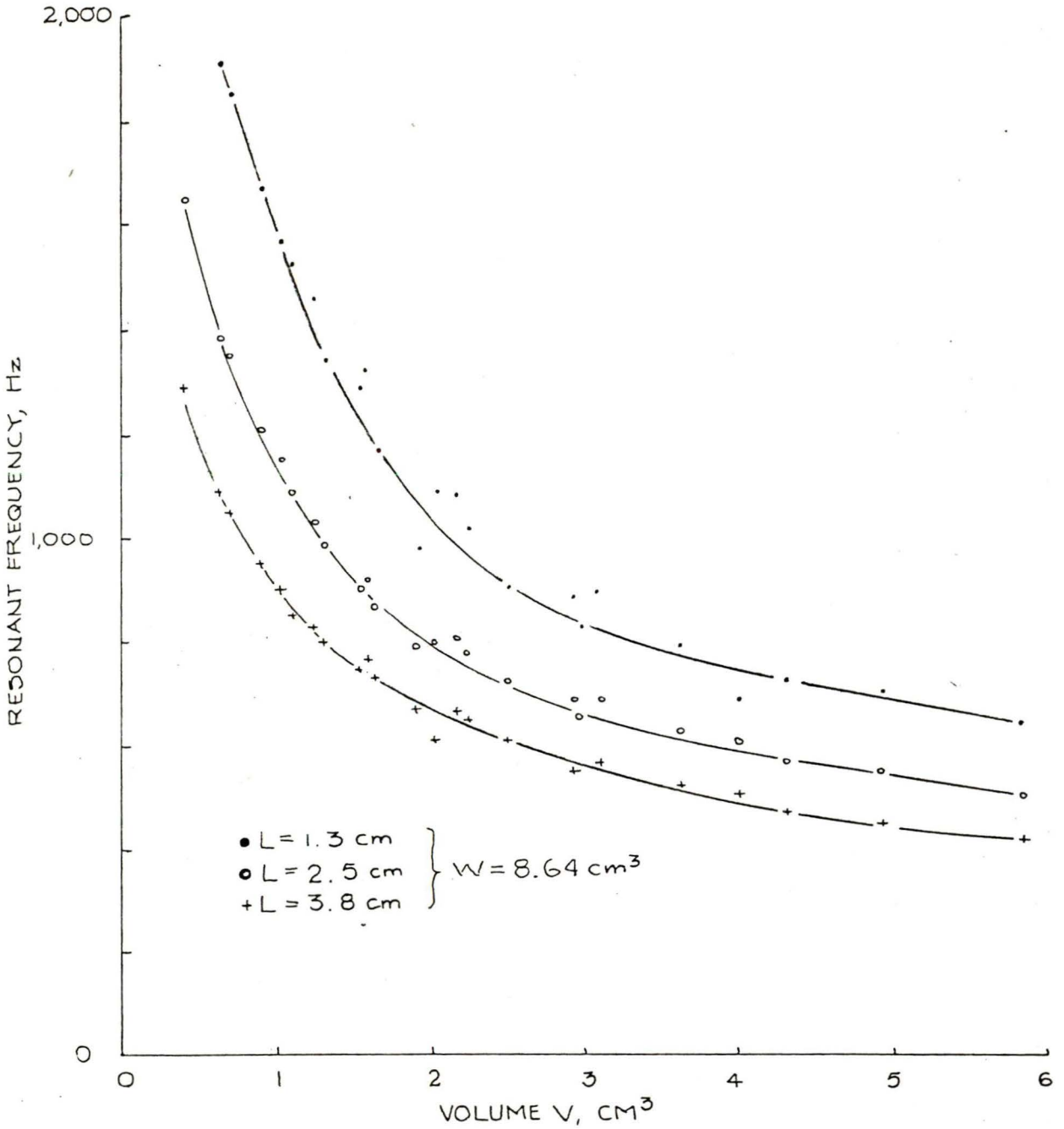

FIGURE 17. EXPERIMENTAL RESONANCE CURVES (ALL TESTS AND EXPERIMENTS WITH W = 8.64 cm^3).

Squaring both sides of the expression

$$f_o = \frac{c}{2\pi} \sqrt{\frac{A}{L}\left(\frac{1}{W} + \frac{1}{V}\right)}$$

gives $$f_o^2 = \frac{c^2}{4\pi^2} \left[\frac{A}{L}\left(\frac{1}{W} + \frac{1}{V}\right)\right] .$$

Since $$A = \pi D^2/4,$$

we can write $$f_o^2 = \frac{c^2}{16\pi} \frac{D^2}{L}\left(\frac{1}{W} + \frac{1}{V}\right) .$$

Let us use the value $c = 33.16 \times 10^3$ cm/sec. Then $c^2 = 1099.59 \times 10^6$ and we can write $c^2/16\pi = 21.88 \times 10^6$. Now

$$f_o^2 \times 10^{-6} = 21.88 \frac{D^2}{L}\left(\frac{1}{W} + \frac{1}{V}.\right)$$

This new function expresses $f_o^2 \times 10^{-6}$ as a linear function of D^2, $1/L$, $1/W$ and $1/V$ (each in the form $y = ax + b$). We can write $(f_o^2 \times 10^{-6}) = (\text{constant})\ (1/L)$ and expect to obtain a linear function when $(F_o^2 \times 10^{-6})$ is plotted against $(1/L)$ with all other variables being held constant. The remaining equations of interest are $(f_o^2 \times 10^{-6}) = (\text{constant}_1)\ (1/V) + (\text{constant}_2)$ and $f_o^2 \times 10^{-6}) = (\text{constant}_3)\ (1/W) + (\text{constant}_4)$.

This type of analysis was continued by plotting $(F_o^2 \times 10^{-6})$ versus $(1/V)$ for the same values of V as in Figure 17. The results (see Figure 18) clearly show that F_o is a function of $(1/V)^{\frac{1}{2}}$, since $F_o^2 \times 10^{-6}$ versus $1/V$ is linear for each group of parameters. More importantly, however, it also becomes clear that the discrepancy between the predicted values of $(f_o \times 10^{-6})$ involve only a difference in slope and intercept.

In each group of experiments analyzed, the intercept of the experimentally determined curves was zero (or practically zero). This was not the case for the predicted curves, since the predicted intercept was a function of $1/W$. This

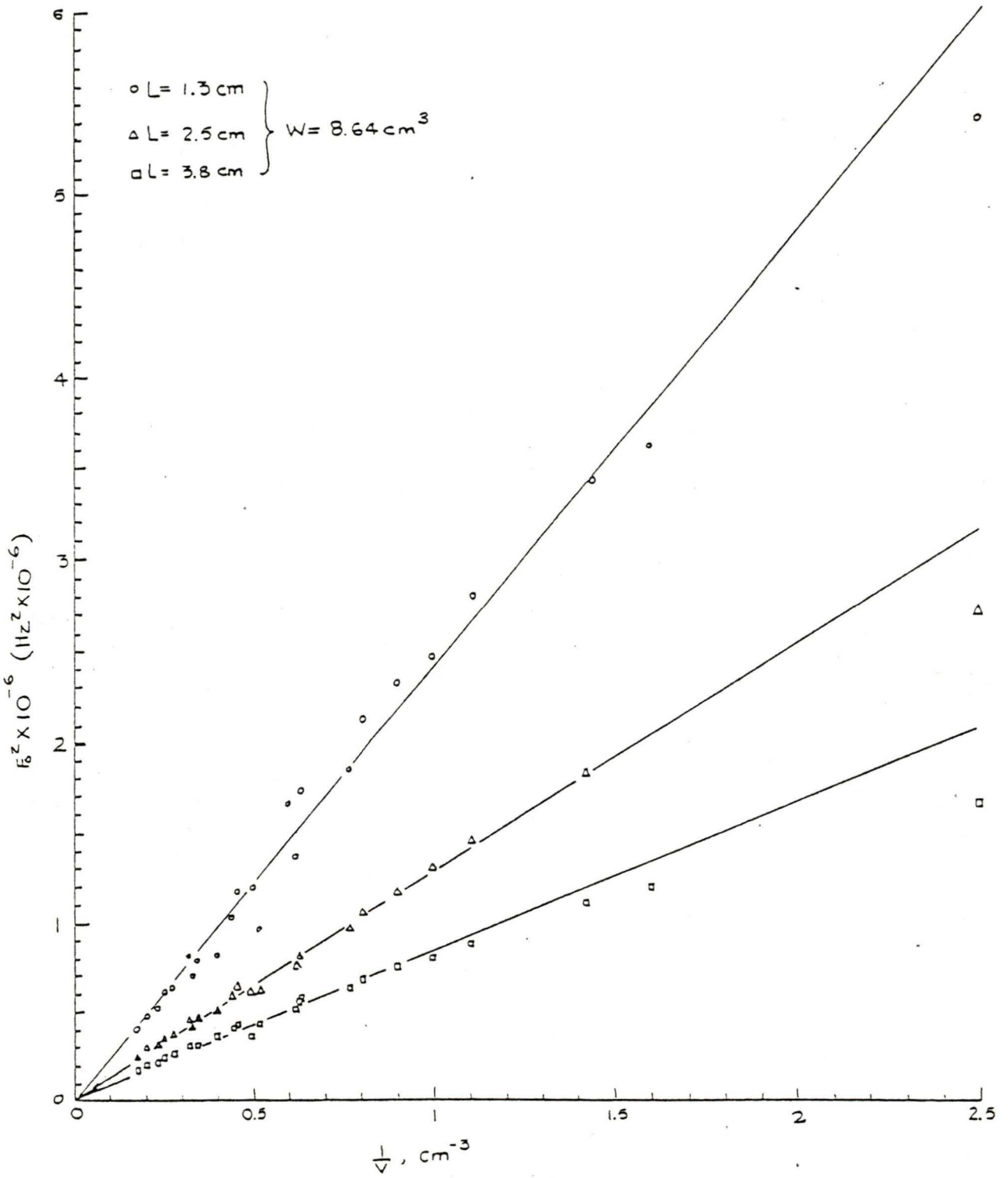

FIGURE 18. LINEAR EVALUATION OF F_o AND V ÀS $(F_o^2 \times 10^{-6})$ AND (1/V).

suggests that the predicted role of W was not realized in these experiments. That this is, indeed, the case is shown by Figure 19. Plotting ($F_o^2 \times 10^{-6}$) versus (1/W) yielded, in the best fit possible, a uniform line ($F_o^2 \times 10^{-6}$) = constant. The value of F_o is not a function of the volume W.

This observation is easily explained. Figure 13 shows the detail of the speaker mount in the test chamber. The apparent volume W was not realized in any experiment since the vibratory motion of the paper speaker cone communicated the pressure excursion directly to the atmosphere outside of the chamber W as well as inside of W. In effect, the true volume was not W, but was virtually infinite and the reciprocal of that volume (in place of 1/W) is practically zero. The proper equation, on the basis of this analysis, should have been $f_o = (c/2\pi)\sqrt{A/LV}$. The zero intercept value for ($F_o^2 \times 10^{-6}$) versus (1/V) is explained.

Figure 20 shows the values of ($F_o^2 \times 10^{-6}$) versus (1/V) compared to the transformed linear relationship derived from the equation above, ($f_o^2 \times 10^{-6}$) = 21.88 (D^2) ((1/L)+(1/V)). Since D remained at 0.45 cm throughout the group of tests, D^2 = 0.202 can be inserted, giving an equation of ($f_o^2 \times 10^{-6}$) = 4.42 ((1/L)+(1/V)). The predicted values from this equation are still consistently above the observed values of $F_o^2 \times 10^{-6}$, although by less than before. The discrepancy results from different slopes.

The experimental lines shown in Figure 20 are "eyeball" lines drawn through the data points. For each value of L, the line can be represented by the form $F_o^2 \times 10^{-6} = K_L$ (1/V). The values of the parameter K_L are given below.

L	K_L	$a = K_L \cdot L/4.42$
1.27	2.50	0.718
2.54	1.29	0.741
3.81	0.85	0.733
	Average value of a =	0.731

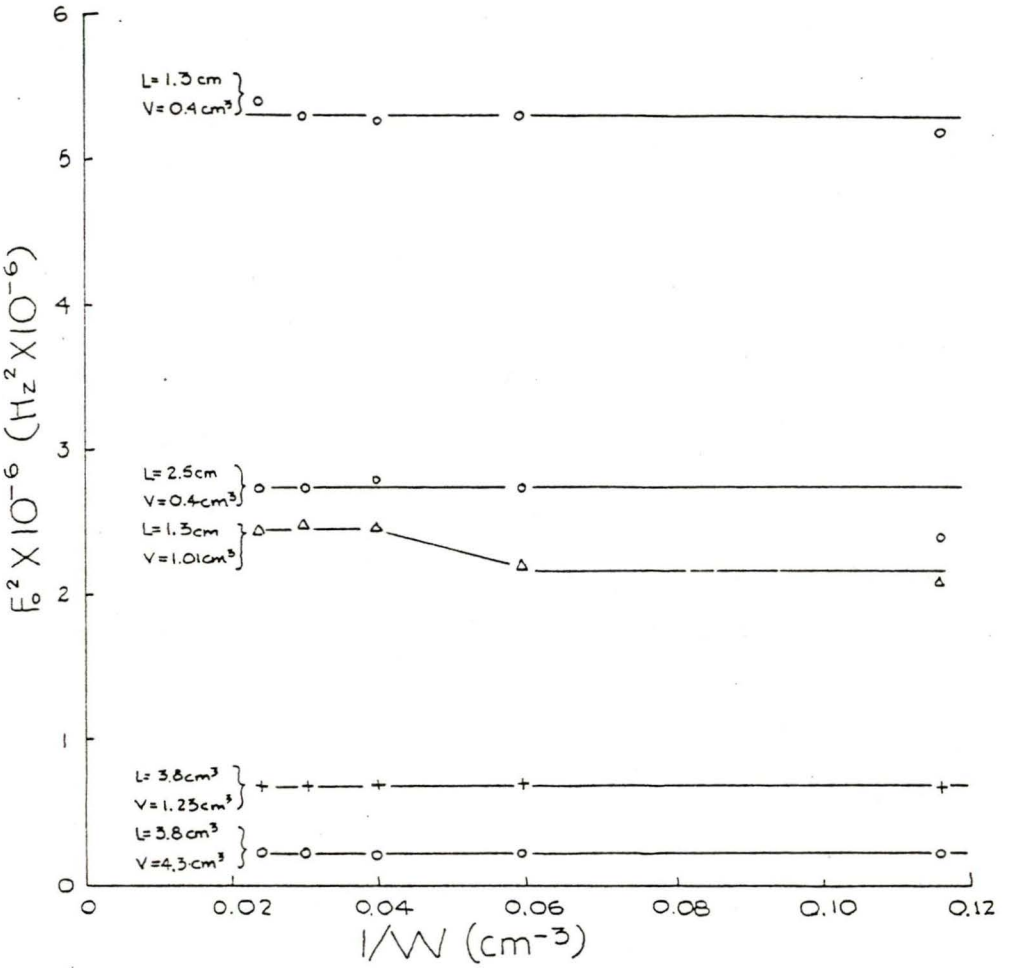

FIGURE 19. LINEAR EVALUATION OF F_o AND W AS ($F_o^2 \times 10^{-6}$) AND (1/W).

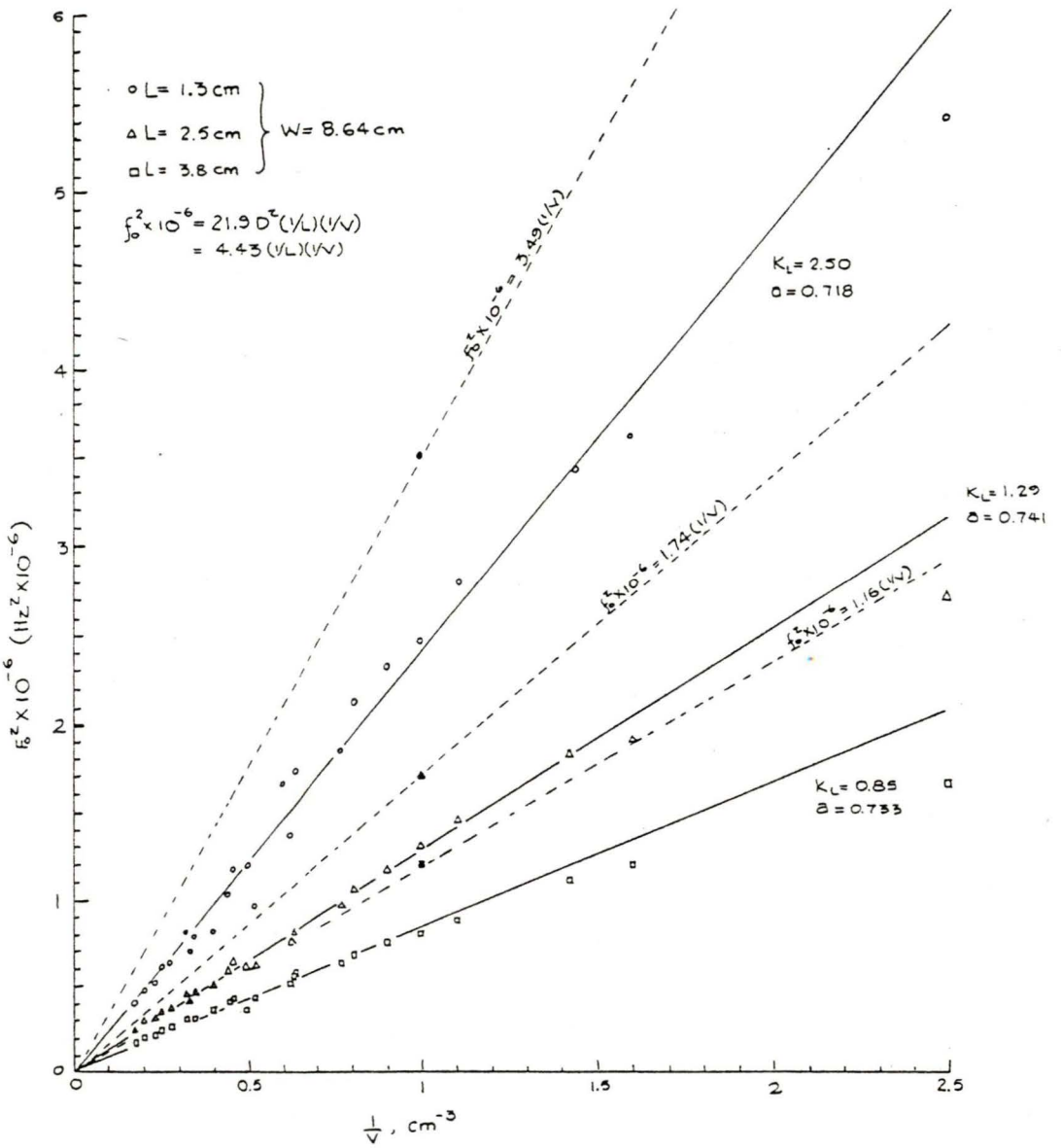

FIGURE 20. LINEAR EVALUATION OF F_O AND V FOR CONSTANT PARAMETER a.

The value of the derived parameter $a = K_L \cdot L/4.42$ was obtained by comparing the theoretical curve $(f_o^2 \times 10^{-6}) = 4.42\,((1/L)+(1/V))$ with each of the experimental curves $(F_o^2 \times 10^{-6}) = K_L\,(1/V)$. The results suggest that the theoretical equation for resonant frequency can be adjusted to the experimentally obtained values by a simple factor a. The new equation is shown below.

$$f_o = \frac{c}{2\pi}\sqrt{\frac{aA}{LV}}.$$

Here a is empirically determined to be about 0.73 for the case when D + 0.45 cm and L varies between 1.27 and 3.81 cm.

There were a total of 6 x 60 = 360 measurements of resonant frequency in these tests. These data were reduced on a Hewlett-Packard calculator, Model 9825A. For each measurement, a value of $a = F_o^2\,(16\pi VL)/(c^2D^2)$ was calculated. The average of these values is shown below.

$$a = 0.73 \pm 0.02 = \sum_{i=1}^{360} \frac{ai}{360} \pm \sqrt{\sum_{i=1}^{360} \frac{(a-ai)^2}{360}}$$

There is, however, no basis in theory for such a "correction factor". A number of authors have proposed a correction to the Helmholtz equations in the form of a "mass end correction" $\delta = (16/3\pi)r$, where r is the radius of the neck opening into the cavity V. The rationale behind the mass end correction is that the movement of air in the regions near the opening of the neck into V suggests that the "effective" neck length is actually $L + \delta$. According to that hypothesis, $f_o = (c/2\pi)\sqrt{A/V(L+\delta)}$.

If this were the case, we would expect that $(F_o^2 \times 10^{-6}) =$ a $4.43\,(1/V)\,(1/L) = 4.43\,(1/V)\,(1/L+\delta)$. Either δ varies with L and a is fixed, or a varies with L and δ is fixed. The data indicate that a is fixed, at least over the range of L values tested. There was no way of making these data correspond to the "mass end correction" hypothesis.

A concept very similar to the "mass end correction" can be formulated in terms of b = l/a. We then have the expression given below for the resonant frequency.

$$f_o = \frac{c}{2\pi}\sqrt{\frac{A}{V(bL)}}.$$

Here bL is the "effective" neck length and, therefore, $b \geq 1$. For these experiments b = 1.38.

These experiments do not indicate whether the factor b (or a) varies with neck diameter, since a constant neck diameter of 0.45 cm was used throughout the experiments. It may be that further experiments in which neck diameter is varied would enable a simple formula for b to be empirically derived.

A fourth way of analyzing the discrepancy between the classical Helmholtz equation and the experimental results is in terms of "acoustical resistance". Morse and Ingard* point out that acoustical resistance becomes a factor when considering sound of frequency more than a few KHz in a tube of less than 1 cm^2 cross-sectional area. In these experiments the neck of the resonator is a tube 1.27-3.81 cm long with cross-sectional area A = 0.16 cm^2.

This concept is most easily examined by an RLC-electrical circuit analog. The classical Helmholtz formula for resonant frequency may be derived by considering a Helmholtz resonator as the physical analog of an LC-circuit, with inductance and capacitance in parallel.

ELECTRICAL CIRCUIT	HELMHOLTZ RESONATOR
C = capacitance	capacitance analog = $V/c^2\rho$**
L = inductance	inductance analog = $\rho L/A$
$f_o = \frac{1}{2\pi}\sqrt{\frac{1}{LC}}$	$f_o = \frac{c}{2\pi}\sqrt{\frac{A}{VL}}$

---

* Morse, P.M. and Ingard, K.U. (1968) Theoretical Acoustics. McGraw-Hill Book Company, New York.

** ρ = gas density.

In this derivation, both electrical resistance and acoustical resistance are ignored. If it is assumed that the inductor in the LC-circuit has also a resistance component R, which we may take to be in series, the "natural frequency" of the circuit is expressed by the formula below.*

$$f_n = \frac{1}{2\pi} \sqrt{\frac{1}{LC} - \frac{R^2}{L^2}}.$$

We might assume that there is an equivalent expression for the Helmholtz resonator. If we let r stand for the acoustical resistance, we get the equation below.

$$f_n = \frac{1}{2\pi} \sqrt{\frac{Ac^2}{VL} - \frac{r^2A^2}{\rho^2L^2}}$$

where r = function (A, ρ, V, L,...).

There are a variety of expressions for r, each derived for a special geometry and circumstance. A number of these expressions were examined and it was found that none fit the values required by the experimental data.

We can, however, write r in terms of the empirical constant a. Assume

$$f_n = F_o = \frac{1}{2\pi} \sqrt{\frac{Ac^2}{VL} - r^2 \left(\frac{A}{\rho L}\right)^2} = \frac{1}{2\pi} \sqrt{\frac{aAc^2}{LV}}.$$

Then we can derive the two expressions

$$a = 1 - r^2 \frac{VA}{Lc^2\rho^2} \quad \text{and} \quad r = c\rho \sqrt{\frac{L(1-a)}{VA}}.$$

---

* Fink, D.G. (1975) Electronics Engineers' Handbook, McGraw-Hill Book Company, New York.

This analysis cannot be carried further in the absence of information about how a might vary with neck diameter D (or cross-sectional area A). It suggests, however, that a theoretically satisfying expression might be derived which would fit the data obtained in the experiments described.

Dimensionally b (and, therefore, a) must be identical, since $f_o = (c/2\pi)\sqrt{A/V(bL)}$ yields $t^{-1}=lt^{-1}(l^2l^{-3}(b^{-1}l^{-1}))^{\frac{1}{2}}=t^{-1}b^{-1/2}$. This indicates r must have dimension $ml^{-4}t^{-1}$ since $r = c\rho\sqrt{L(1-a)/VA}$ yields $lt^{-1}ml^{-3}(ll^{-3}l^{-2})^{\frac{1}{2}}=ml^{-4}t^{-1}$. The dimensional elements of the analog are given below.

ELECTRICAL	ACOUSTICAL
R: $\mu l t^{-1}$	r: $ml^{-4}t^{-1}$
L: μl	$\rho L/A$: ml^{-4}
C: $\mu^{-1}l^{-1}t^2$	$V/C^2\rho$: $m^{-1}l^4t^2$
f: t^{-1}	f: t^{-1}

For the purposes of design, let us specify a neck diameter of 0.45 cm and use the expressions below.

$$f_o = \frac{c}{2\pi}\sqrt{\frac{A}{V(bL)}} = 5.28 \times 10^3 \sqrt{0.115/VL}$$

$$VL = 3.21 \times 10^6/f_o^2$$

Here V is in cm^3 and L is in cm.

The experimental procedure also provided a measure of P_m = max P. The values of P_m varied between about 0.15 psi and 0.5 psi for the speaker driven Helmholtz resonator. The complex character of the relationship between P_m and f_o, V, W and L is illustrated in Figure 21. Here eight different EXPERIMENTS are shown in which V, W and L differ.

Possible P_m varies in some sinusoidal fashion (see TESTS 4, 7, 15 and 23 in Figure 21) with f_o or V. Comparing some EXPERIMENTS, it appeared that P_m increased with W. It

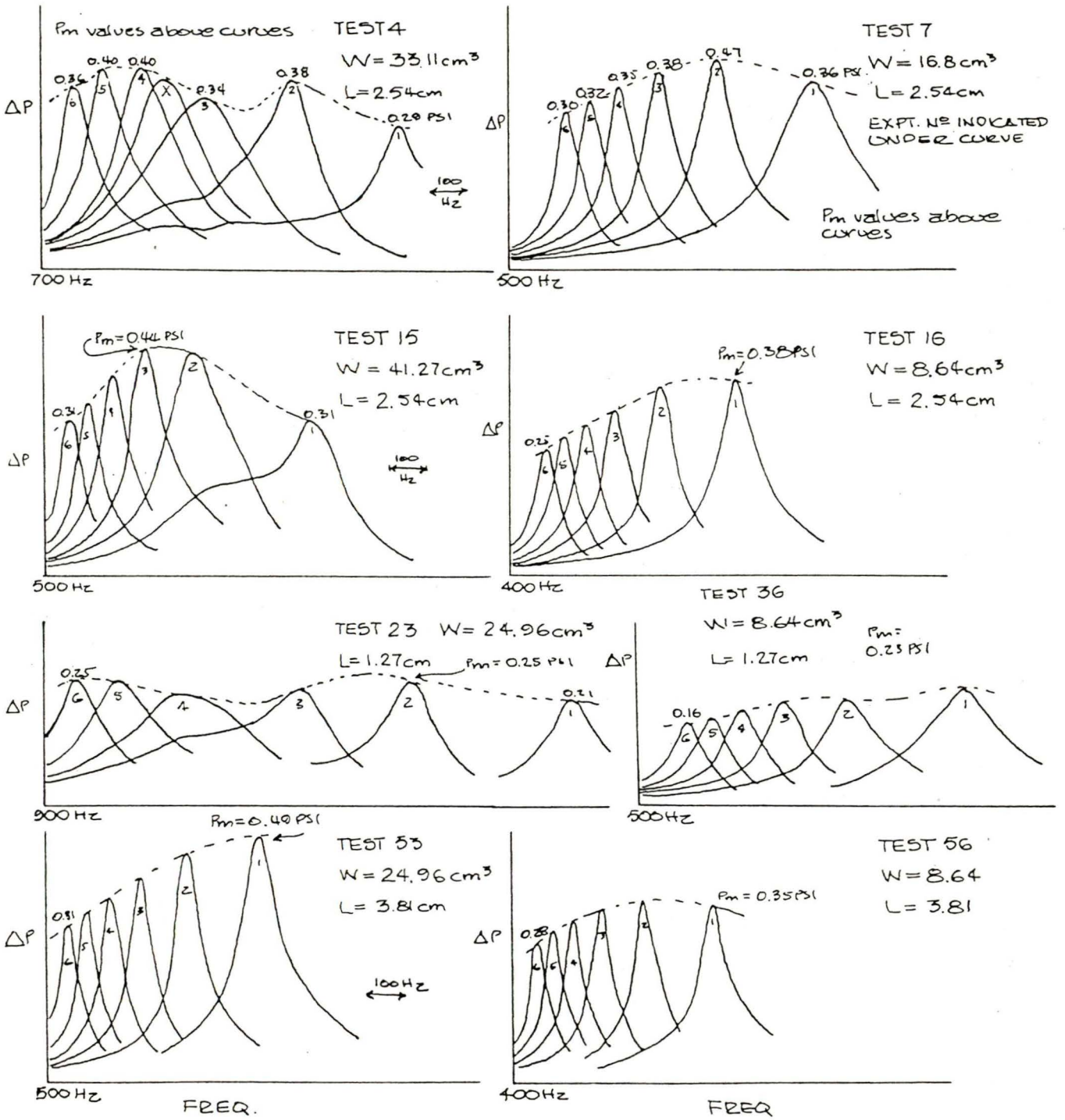

FIGURE 21. PRESSURE EXCURSION VERSUS FREQUENCY FOR SOME EXPERIMENTS.

must be noted, however, that any speaker has its own resonant frequency f_s, at which it delivers its maximum power output. At other frequencies its output is less, sometimes considerably less, than at f_s.

There was, however, one relatively clear trend: P_m increased with neck length L. This may be seen in Figure 22, where P_m versus f_o is shown for every EXPERIMENT. The lines drawn through the clusters of data are not "fitted", but the general increase in P_m with L is evident. The reason for this increase is not clear, since the empirically derived expression for the acoustical resistance r indicates that r increases with the square root of the neck length. One might think that an increasing acoustical resistance would decrease the pressure excursion within the resonator.

The graphically determined values of Q and P_m were compared, but no relationship was observed. Because of the geometrical complexity of the system, Q was not further investigated.

These experiments suggested that the design of a Helmholtz resonator was rational and predictable on the basis of empirically derived equations. In the experimental reports which follow, various piezoceramic acoustical transducers were used to excite the double-chamber Helmholtz resonator. This investigation was part of the program detailed in the discussion on page 20.

The experimental design is shown in Figure 23. Either ceramic audio tone transducers (CATT) from Gulton Industries, Inc. or Linden Laboratories, Inc., Piezoceramic Benders were used to excite the double Helmholtz resonator.

Figure 24 shows the first attempt to excite the resonator with a piezoelectric device. Two very clear resonance peaks were observed. One, as predicted, was the resonance frequency of the Helmholtz resonator. The other was the natural vibration frequency, fp, of the piezoceramic transducer.

It was assumed that the maximum ΔP would occur when Fp = Fo, that is, when the natural frequency of the piezoceramic transducer equaled the resonant frequency of the Helmholtz resonator. Figures 25 and 26 (TESTS 65 and 66) show that this is, indeed, the case. Experiment 6, TEST 65, shows that:

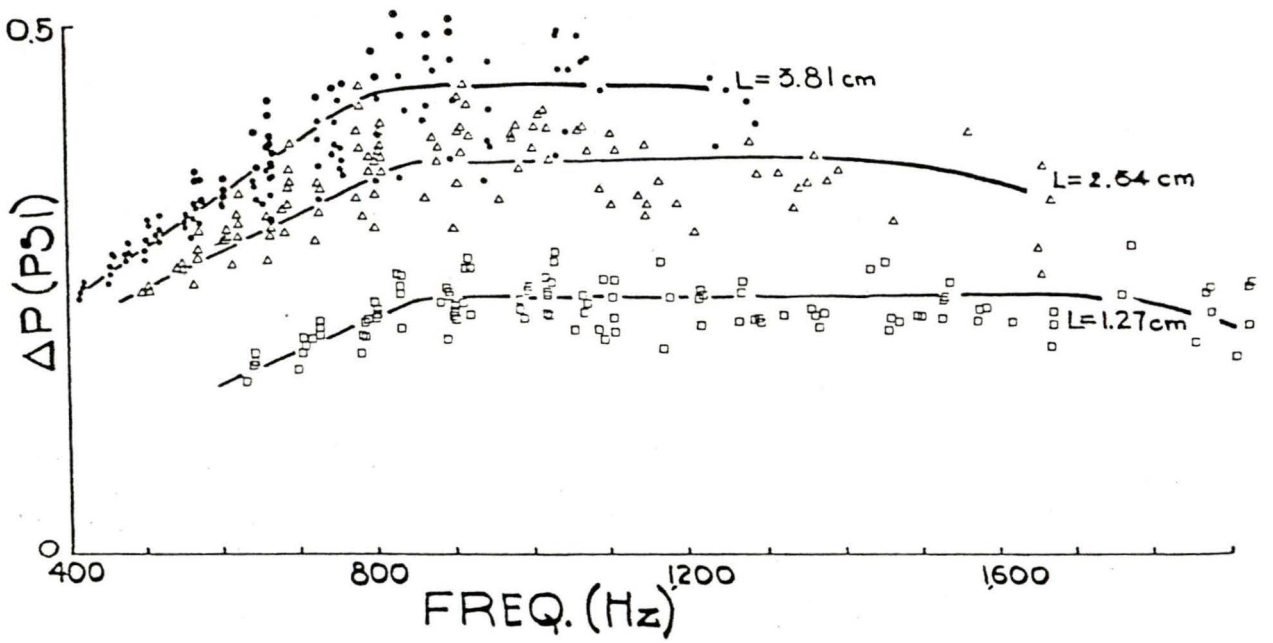

FIGURE 22. P_m VERSUS F_o FOR EVERY EXPERIMENT.

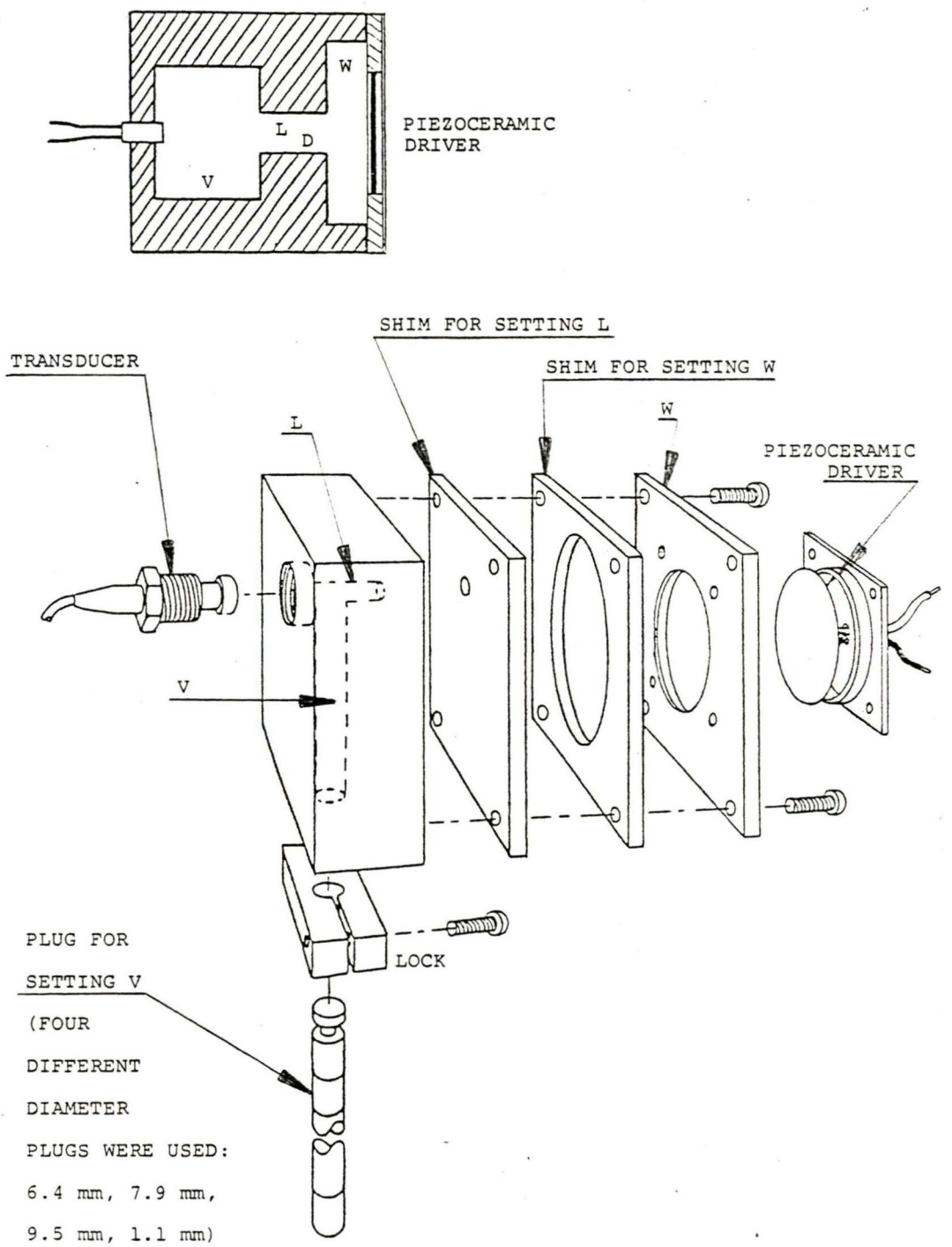

FIGURE 23. DOUBLE-CHAMBER RESONATOR DESIGNED FOR TESTING THE RELATIONSHIP BETWEEN F_o AND THE RESONATOR GEOMETRY.

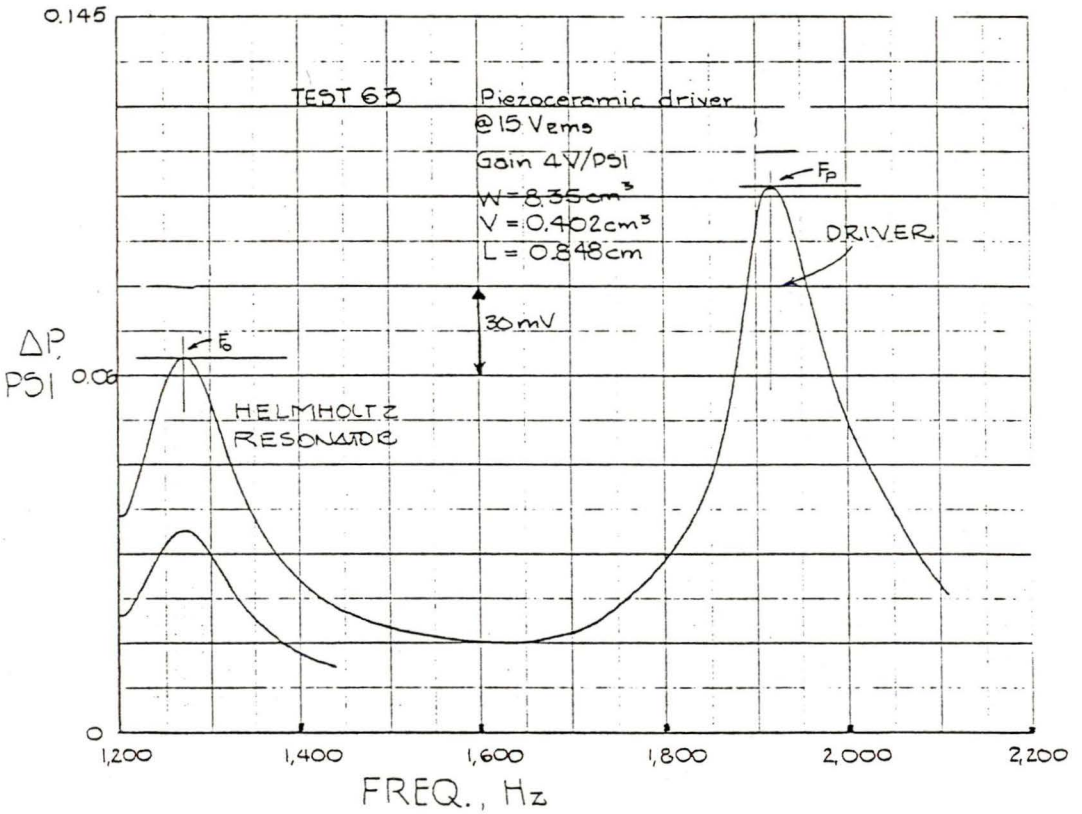

FIGURE 24. A RESONATOR EXCITED BY A PIEZOCERAMIC DRIVER.

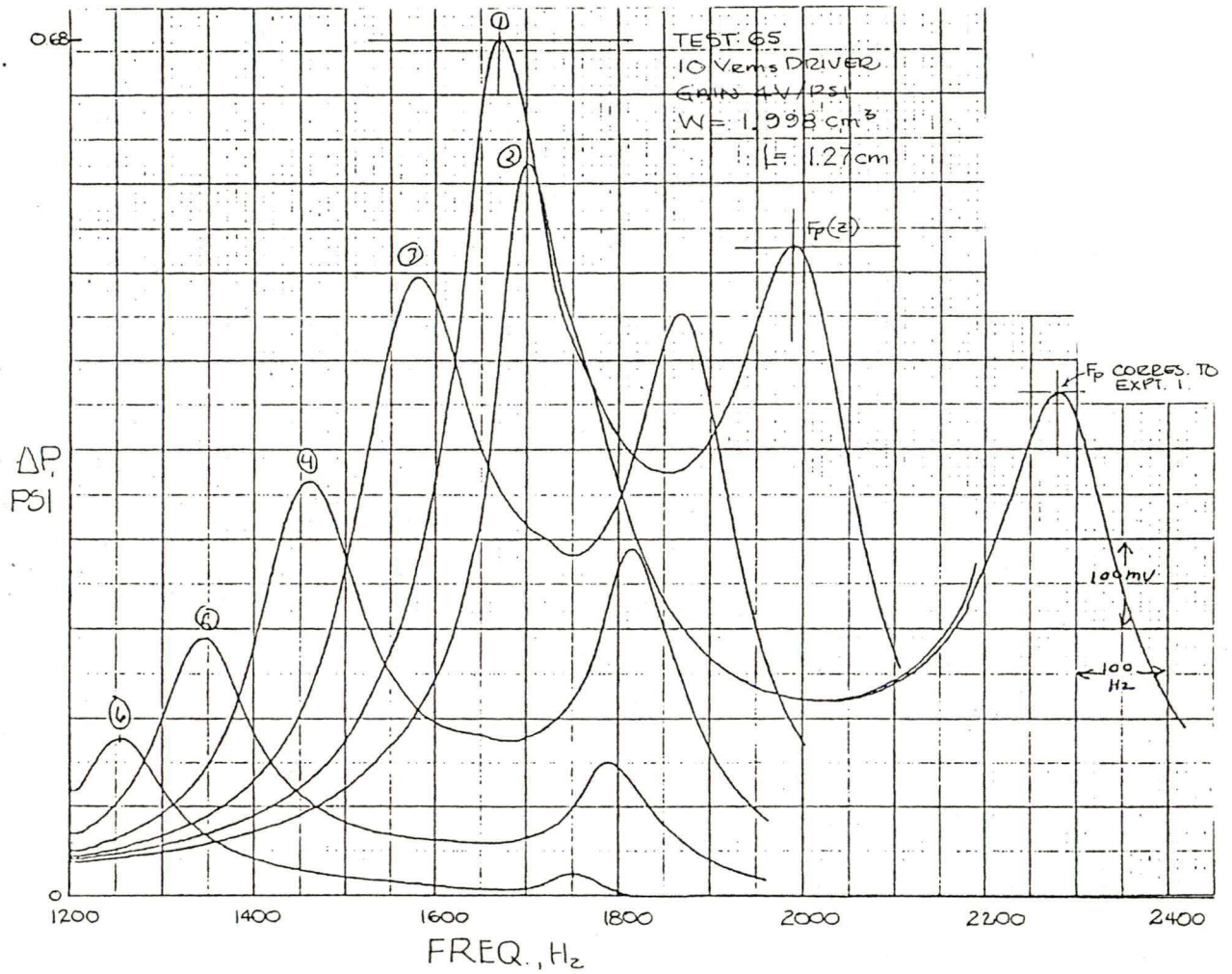

FIGURE 25. CHANGING THE RESONATOR GEOMETRY TO MATCH THE RESONANT FREQUENCY OF THE PIEZOCERAMIC DRIVER.

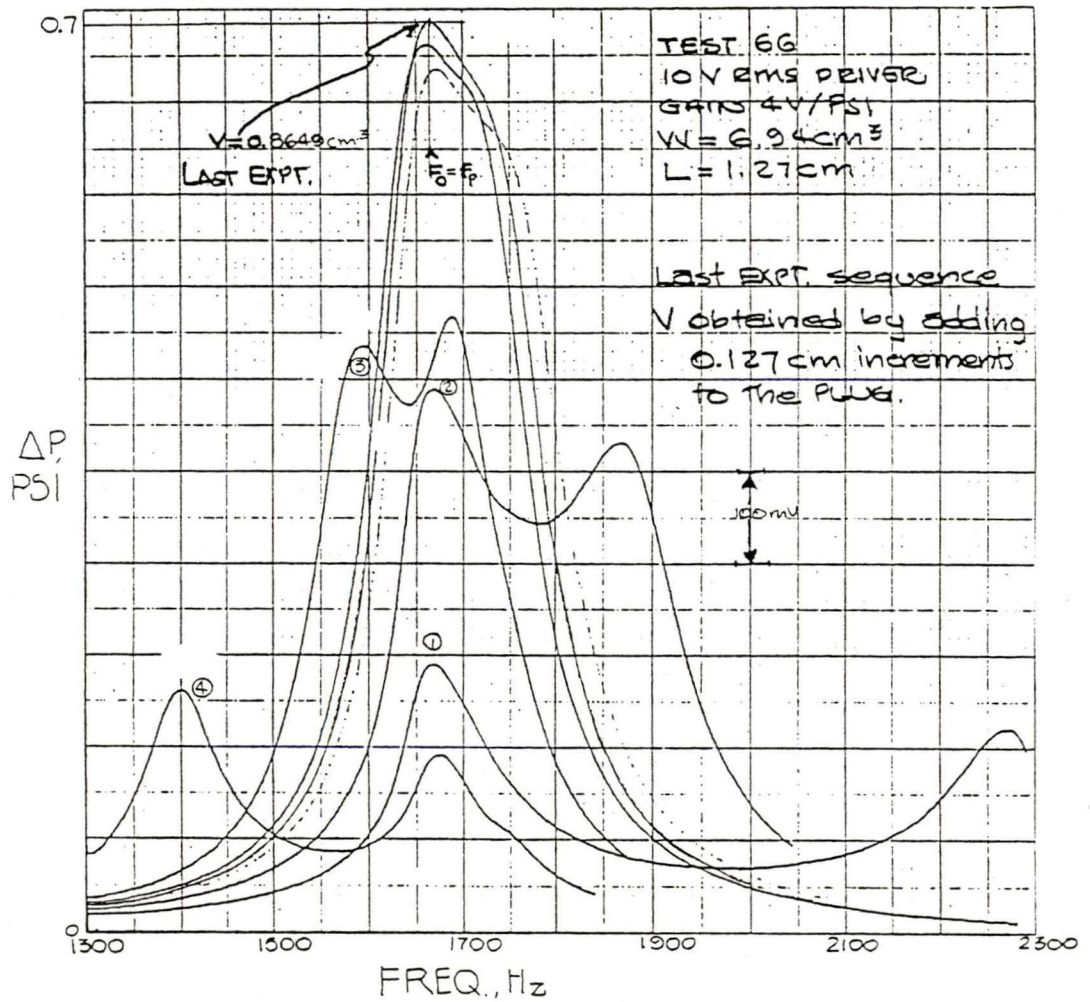

FIGURE 26. CLOSER MATCHING OF F_o AND F_p OBTAINED BY ADJUSTING V.

W = 1.998 cm^3 V = 1.911 cm^3 L = 1.27 cm D = 0.4496 cm

Fo = 1255 Hz Fp = 1751 Hz Diff. Fo-fp/fp = 39.5%

Pm = 0.1254 Pm = 0.0171

In Experiment 1, where V = 0.402 cm^3:

Fo = 1660 Hz Fp = 1990 Hz Diff. Fo-fp/fp = 19.88%

Pm = 0.68 psi Pm = 0.52 psi

Finally, in the last EXPERIMENT of TEST No. 66:

V = 0.8649 cm^3 W = 6.94 cm^3

Fo = Fp = 1675 Hz and Pm = 0.70 psi.

Two immediate conclusions may be drawn from these data:

- As Fo approaches Fp [(FO-Fp)/Fp = 0] there is a dramatic rise in the peak-to-peak pressure excursion $\Delta P \rightarrow$ max ΔP = Pm.
- Although the actual resonant frequency of the piezo-ceramic device may be only a function of its construction, when mounted in the Helmholtz resonator the coupled frequency F_p is also a function of resonator geometry.

An even more obvious example of these two conclusions is shown in Figure 27. For V = 0.704 the twin-peaked frequency curve shows (Fo = 1680 Hz, ΔP = 0.31 psi) and (Fp-1837 Hz, ΔP = 0.30 psi). For V = 1.005 cm^3 (Fo = 1583, ΔP = 0.31 psi) and (Fp = 1673 Hz, ΔP = 0.35 psi). When V was adjusted to 0.825 cm^3 Fo = Fp = 1695 and Pm = 0.63 psi. This is an increase in average peak-to-peak pressure of almost two fold (1.97 times).

Figure 28 shows the effect of changing volume by increments of 0.040 cm^3. Maximum ΔP is achieved at 0.704 cm^3 + 3 x 0.04 cm^3 = 0.824 cm^3, where Fo = Fp = 1680 Hz. Here Pm = 0.68 psi. A change in volume by 0.04 cm^3 in either direction shifts the frequency Fo by about $\pm$ 20 Hz, broadens the curve (a reduction in Q) and reduces the value of P by as much as -0.064 psi (about 9.4%).

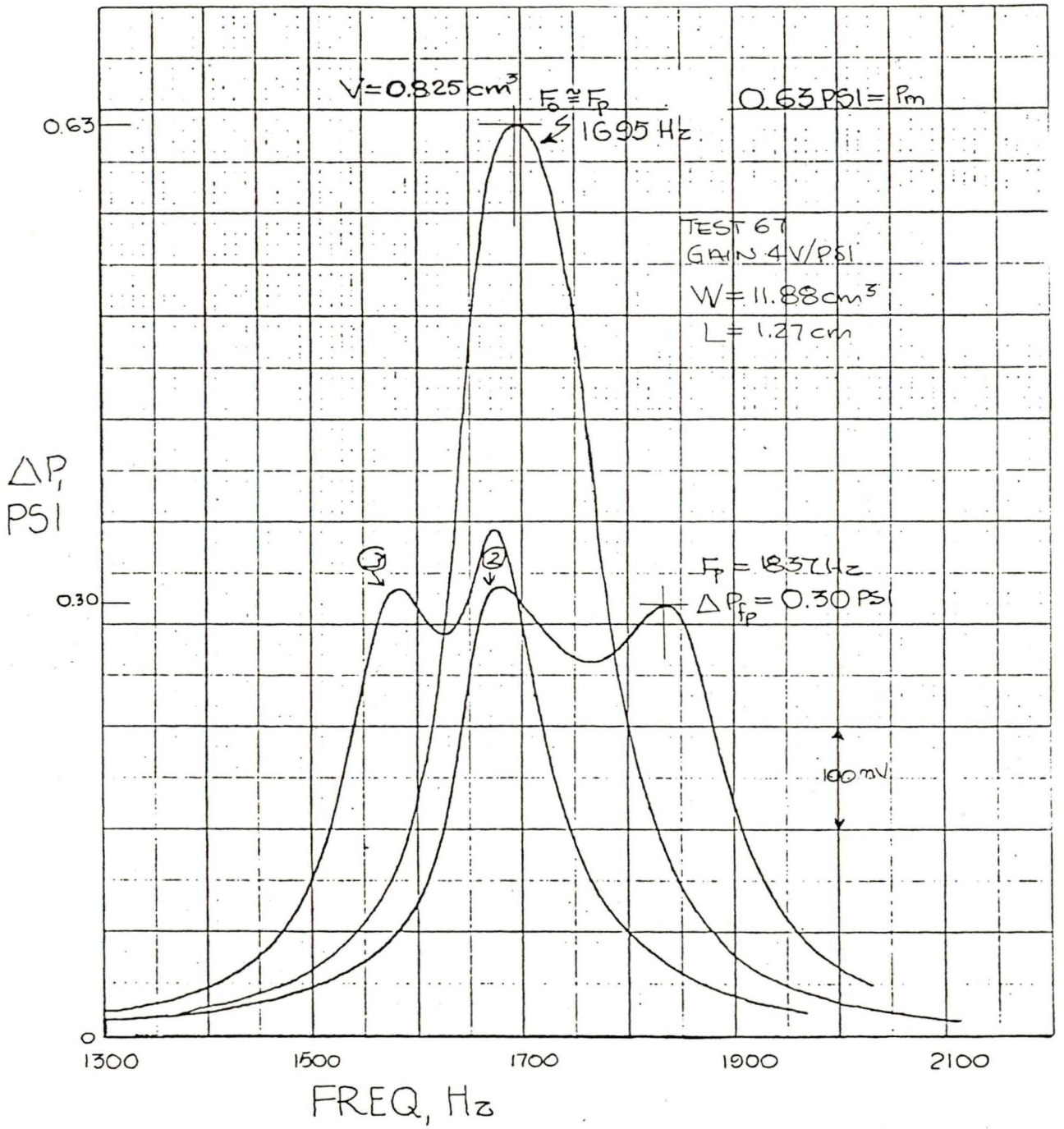

FIGURE 27. F_o, F_p AND P_m FOR CHANGING VALUES OF V.

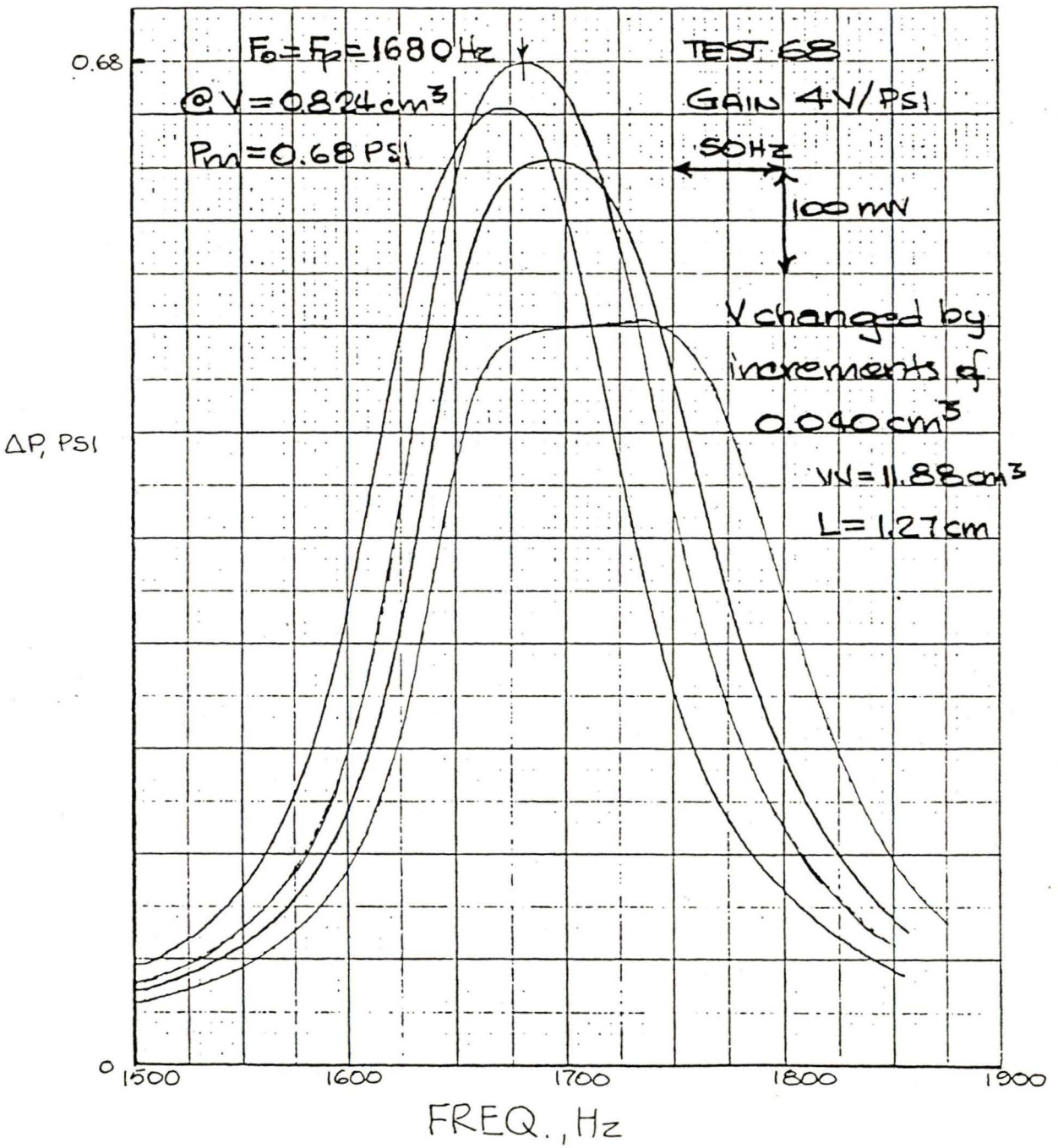

FIGURE 28. F_o, F_p AND P_m FOR SMALL INCREMENTAL CHANGES IN VOLUME V.

Another way of looking at these data is to observe that for frequency values in the neighborhood of Fo = Fp, a change in either Fo or Fp of only 1% results in a reduction of ΔP by as much as $9^{+}\%$. The significance of this 1:10 relationship between pressure excursion and resonant frequency will become more apparent as attempts to stabilize Fp are discussed.

Over a span of minutes, the system consisting of piezoceramic driver and Helmholtz resonator appeared to be relatively stable. Figure 29 shows the results of repeated experiments, 3-minutes apart. The total time span was 45 minutes.

Changing piezoceramic drivers, however, appeared to have a dramatic effect. In Figure 30 are shown the results of replacing the piezoceramic driver of previous tests with three "identical" piezoceramic drivers of the same stock. Two gave similar results, although clearly Fp shifted slightly. For the third, Fp was considerably lower and resulted in $Fp << Fo$, with a significant reduction in ΔP.

A considerable part of this variation appeared to be in the mounting of the piezoceramic driver. This is best demonstrated in Figure 31. The piezoceramic driver was rotated through 360°. Clearly orientation had a great deal to do with the Fp value.

That this is a matter of mounting is shown in Figure 32. Highly localized heating and cooling of one screw on the piezoceramic driver indicated that the mounting geometry of the piezoceramic driver was critical. Here we see a spectrum of resonance curves made while first continuously heating one mounting screw, then cooling the same mounting screw. Such temperature changes make minute changes in the tightness of the mount.

The highly localized nature of the effect implied that the mounting screw "tightness" was a critical factor and posed a very serious design problem.

Some further effort was made to study various piezoelectric driver mounts, but the results were discouragingly in line with those described above. The problem appeared to be a function of two critical design limitations.

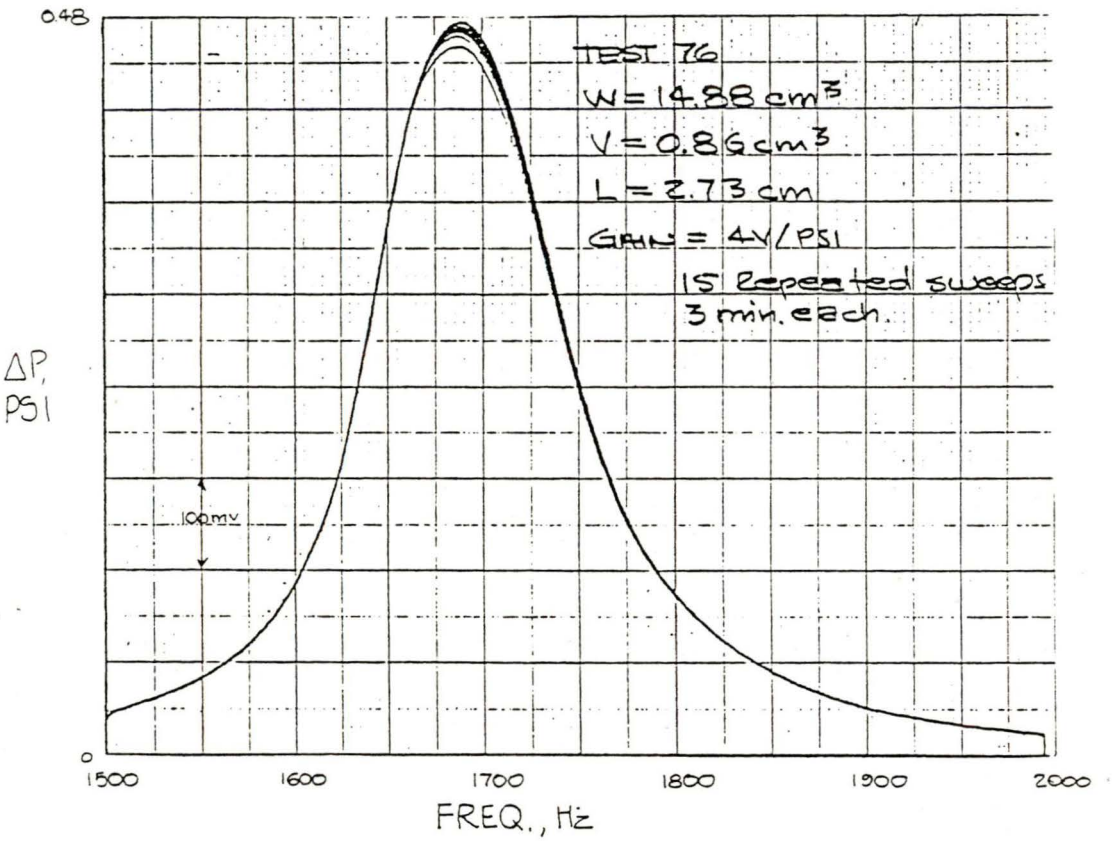

FIGURE 29. RESONANCE FREQUENCY STABILITY WITH TIME IN A PIEZOCERAMIC-DRIVEN HELMHOLTZ RESONATOR.

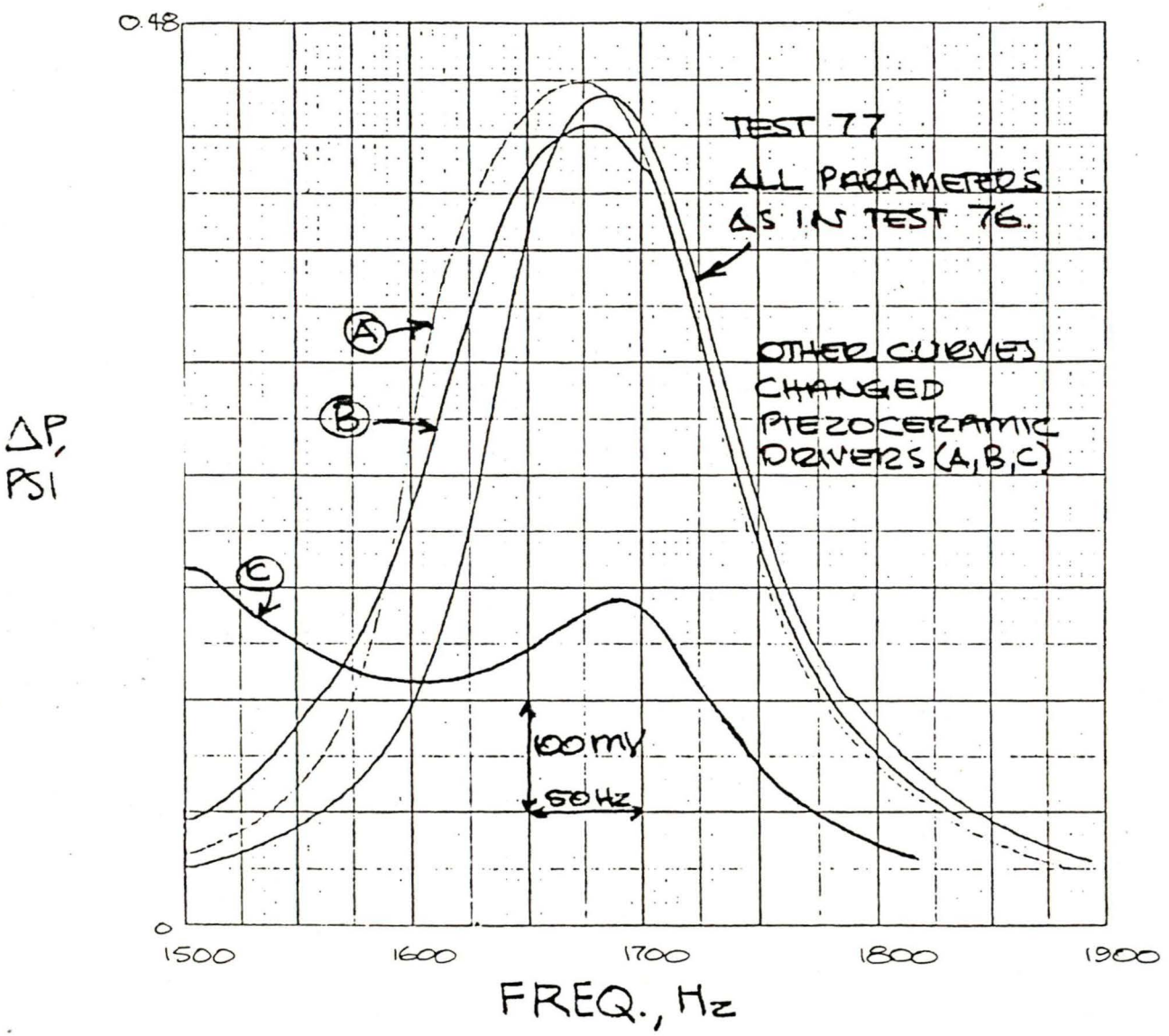

FIGURE 30. CHANGING PIEZOCERAMIC DRIVERS.

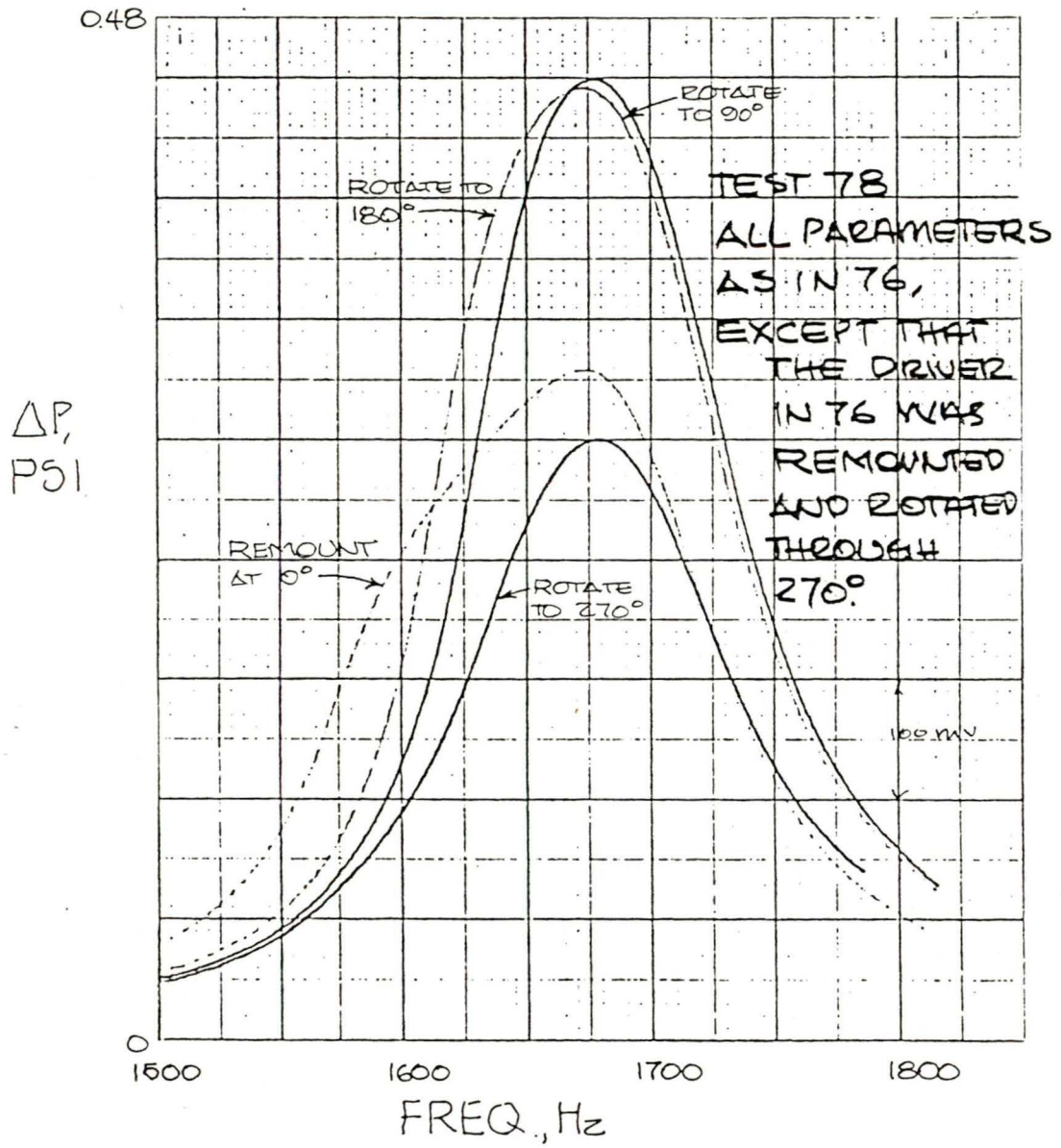

FIGURE 31. CHANGE IN F_o WHEN ROTATING ONE PIEZOCERAMIC DRIVER THROUGH 270°.

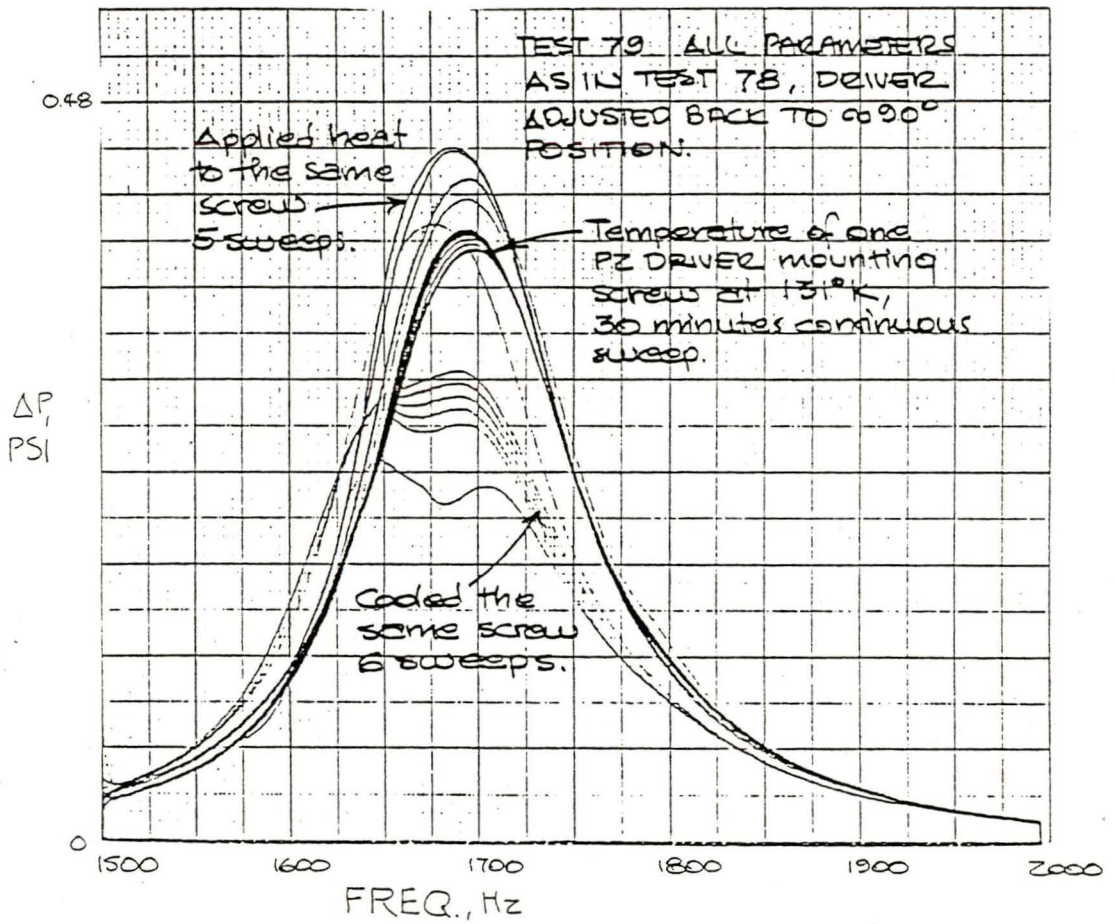

FIGURE 32. THE EFFECT OF HEATING AND COOLING ONE MOUNTING SCREW ON THE PIEZOCERAMIC DRIVER.

- One percent variations in the matching of Fo and Fp resulted in almost ten percent variations in the peak-to-peak pressure excursion within the resonance chamber. This means that both Fo and Fp have to be highly predictable and very stable if a practical instrument is to be designed.

- There appeared to be considerable variation among piezoceramic drivers and an even more serious variation with mounting. Further, the frequency Fp was clearly affected by the geometry of the system and in a manner too complicated to be elucidated by less than a detailed study. These findings imply that meeting the requirement of the first design limitation, producing a predictable and stable piezoceramic driver, is unlikely without extensive study. With the present state of knowledge, each Helmholtz-resonator SAMPLE CELL would have to be specifically adjusted for Fo to match Fp and subsequent variations in mounting and ambient temperature might seriously change this matching.

EVALUATION OF THE HELMHOLTZ RESONATOR SAMPLE CELL CONCEPT

The finding detailed in the previous section of this report brought about a re-evaluation of the project procedures and goals.

It had been initially assumed that the major developmental problem with the Helmholtz resonator SAMPLE CELL concept would be to identify the geometrical relationships necessary to design the working SAMPLE CELL. As it turned out, these relationships were identified with relative ease and the problem of designing a Helmholtz resonator SAMPLE CELL was, in effect, solved.

A new and design-limiting problem was identified during this developmental research: The critical mounting and geometry of the piezoceramic driver. Although it was clear that this was a practical design problem rather than a theoretical limitation on the concept, it was also clear that a substantial developmental research program might be necessary before this problem could be solved.

Two courses were open for continuation of the project.

- Continue this line of research, taking the chance that funds and time would be adequate to perfect the Helmholtz resonator SAMPLE CELL into a reliable and cost-efficient working device.

- Abandon development of the Helmholtz resonator SAMPLE CELL for this project and concentrate on development of the simpler and partially tested pump-modulated SAMPLE CELL.

The second course was adopted after re-examination of the existing pump-modulated SAMPLE CELL prototypes. A pump-modulated SAMPLE CELL was designed, based on the prototype, and a contract modification was requested to facilitate development of the pump-modulated system.

DESIGNING THE PUMP-MODULATED DETECTOR

The design of the miniature CO_2 and CH_4 DETECTORS was a logical continuation of the concepts developed under Contract No. H0230050.* The primary developmental effort in the present project, once it was decided to produce the pump-modulated DETECTOR design, was directed toward miniaturization and production feasibility. The most important difference between the miniature CO_2/CH_4 DETECTOR and the prototype developed in Contract No. H0230050 was the pump-modulated SAMPLE CELL. The choice of pump-modulation posed a number of design problems.

THE PUMP-MODULATED SAMPLE CELL

The pump-modulated SAMPLE CELL consists of six components.

- THE CELL
- THE PUMP MECHANISM
- THE SOURCE
- THE PRESSURE TRANSDUCER
- THE FILTER
- THE DETECTOR

These components are shown in Figure 33, an exploded view of the SAMPLE CELL.

---

* A "Portable Compact Low-cost NO_2, CO and CH_4 Gas Analyzer for In-mine Personnel Safety Monitoring". Final Report on Contract No. H0230050. July 1977. Andros Incorporated, Berkeley, California.

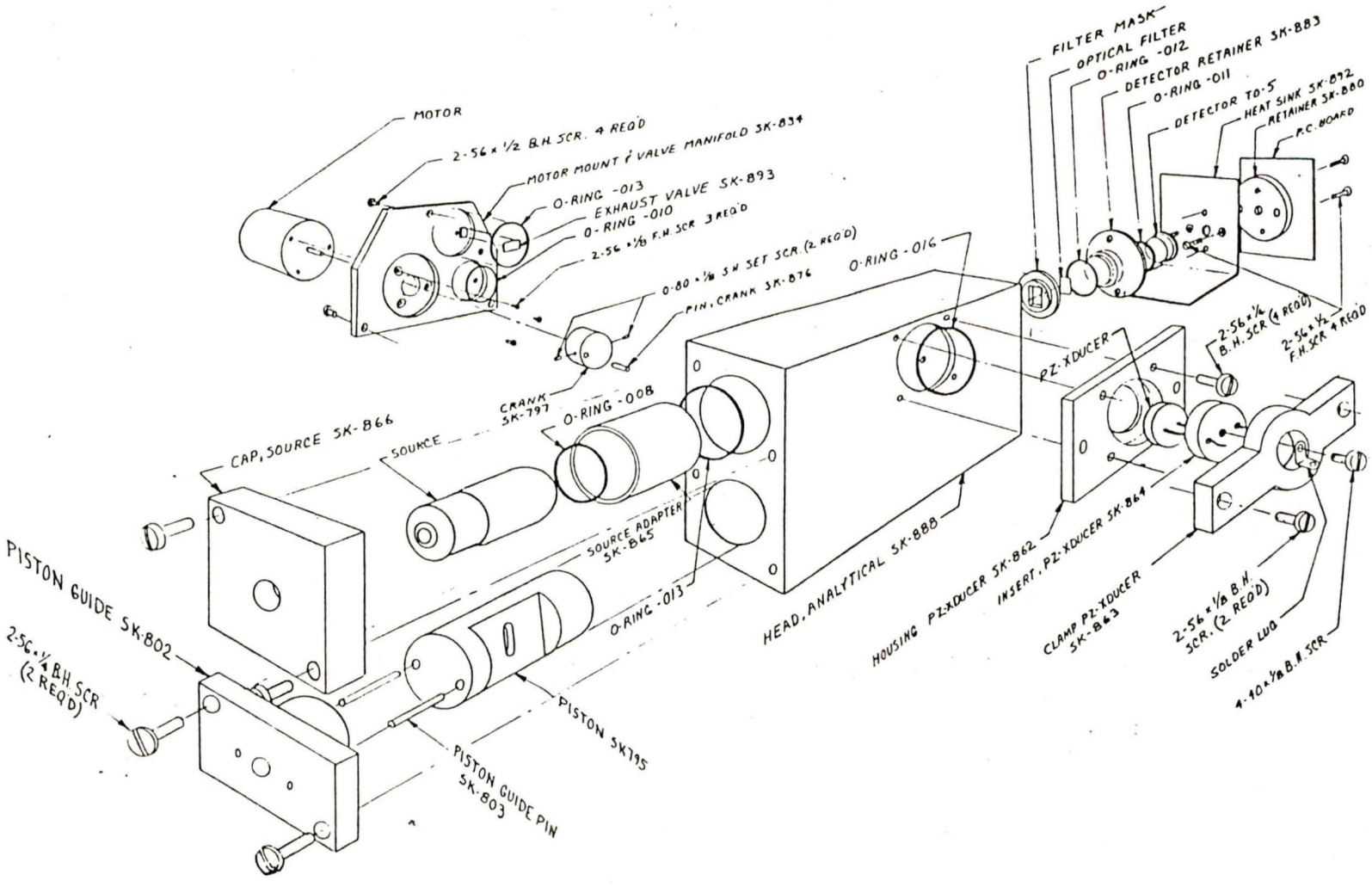

FIGURE 33. VIEW OF THE SAMPLE-CELL ASSEMBLY.

• THE CELL AND PUMP MECHANISM

It was initially decided to manufacture the PUMP and SAMPLE CELL as an integral unit machined from a single plastic "block". The material chosen was the General Electric polycarbonate "Lexan", a tough and easily machined material. It was felt that an integral unit would be more compact, lend structural integrity to the DETECTOR and be less costly. With a view toward future production, the use of plastic suggested the possibility of injection molding the CELL "block".

The SAMPLE CELL dimensions were determined as a balance between the requirement for miniaturization and an effort to maximize the signal-to-noise ratio of the system. The critical dimensions of the integral SAMPLE CELL/PUMP were L_p, the CELL light path and V_s, the piston-stroke volume of the modulating PUMP.

The relationship between SAMPLE CELL dimensions and signal-to-noise ratio is illustrated by observing that the peak-to-peak voltage of the f_1 signal varies according to the *change in the number of absorbing gas molecules in the light path as the CELL pressure varies over ΔP.* For any given light-absorbing gas concentration, the greater change in number of gas molecules in the light path, the greater the signal amplitude (V_{f1} = (constant) ΔPa [C], where [C] = absorbing-gas concentration and a = absorption strength of the sample gas within the filter pass band).

Rather than reexamine this problem for the miniature DETECTORS, we used the experience in designing the prototype* developed in Contract No. H0230050. The prototype gave less than 1% p-p noise when measuring 0.8% CO_2. The gas law enabled us to derive new dimensions with similar minimum parameters.

---

* Pages 94-98, "A Portable Compact Low-cost NO_2, CO and CH_4 Gas Analyzer for In-mine Personnel Safety Monitoring". Final Report on Contract No. H0230050. July 1977. Andros Incorporated, Berkeley, California.

In this analysis we will ignore the difference between the DETECTOR area and the CELL cross-section area and simply assume that all rays of light from the SOURCE traverse the cell and land on the DETECTOR. This fiction is useful only for the purposes of comparison.

The gas law states PV = nRT for a perfect gas. Here R = 1206, the gas constant for a system with length in cm and pressure in psi, T = 293° Absolute (about 68° F) and n = M/N, where N = Avogadro's number and M = the number of gas molecules in the volume V at pressure P. For a SAMPLE CELL, $M = NPV/RT = (6.02 \times 10^{23})\ PV/(1206)\ (293) = (1.70 \times 10^{18})$ PV molecules.

Assume the pressure excursion ΔP is a positive pressure increase above the atmospheric pressure of 14.7 psi. At atmospheric pressure, let M_o be the number of gas molecules in the CELL. At $P + \Delta P$, let M_1 be the number of gas molecules in the CELL. If the CELL diameter is D and the length of the cylindrical light path in the CELL is L_p, we can write an expression for the *change* in the number of gas molecules $\Delta M = M_1 - M_o$.

$$\Delta M = (1.7 \times 10^{18})(P + \Delta P - P)\pi D^2 L_p/4 = (1.34 \times 10^{18})\ \Delta P D^2 L_p.$$

The change in the number of gas molecules per unit length of light path, written $\Delta M/L_p = (1.34 \times 10^{18})\ \Delta P D^2$, is a good measure of the potential signal level (depending on the concentration of absorbing gas) in the DETECTOR. Increasing any of the parameters that increase this change will improve the signal-to-noise level.

The SAMPLE CELL in the prototype developed under Contract No. H0230050 had dimensions $L_p = 5.08$ cm and D = 1.27 cm. The normal pressure excursion used was $\Delta P = 0.25$ psi. This gives a value of $\Delta M/L_p = 0.540 \times 10^{18}$ molecules per cm (and a total change of 2.74×10^{18} molecules along the light path). We may take this value of $\Delta M/L_p$ as a *lower limit* for the design of the miniature CO_2/CH_4 DETECTOR. In the miniature system the dimensions of the SAMPLE CELL must be such that along the light path $\Delta M/L_p > 0.54 \times 10^{18}$ molecules per cm.

Applying the gas law to the miniature CO_2/CH_4 DETECTOR CELL gives $\Delta M = (1.34 \times 10^{18})\ \Delta P D^2 L_p = 2.74 \times 10^{18}$ molecules (to meet the above requirement). This reduces to $2.045 = \Delta P D^2 L_p$ for the relationship between ΔP, D and L_p which matches the Contract H0230050 prototype in *total* number of gas molecules in the light path. This relationship is graphed in Figure 34. We see that preserving the total number of molecules in the light path will not permit a CELL diameter of much less than 1 cm unless values of ΔP and L_p are chosen which are quite large. A value of 2.5 cm for L_p (about half the prototype CELL-path length) and D = 1 cm require a pressure excursion of between 0.5 psi and 0.75 psi.

We can also apply the gas law to the PUMP. When the piston is fully drawn and the valves have closed, the interior pressure is atmospheric pressure (14.7 psi). When the piston is at "top-dead-center", this entire amount of gas has been injected into the SAMPLE CELL (see Figure 33). This gives the equation $\Delta M = (1.70 \times 10^{18})\ (14.7)\ V_s$, where V_2 is the stroke volume and is equal to $\pi D_s^2 L_s/4$. The number of molecules of gas added to the SAMPLE CELL with each PUMP stroke is, therefore, $\Delta M = (19.63 \times 10^{18})\ D_s^2 L_s$. Setting this value equal to the total number of gas molecules in the prototype light path gives $D_s^2 L_s = 0.1396$. This relationship is shown in tabular form below.

$D_s = 0.75$ cm	$L_s = 0.25$ cm
$D_s = 1.00$ cm	$L_s = 0.14$ cm
$D_s = 1.25$ cm	$L_s = 0.09$ cm

The small values of stroke length, given diameters of the piston which fall around 1 cm, are fortunate. It was decided to drive the PUMP with a miniature precision motor manufactured by Faulhaber Shönaich (Model 235/110). It was selected for physical size (2.7 cm x 2.1 cm) and low required power input. The motor, in this application, was *derated* by a factor of 10 from its rated power output. From Figure 33, note that this miniature motor turns a wheel bearing an eccentric pin which rides in a slot in the glass-filled Teflon piston. This design, given the miniature motor and the motor

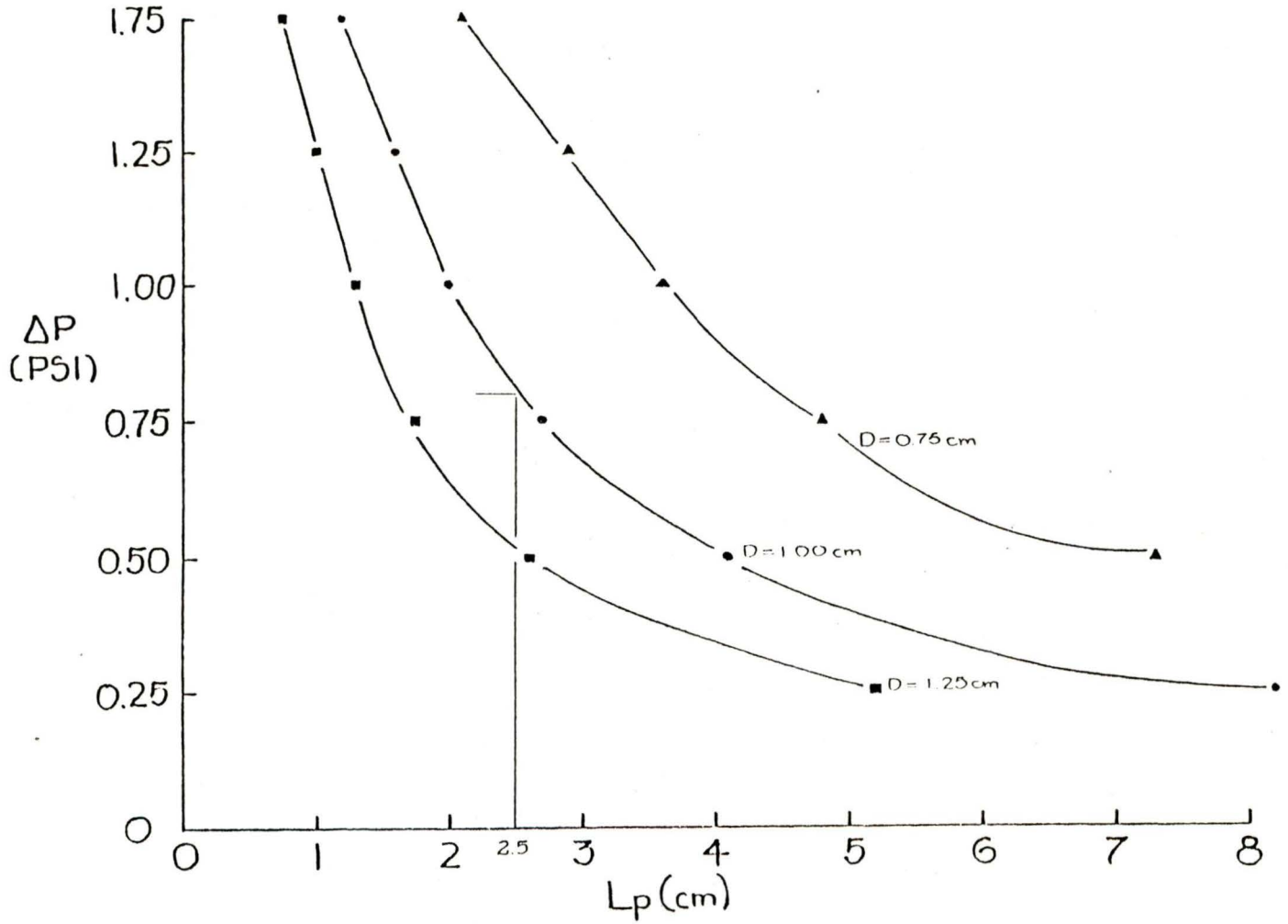

FIGURE 34. VALUES OF D, L_p and ΔP WHICH GIVE A TOTAL $\Delta M = 2.74 \times 10^{18}$ MOLECULES OF GAS.

dimensions, works best when the piston-stroke is very short. A stroke length of L_s = 0.3 cm was chosen as the shortest length compatible with the shaft diameter, pin diameter, etc. In the equation for ΔM, this value yields $\Delta M = 5.9\ D_s^2 \times 10^{18}$ molecules.

Figure 34 indicates that L_p = 2.5 cm and D = 1 cm fit the requirements set by the prototype. If, for ease of machining, we set $D_s = D = 1$ cm, we get ΔM (from the PUMP) = 5.9×10^{18}. Then $\Delta M/L_p = (5.9 \times 10^{18})L_p$ for the miniature CO_2/CH_4 SAMPLE CELL. Various values of L_p give the following values for the number of molecules per cm along the light path and for the calculated pressure excursion.

L_p	$\Delta M/L_p$	CALCULATED ΔP
3 cm	1.97×10^{18} molecules/cm	1.47 psi
2.5 cm	2.36×10^{18} molecules/cm	1.76 psi
2 cm	2.95×10^{18} molecules/cm	2.20 psi

A light-path length of 2.50 cm was chosen. This gives a change of more than twice as many molecules/cm in the light path as was the case for the prototype ANALYZER built for Contract No. H0230050. It was felt that a good safety margin was necessary because of other factors which might reduce the signal-to-noise ratio and because it was recognized that the PUMP might not efficiently deliver such a high pressure excursion. The production dimensions for the CELL and PUMP were:

L_p = 2.50 cm

D = 0.95 cm (The interior of the CELL was fitted with a highly polished aluminum sleeve to enhance internal reflection and maximize light transmission.)

L_s = 0.3 cm (An approximate measurement based on the crank eccentricity, the actual stroke length varied around this figure.)

D_s = 0.95 cm

The measured pressure excursion varied from P = 0.75 psi to ΔP = 1.11 psi. A figure of 0.75 psi is considerably less than the calculated pressure excursion and appears to be the result of late valve closure and valve leakage. A pressure excursion of 0.75 psi is still within the design requirements (see Figure 34) and gives a computed $\Delta M/L_p = 0.91 \times 10^{18}$ molecules/cm ($> 0.54 \times 10^{18}$ molecules/cm, the lower limit determined from the prototype) and a change in the total number of molecules in the light path of 2.28×10^{18} molecules (compared to 2.74×10^{18} molecules in the Contract H0230050 prototype). The pressure modulation is shown in Figure 36B.

- THE SOURCE

The SOURCE requirements were: Sufficient infrared output with low power consumption; capability of being modulated; long operating life; operating safety in a methane atmosphere; moderate cost.

The modulation requirement ruled out many conventional IR sources. Low power requirement and cost considerations suggested that the best SOURCE would be a filament lamp operating at low voltage (since lamp lifetime varies as the inverse 12-th power of the operating voltage).

Lamp efficiency at the wavelengths of interest was first estimated by measuring infrared transmission through glass sheets (and quartz) of the thickness of the glass envelope on filament lamps.

MATERIAL	TRANSMISSION at 3.4μm	TRANSMISSION at 4.3μm
0.02 cm glass	81%	68%
0.08 cm glass	55%	45%
0.20 cm quartz	90%	15%

This test indicated more than adequate transmission at the wavelengths of interest and thicknesses of ordinary filament bulbs (e.g., a General Electric No. 57 lamp has an envelope thickness of 0.03 cm).

Two groups of small filament lamps appeared as candidates for the SOURCE: High-power/low voltage lamps and low-power/high-voltage lamps. Since it was expected to operate the SOURCE at low voltage (3 to 4 volts), it was important to compare the output and operating characteristics of these two kinds of lamps. A General Electric No. 3027 high-power/low-voltage lamp and a General Electric No. 57 low-power/high-voltage lamp were tested by mounting the lamps in *place of the normal source* in a spectrophotometer (in which the reference beam was blocked) and adjusting the gain for "100% transmission" at 3μm and at the rated operating voltage of the lamp being tested. The results of these tests are shown in Figure 35. Measurements of percent output were made at various operating voltages and at the wavelengths 3.4μm and 4.1μm.

Both lamps exhibited a strictly linear relationship between operating voltage and percent output at the wavelengths of interest. There was little difference in either lamp between the percent output at 3.4μm or 4.1μm. At an operating voltage of 3 volts, there was a 10% difference in the percent output of the low-power/high-voltage lamp compared to the high-power/low-voltage lamp. At that voltage, however, there was a 13-fold reduction in the current required to operate the high-voltage/low-power lamp. In the test of the high-voltage/low-power lamp the gain of the spectrophotometer was initially left at the setting used for the low-voltage/high-power lamp test. At its operating voltage of 14 volts (3.36 watts) the percent output reading was 80%.

These data indicated that in exchange for a modest reduction in light output at the wavelengths of interest, one might gain a substantial reduction in operating power and a considerable increase in operating life. The high-voltage/low-power series of General Electric lamps that were considered are listed below.

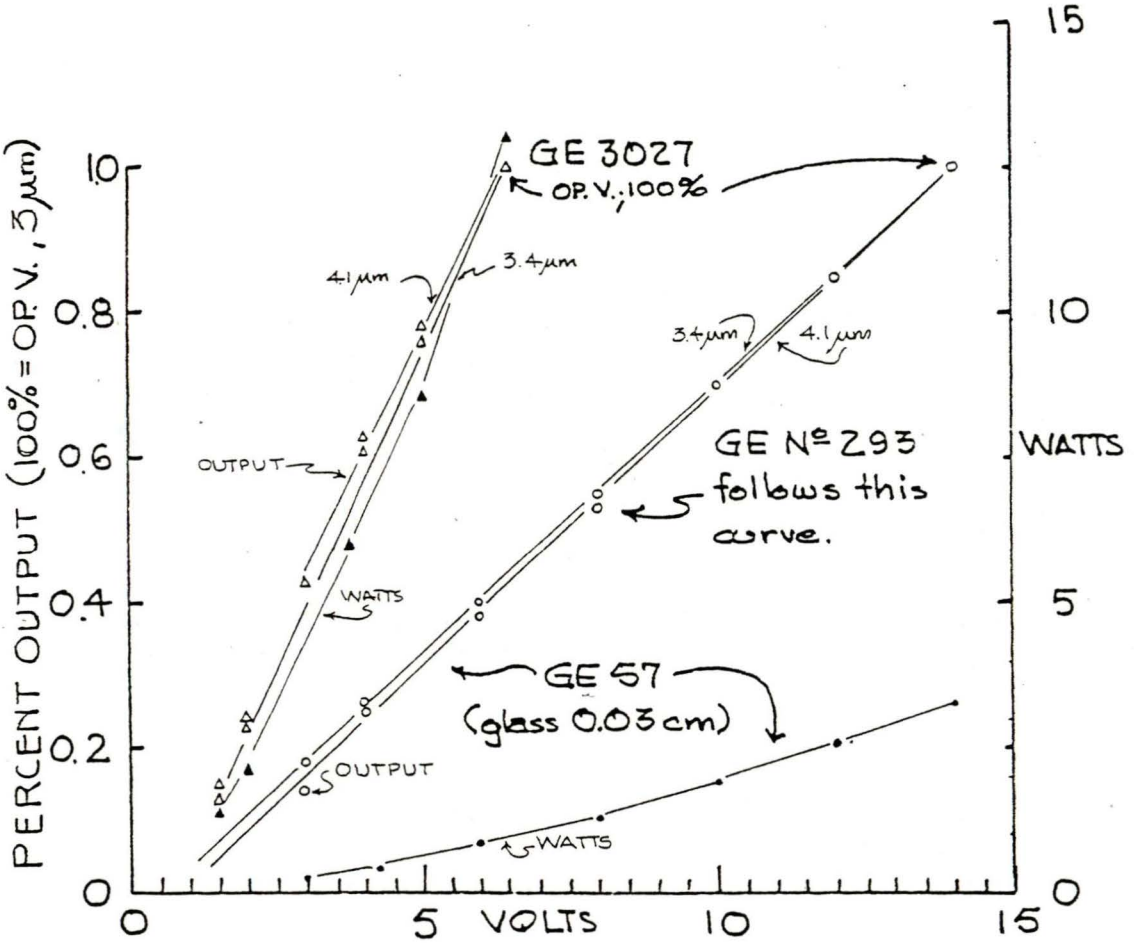

FIGURE 35. LAMP STRENGTH AT 3.4μm AND 4.1μm.

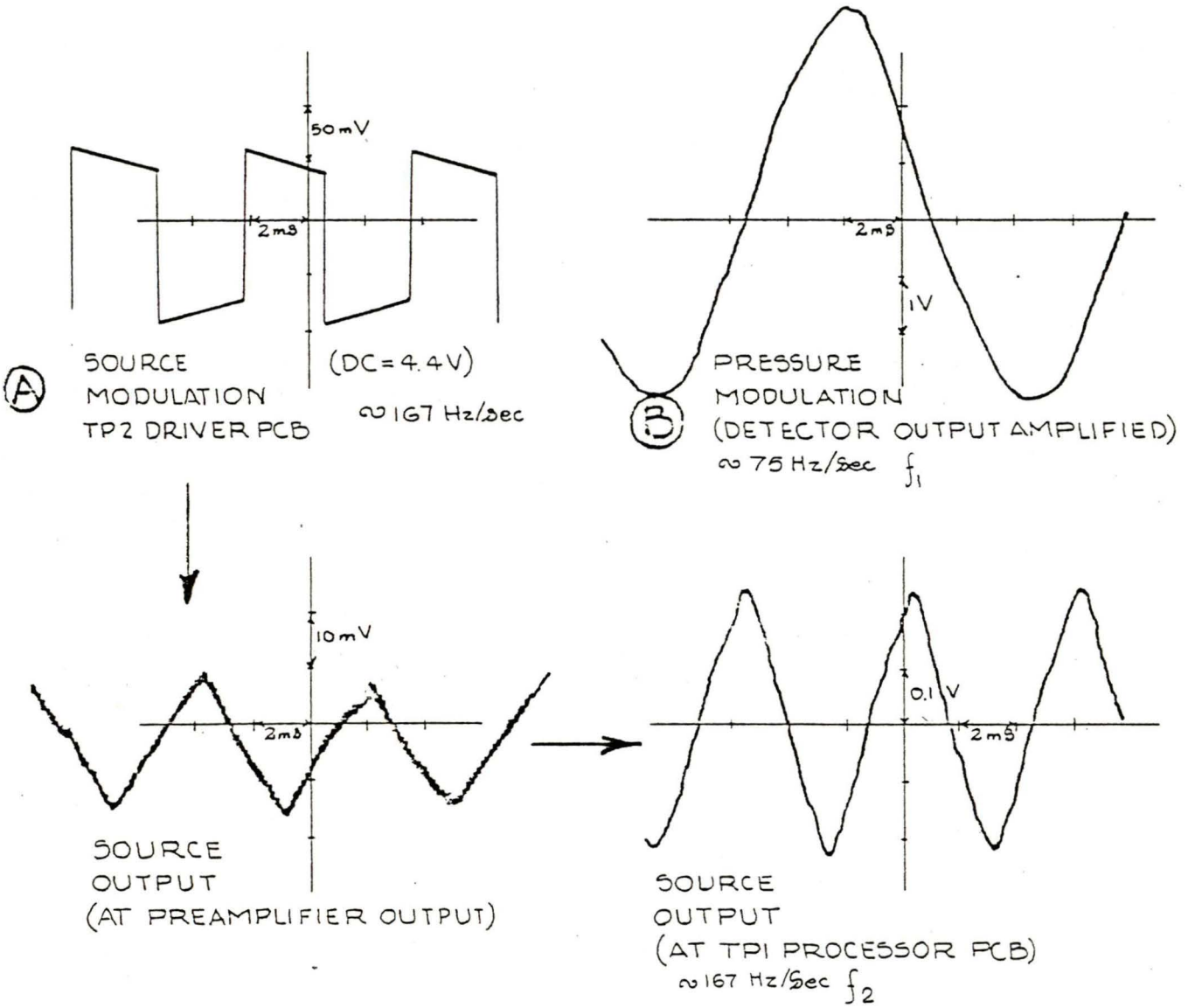

FIGURE 36. TRACINGS FROM OSCILLOSCOPE PHOTOGRAPHS OF:

(A) MODULATION OF THE SOURCE VOLTAGE AND RESULTING MODULATION OF THE SOURCE OUTPUT;

(B) AMPLIFIED DETECTOR OUTPUT SHOWING RESULT OF PRESSURE MODULATION.

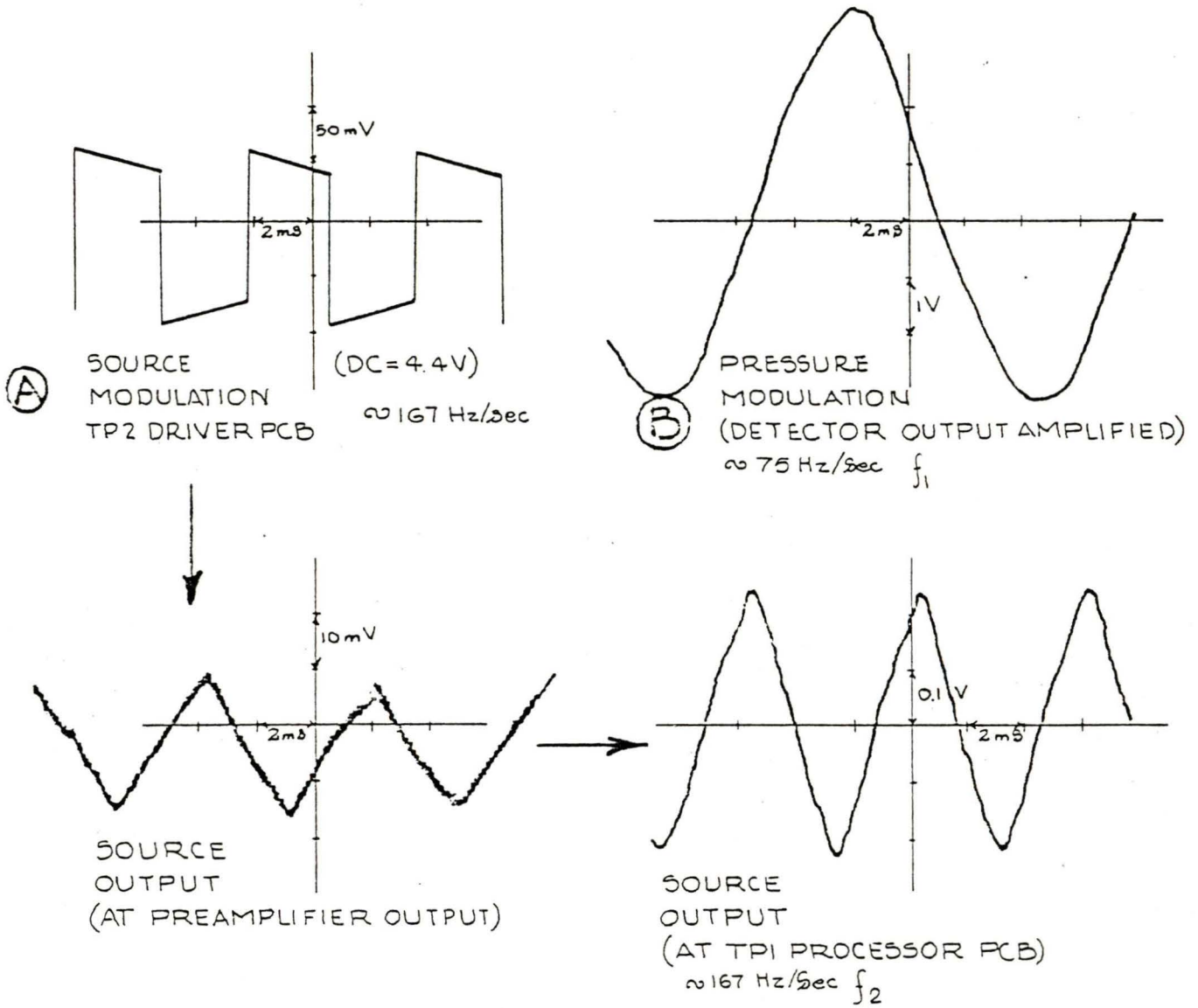

FIGURE 36. TRACINGS FROM OSCILLOSCOPE PHOTOGRAPHS OF:

(A) MODULATION OF THE SOURCE VOLTAGE AND RESULTING MODULATION OF THE SOURCE OUTPUT;

(B) AMPLIFIED DETECTOR OUTPUT SHOWING RESULT OF PRESSURE MODULATION.

The lamps were tested at 6 volts, 210 mA (1.26 watts). The General Electric No. 57 was found to ignite the mixture when broken. The General Electric No. 31, already known not to be intrinsically safe, also ignited the mixture when broken. Five General Electric No. 293 lamps were tested and all five failed to ignite the mixture when broken.

Sufficient confidence was generated as a result of this test to proceed with the use of the General Electric No. 293 lamp in the CO_2/CH_4 DETECTORS. This lamp has been submitted to the Mining Safety and Health Administration for testing for intrinsic safety. The General Electric No. 293 lamp has a rated life of 7,500 hours average at 14 volts. In theory the life at a lower operating voltage may be computed as the rated life multiplied by the 12-th power of the ratio of rated voltage to operating voltage, in this case $7,500 \times (14/4)^{12} = 25 \times 10^{10}$ hours. This formula breaks down, however, at differences of more than a few percent. It may be assumed, however, that the lamp used at the operating voltage of the SOURCE will have a substantial longer than average life.

- THE TRANSDUCER

In earlier designs of pressure-modulated DETECTORS, Andros has used the National Semiconductor LX-1600 Series Transducer. For the miniature CO_2/CH_4 DETECTOR design two low-cost piezoelectric discs were examined. These are the GULTON G1195 and the FERROXCUBE PXE-5 piezoelectric discs. These piezoelectric discs, although not zero and span stable over a wide temperature range, as is the National Semiconductor transducer, have the advantage of a 50:1 cost reduction. The two piezoelectric discs tested did exhibit a slight span temperature coefficient (the test results matched the manufacturers' rated values), but this is readily compensated for in the PROCESSOR at no substantial cost. The mounting of the piezoelectric disc PRESSURE TRANSDUCER is shown in Figure 33.

- THE FILTER

The CO_2 and CH_4 DETECTOR FILTERS chosen were thin film interference filters from Optical Coating Laboratories, Inc.

The lamps were tested at 6 volts, 210 mA (1.26 watts). The General Electric No. 57 was found to ignite the mixture when broken. The General Electric No. 31, already known not to be intrinsically safe, also ignited the mixture when broken. Five General Electric No. 293 lamps were tested and all five failed to ignite the mixture when broken.

Sufficient confidence was generated as a result of this test to proceed with the use of the General Electric No. 293 lamp in the CO_2/CH_4 DETECTORS. This lamp has been submitted to the Mining Safety and Health Administration for testing for intrinsic safety. The General Electric No. 293 lamp has a rated life of 7,500 hours average at 14 volts. In theory the life at a lower operating voltage may be computed as the rated life multiplied by the 12-th power of the ratio of rated voltage to operating voltage, in this case $7,500 \times (14/4)^{12} = 25 \times 10^{10}$ hours. This formula breaks down, however, at differences of more than a few percent. It may be assumed, however, that the lamp used at the operating voltage of the SOURCE will have a substantial longer than average life.

- THE TRANSDUCER

In earlier designs of pressure-modulated DETECTORS, Andros has used the National Semiconductor LX-1600 Series Transducer. For the miniature CO_2/CH_4 DETECTOR design two low-cost piezoelectric discs were examined. These are the GULTON G1195 and the FERROXCUBE PXE-5 piezoelectric discs. These piezoelectric discs, although not zero and span stable over a wide temperature range, as is the National Semiconductor transducer, have the advantage of a 50:1 cost reduction. The two piezoelectric discs tested did exhibit a slight span temperature coefficient (the test results matched the manufacturers' rated values), but this is readily compensated for in the PROCESSOR at no substantial cost. The mounting of the piezoelectric disc PRESSURE TRANSDUCER is shown in Figure 33.

- THE FILTER

The CO_2 and CH_4 DETECTOR FILTERS chosen were thin film interference filters from Optical Coating Laboratories, Inc.

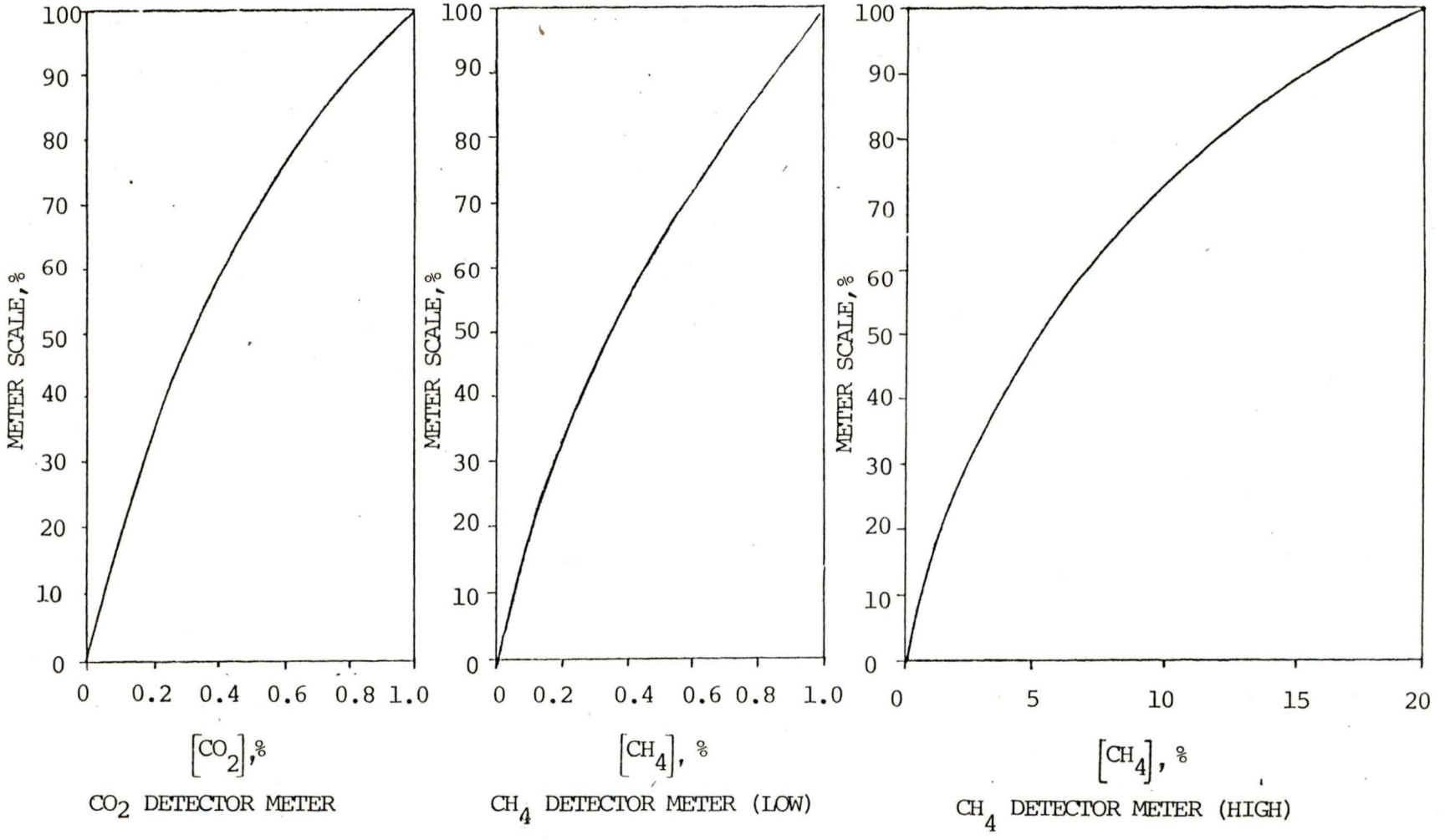

FIGURE 38. METER-CALIBRATION CURVES FOR THE CO_2/CH_4 DETECTORS.

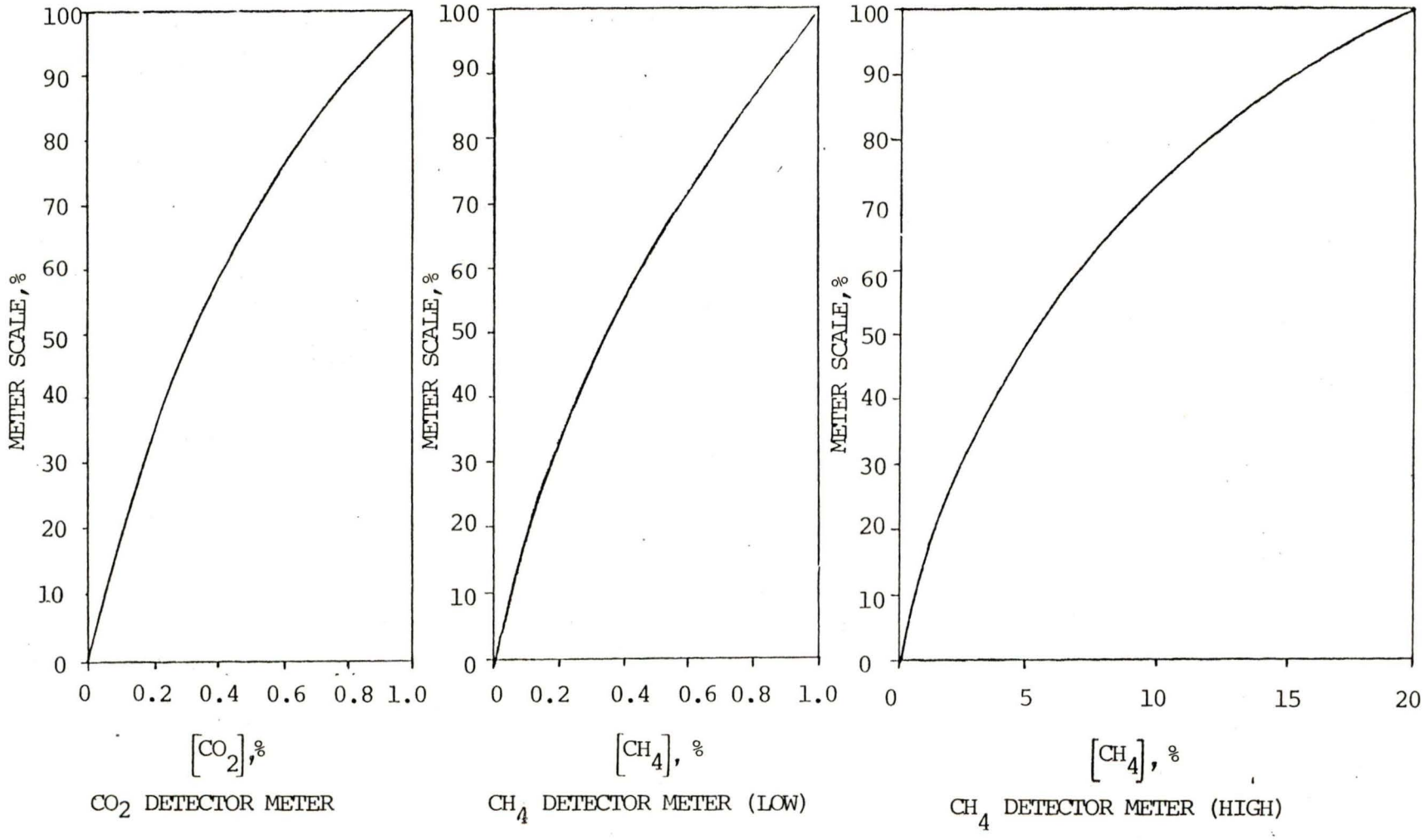

FIGURE 38. METER-CALIBRATION CURVES FOR THE CO_2/CH_4 DETECTORS.

In the miniature CO_2/CH_4 DETECTOR design, the pressure excursions were not constant because of valve wear, piston slip, etc. No attempt was made to achieve constancy as there is no practical device by which this could be achieved. Instead, the pressure signal from the TRANSDUCER was applied to the denominator input of the analog divider. The numerator input of the analog divider was derived from the f_1 frequency optical signal. This accomplishes the same elimination of drift and error (error x f_1 signal/error = f_1 signal). The PROCESSOR diagrams may be found in the DOCUMENTATION section.

- THE DRIVER

The DRIVER circuit developed for Contract No. H0230050 was modified for the miniature CO_2/CH_4 DETECTOR design.

An AC amplifier was added to amplify the PRESSURE TRANSDUCER output. The output of this amplifier goes into two circuits (for diagrams, see the DOCUMENTATION section report). One circuit begins with a full-wave precision rectifier, followed by a low-pass filter whose output is an "average-pressure" signal. The other circuit begins with a limiter and converts the pressure signal (AC) into a square wave. That output is used to demodulate the f_1 frequency signal on the PROCESSOR PCB.

An oscillator and "flip-flop" circuit was added for the f_2 frequency modulation. The output of the "flip-flop" circuit was used to drive the SOURCE and to control the reference gate at the f_2 frequency demodulator on the PROCESSOR PCB. This provides span stabilization.

A MOTOR speed control was also added. Since the MOTOR was operated in a constant voltage mode, a voltage divider and emitter-follower circuit were required.

THEORY OF OPERATION

The Andros Incorporated Detector is a unique pressure modulated nondispersive infrared (NDIR) gas analyzer. Pressure modulated analyzers are characterized by simplicity, low cost, reliability and long-term zero and span stability.

The block diagram in Figure 39 shows the main system components. Infrared radiation from the source passes through the sample cell, traverses a narrow band interference filter and is collected by the detector. The gas in the sample cell is pressure modualted in a periodic manner at frequency F_1 by the sample pump which also continuously flows gas through the sample cell. The pressure, and hence density, modulation of gas in the sample cell will cause a periodic variation in absorption of the radiation passing through the cell if there is any gas in the sample which absorbs radiation. The analyzer is made specific to CO_2 by the use of the narrow band-pass filter. This filter is selected such that it passes only radiation centered on the absorption band of CO_2 at 4.25μm.

The infrared energy from the source is also modulated at frequency F_2 by imposing an AC component on the DC source voltage. A reference demodulator is used to detect the resulting optical signal and control an AGC element such that the magnitude of this signal is kept constant. This amounts to a division of the absorption signal at F_1 by the reference signal at F_2 and thus the concentration of CO_2 is proportional to the ratio of the F_1 signal to the F_2 signal. This renders the span of the unit stable against many possible variations such as a change in source power, window or filter transmission as well as changes in the responsivity of the detector, since any change in these parameters has the same effect on both the F_1 and F_2 signals.

The pressure modulation technique provides long-term zero stability, since the F_1 signal is simply not present when the gas of interest is absent.

To compensate for any variation in the pressure modulation that results from valve wear, motor speed variation, etc., the pressure transducer output is rectified, filtered and applied to the denominator of an analog divider. The numerator of this divider is the F_1 signal which has been phase-sensitive demodulated and filtered. The output of the divider drives the meter.

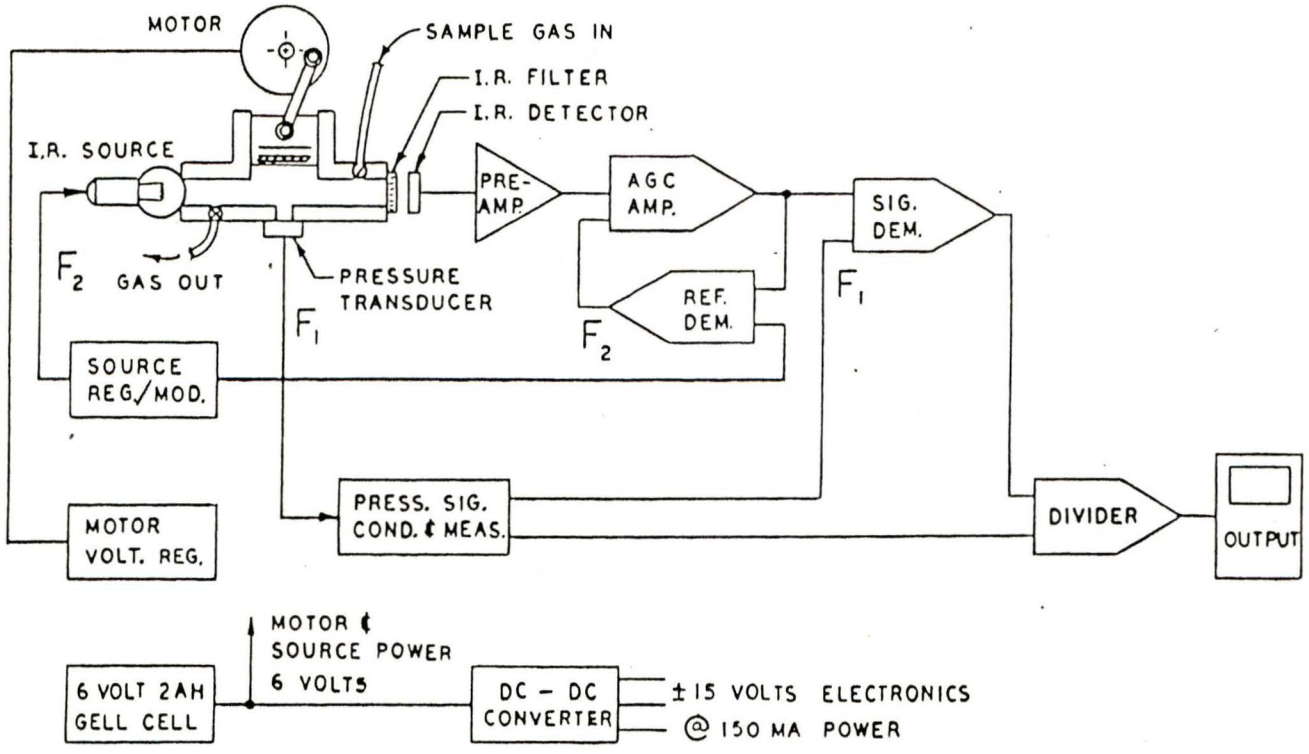

FIGURE 39. SYSTEM BLOCK DIAGRAM.

INITIAL TESTING AND MODIFICATION

On August 30, 1978, Andros delivered four CO_2 DETECTORS (Model 312) and three CH_4 DETECTORS (Model 322) to the Bureau of Mines. These instruments had serial numbers SN2-SN8.

USBM acceptance testing of the instruments began on August 31 and continued through September. The results of these tests are incorporated in this report in Appendix B. In essence, however, it was found that under high ambient ("soak") conditions of CO_2 or CH_4 the instruments could not be calibrated to standard or "zero" gas. The USBM concluded that leaks in the PUMP assembly resulted in a portion of the gas in the SAMPLE CELL being drawn from the ambient gas inside the instrument case instead of via the INLET PORT. The instruments were returned to Andros for further testing and modification.

On December 18, 1978, Andros proposed an extension to the contract in order to carry out modifications to correct the leakage. This extension was granted.

Under the contract extension, the pressure-modulator PUMP was redesigned so that all inlet gases originate from a common line exterior to the DETECTOR case. Revised optical heads were fabricated for the instruments and all of the DETECTORS were tested for gas-tight integrity.

During testing, it was observed that a BATTERY CHARGER of greater capacity was necessary, so a new BATTERY CHARGER was provided to replace the original unit.

It was found that shielding by the case changed calibration adjustments made while the case was off. Access ports for the "zero" and span controls were drilled in the DETECTOR cases. This improves stability and also enables field adjustment without removing the case.

A new aluminium SAMPLE-CELL mount was designed to replace the original plastic mount, a new motor mount was designed and the preamplifier was decoupled from the main PROCESSOR PCB. These changes were made to reduce microphonics and to increase the stability of the DETECTOR.

A CALIBRATION KIT was provided with each instrument. This consisted of a CALIBRATION ADAPTOR, an O-RING and a supply of BALLOONS used to adjust gas pressure.

Revisions to the mechanical and electronic schematics were prepared and included in the new INSTRUCTION MANUALS.

The modified units were shipped to the Bureau of Mines on May 23, 1979.

CONCLUSIONS AND RECOMMENDATIONS

The four Andros CO_2 DETECTORS and three Andros CH_4 DETECTORS delivered to the Bureau of Mines substantially met the modified contract requirements for portable gas detectors (see pages 11 - 12 of this report). Each instrument is a miniature, portable CO_2 or CH_4 DETECTOR designed for in-mine use. The performance of all but one of the components of the CO_2/CH_4 DETECTORS indicate that a reliable and reasonably inexpensive instrument could be produced for widespread industry use.

In our estimation, however, one component in the instruments falls short of the qualities we had hoped for. We feel that until a better design is found for that component, the CO_2/CH_4 DETECTOR design developed in this project may have a limited future as a widely used instrument. The rationale behind this conclusion may be appreciated by distinguishing between shortcomings of a particular instrument and major instrument design limitations.

On pages 19 - 22 we discussed some of the design-limiting problems associated with the pump-modulated DETECTOR, particularly the problems of low modulation frequency and vibration. As was noted in the section entitled INITIAL TESTING AND MODIFICATION, a number of major modifications were made to reduce vibration and microphonics resulting from vibration.

Throughout the development of the pump-modulated instrument we found difficulties with microphonics resulting from vibration. This factor appeared to be the major limiation on span and zero stabilization. The low frequencies of this vibration, because of the low-frequency modulation inherent in the pump-modulation design, made the problem more acute. At one point in the development an opposed dual-piston pump design was tested in the hope that vibration from the reciprocating pump could be damped in this manner. The results were not encouraging and the single-piston design was used.

The important factor in this design limitation is cost. Although it was possible to significantly reduce pump vibration and microphonics in the development models of the CO_2/CH_4 DETECTORS, such individual adjustment and precision construction in production models is possible only at an increased cost. In our view, practical portable CO_2/CH_4 DETECTORS must be inexpensive as well as reliable if they are to be widely accepted throughout industry.

It is our belief that an alternate (other than pump driven) means of generating pressure modulation in the sample cell is the key breakthrough needed to reduce the cost of this instrument. In the past Andros has fabricated Hemlholtz resonator sample cells, driven by both piezoceramic and electromagnetic means.

The performance of other components of the CO_2/CH_4 DETECTORS makes quite clear that, provided the problem of vibration and microphonics is solved, a very reliable and modestly priced portable instrument might be produced. It is our recommendation that a further examination of both non-resonant piezoceramic drivers and electromagnetic drivers for a miniature Helmholtz resonator sample cell be made. The objective of such a project would be to focus on the sample cell construction, driver mechanism, low power consumption and small overall size in order to produce inexpensive and reliable CO_2 and CH_4 detectors.

APPENDIX A

DOCUMENTATION

APPENDIX A

DOCUMENTATION

Item No.	Drawing No.	Description
1	11319	System block diagram
2	11432	Preamp schematic diagram
3	11659	Processor schematic diagram
4	11661	Drivers schematic diagram
5	11450	System wiring diagram

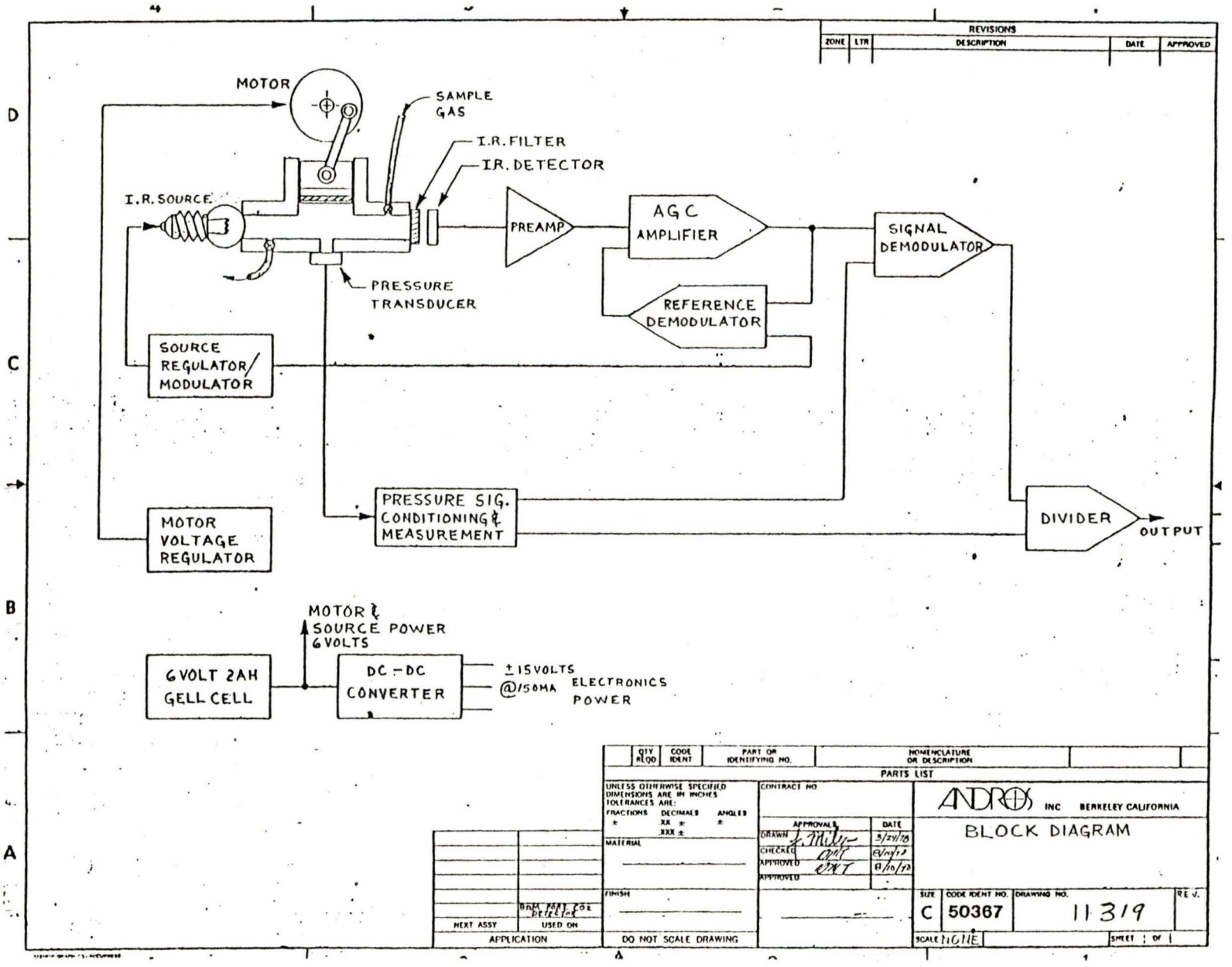
REVISIONS
ZONE | LTR | DESCRIPTION | DATE | APPROVED
MOTOR
SAMPLE GAS
I.R. FILTER
IR. DETECTOR
I.R. SOURCE
PREAMP
AGC AMPLIFIER
SIGNAL DEMODULATOR
PRESSURE TRANSDUCER
REFERENCE DEMODULATOR
SOURCE REGULATOR/ MODULATOR
PRESSURE SIG. CONDITIONING & MEASUREMENT
DIVIDER
OUTPUT
MOTOR VOLTAGE REGULATOR
MOTOR & SOURCE POWER 6 VOLTS
6 VOLT 2AH GELL CELL
DC-DC CONVERTER
±15 VOLTS @150MA
ELECTRONICS POWER
PARTS LIST
QTY REQD | CODE IDENT | PART OR IDENTIFYING NO. | NOMENCLATURE OR DESCRIPTION
UNLESS OTHERWISE SPECIFIED DIMENSIONS ARE IN INCHES
TOLERANCES ARE:
FRACTIONS ± DECIMALS XX ± XXX ± ANGLES ±
MATERIAL
FINISH
DO NOT SCALE DRAWING
CONTRACT NO
APPROVALS | DATE
DRAWN | CHECKED | APPROVED | APPROVED
NEXT ASSY | USED ON
APPLICATION
ANDROS INC BERKELEY CALIFORNIA
BLOCK DIAGRAM
SIZE C | CODE IDENT NO. 50367 | DRAWING NO. 11319 | REV.
SCALE NONE | SHEET 1 OF 1

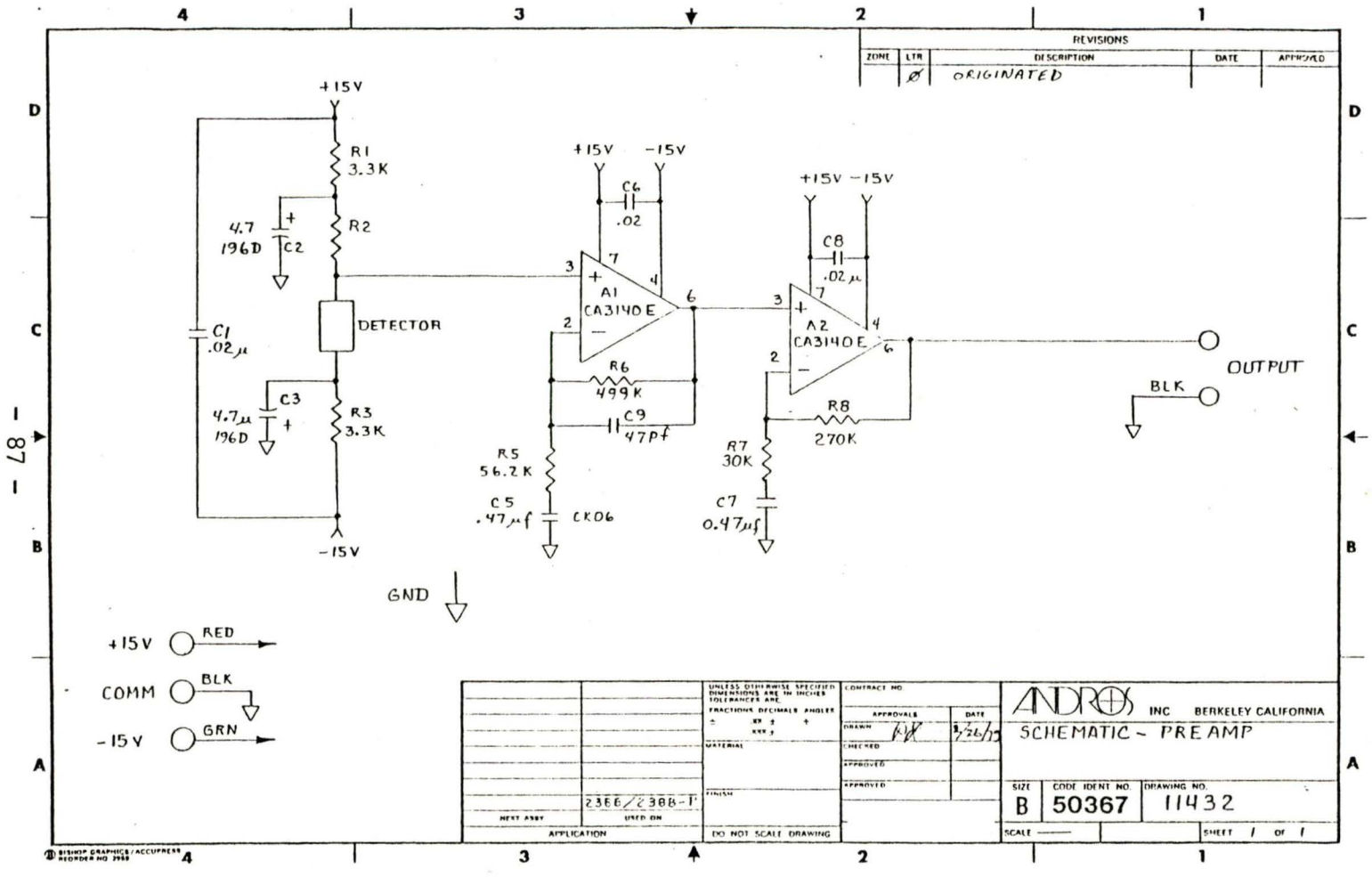
REVISIONS
ZONE | LTR | DESCRIPTION | DATE | APPROVED
Ø ORIGINATED
+15V
R1 3.3K
4.7 196D C2
R2
C1 .02μ
DETECTOR
4.7μ 196D C3
R3 3.3K
-15V
GND
+15V -15V
C6 .02
A1 CA3140E
R6 499K
C9 47Pf
R5 56.2K
C5 .47μf CK06
+15V -15V
C8 .02μ
A2 CA3140E
R8 270K
R7 30K
C7 0.47μf
OUTPUT
BLK
+15V RED
COMM BLK
-15V GRN
UNLESS OTHERWISE SPECIFIED DIMENSIONS ARE IN INCHES TOLERANCES ARE
FRACTIONS DECIMALS ANGLES
± .XX ± ±
.XXX ±
MATERIAL
FINISH
DO NOT SCALE DRAWING
CONTRACT NO.
APPROVALS DATE
DRAWN DH 3/26/73
CHECKED
APPROVED
APPROVED
NEXT ASSY 2366/2388-1
USED ON
APPLICATION
ANDROS INC BERKELEY CALIFORNIA
SCHEMATIC - PREAMP
SIZE B
CODE IDENT NO. 50367
DRAWING NO. 11432
SCALE —
SHEET 1 OF 1
BISHOP GRAPHICS / ACCUPRESS REORDER NO. 3959

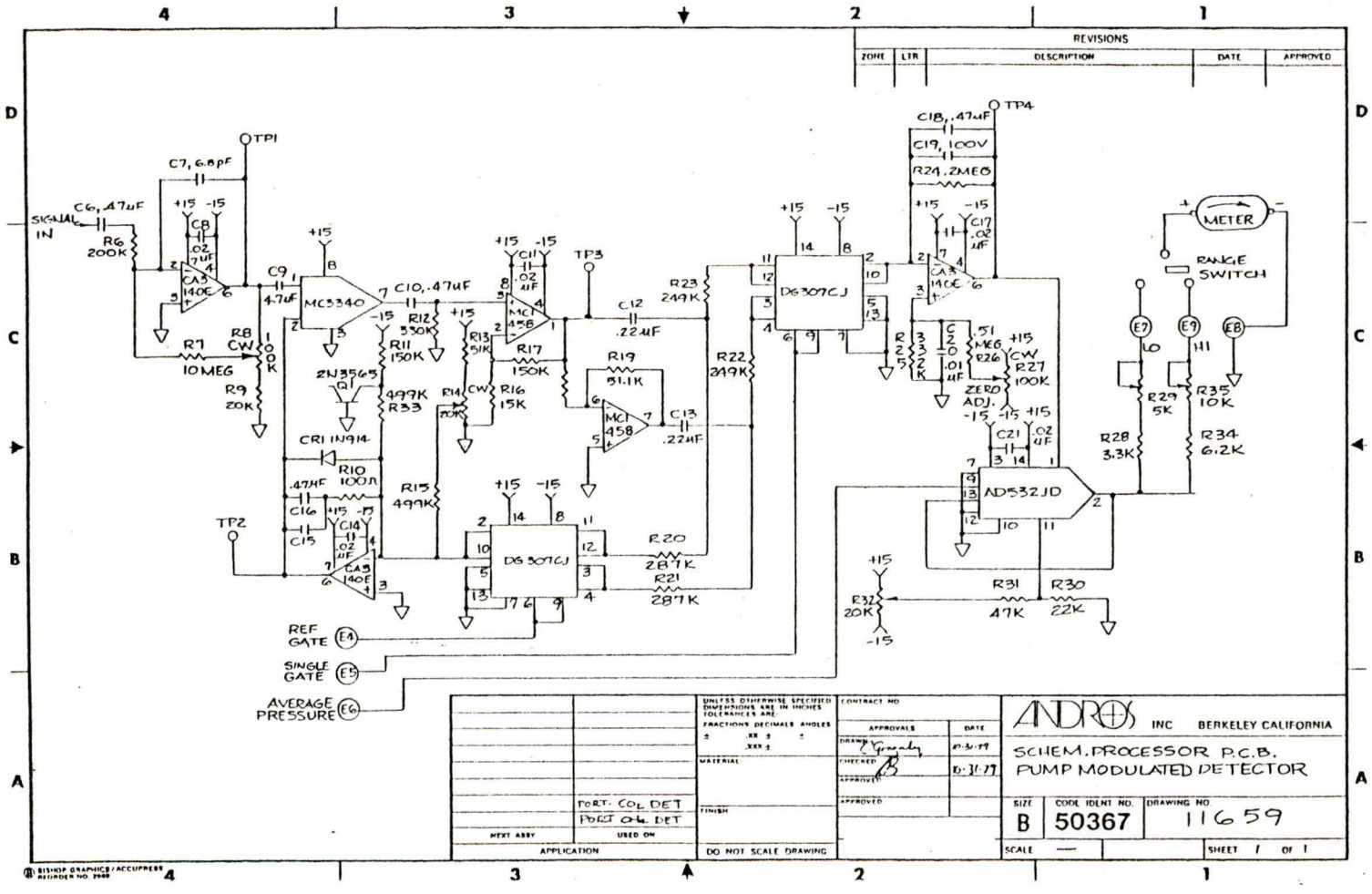
REVISIONS
ZONE | LTR | DESCRIPTION | DATE | APPROVED
TP1
TP2
TP3
TP4
C7, 6.8pF
C6, .47uF
SIGNAL IN
R6 200K
C8 .02 uF
CA3 140E
C9 4.7uF
MC3340
C10, .47uF
R12 330K
R11 150K
499K R33
2N3565 Q1
R7 10 MEG
R8 CW 100K
R9 20K
CR1 IN914
C16 .47uF
C15
C14 .02 uF
R10 100Ω
R13 499K
C11 .02 uF
MC1458
R13 51K
R14 CW 20K
R16 15K
R17 150K
C12 .22uF
R19 51.1K
MC1458
C13 .22uF
R23 249K
R22 249K
DG307CJ
R20 287K
R21 287K
C18, .47uF
C19, 100V
R24, 2MEG
C17 .02 uF
R32 20K
R31 47K
R30 22K
C20 .01 uF
R25 332K
51 MEG R26
CW R27 100K
ZERO ADJ.
C21 .02 uF
AD532JD
R28 3.3K
R29 5K
R34 6.2K
R35 10K
METER
RANGE SWITCH
E7 LO
E9 HI
E8
REF GATE E4
SINGLE GATE E5
AVERAGE PRESSURE E6
+15
-15
UNLESS OTHERWISE SPECIFIED DIMENSIONS ARE IN INCHES TOLERANCES ARE FRACTIONS DECIMALS ANGLES
MATERIAL
FINISH
DO NOT SCALE DRAWING
CONTRACT NO
APPROVALS DATE
DRAWN 10-3-77
CHECKED 10-31-77
APPROVED
PORT. COL DET
PORT O-L DET
NEXT ASSY USED ON
APPLICATION
ANDROS INC BERKELEY CALIFORNIA
SCHEM. PROCESSOR P.C.B.
PUMP MODULATED DETECTOR
SIZE B
CODE IDENT NO. 50367
DRAWING NO. 11659
SCALE —
SHEET 1 OF 1
BISHOP GRAPHICS / ACCUPRESS NO. 2040

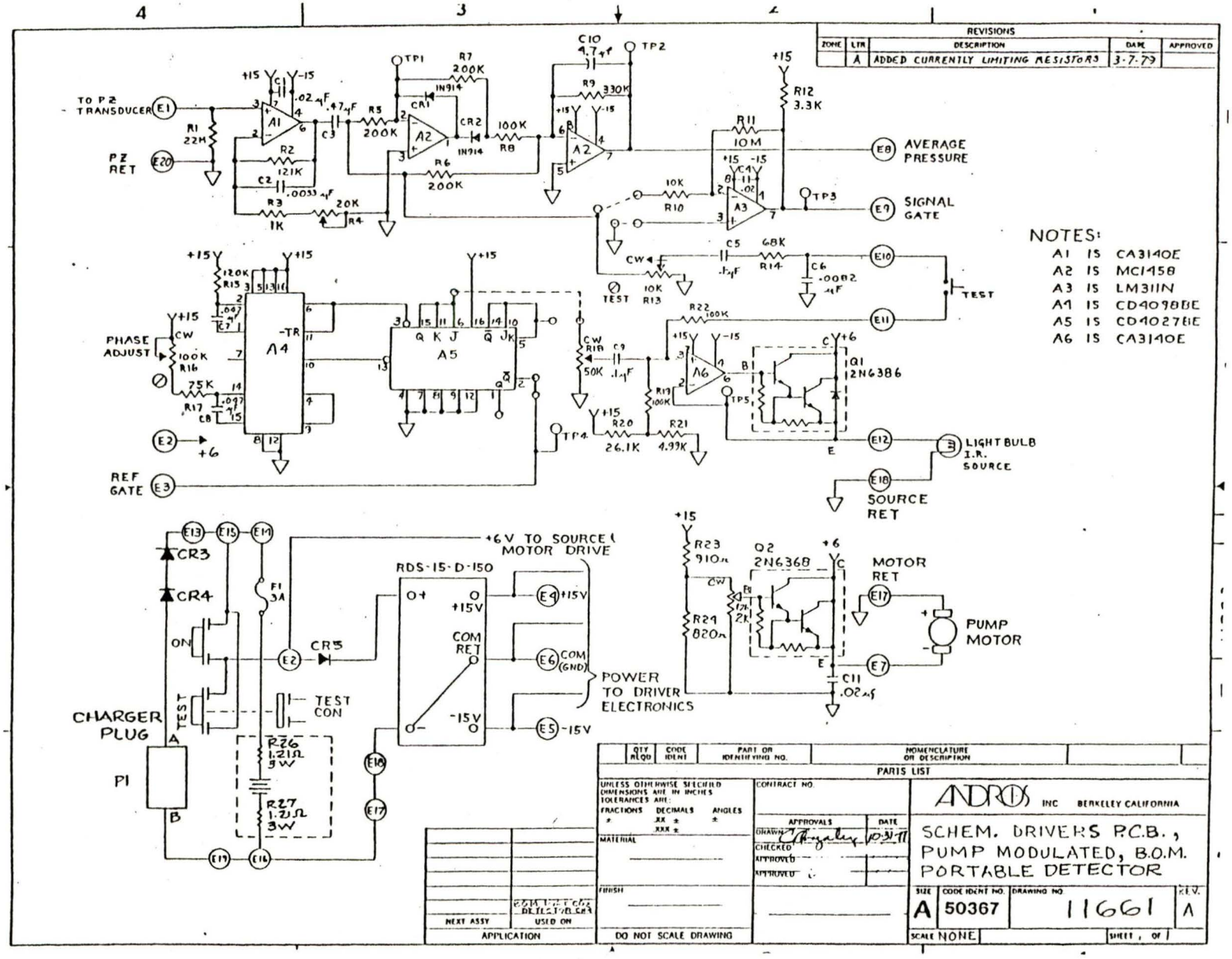
REVISIONS
ZONE | LTR | DESCRIPTION | DATE | APPROVED
A | ADDED CURRENTLY LIMITING RESISTORS | 3-7-79
TO PZ TRANSDUCER
PZ RET
AVERAGE PRESSURE
SIGNAL GATE
TEST
PHASE ADJUST
REF GATE
+6
LIGHT BULB I.R. SOURCE
SOURCE RET
+6V TO SOURCE MOTOR DRIVE
RDS-15-D-150
+15V
COM RET
-15V
POWER TO DRIVER ELECTRONICS
CHARGER PLUG
TEST CON
MOTOR RET
PUMP MOTOR
NOTES:
A1 IS CA3140E
A2 IS MC1458
A3 IS LM311N
A4 IS CD4098BE
A5 IS CD4027BE
A6 IS CA3140E
PARTS LIST
UNLESS OTHERWISE SPECIFIED DIMENSIONS ARE IN INCHES
TOLERANCES ARE:
FRACTIONS DECIMALS ANGLES
CONTRACT NO.
APPROVALS DATE
DRAWN 10-31-11
CHECKED
APPROVED
APPROVED
MATERIAL
FINISH
DO NOT SCALE DRAWING
NEXT ASSY USED ON
APPLICATION
ANDROS INC BERKELEY CALIFORNIA
SCHEM. DRIVERS P.C.B., PUMP MODULATED, B.O.M. PORTABLE DETECTOR
SIZE A
CODE IDENT NO. 50367
DRAWING NO 11661
REV. A
SCALE NONE
SHEET 1 OF 1

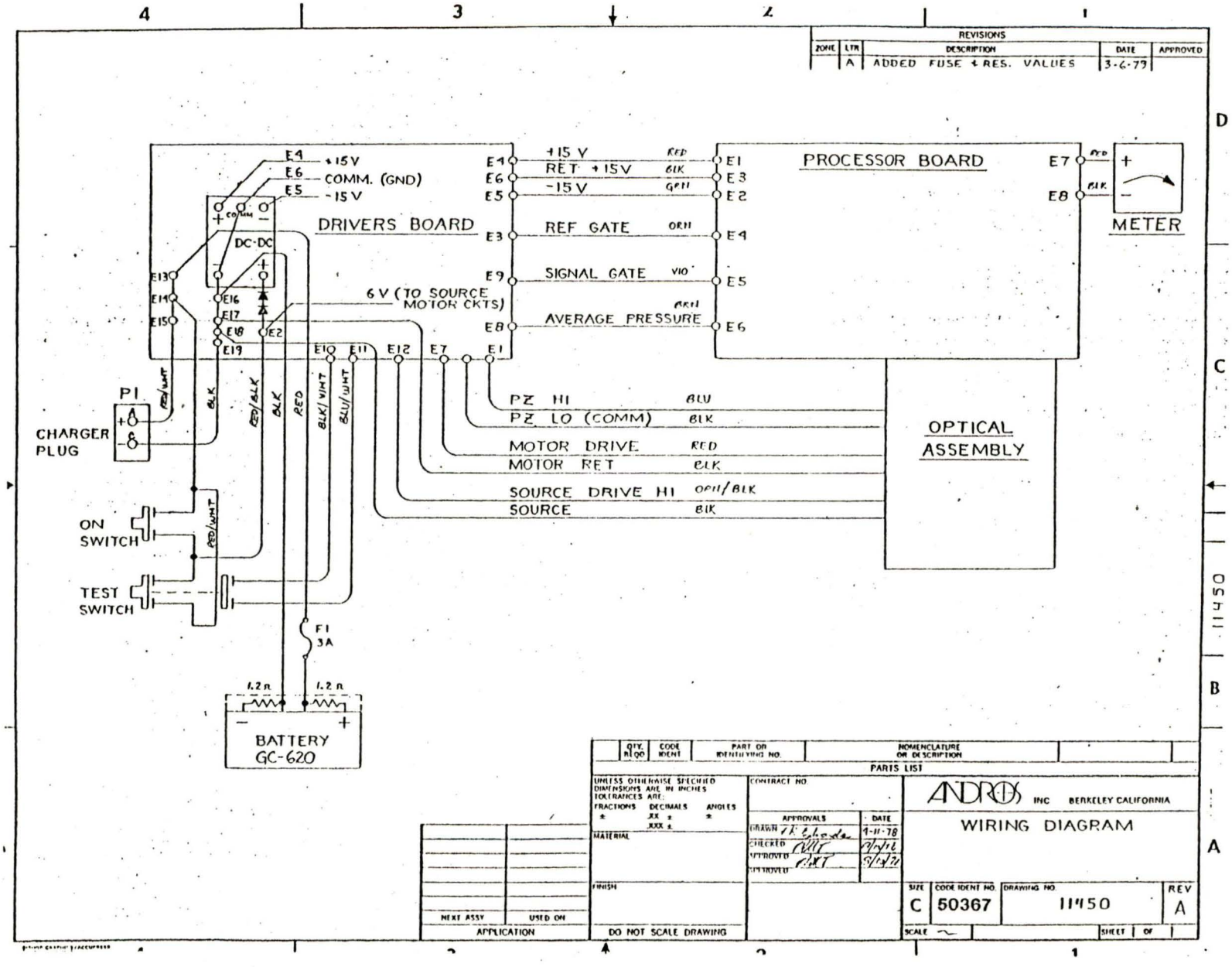
REVISIONS
ZONE | LTR | DESCRIPTION | DATE | APPROVED
A | ADDED FUSE & RES. VALUES | 3-6-79
DRIVERS BOARD
PROCESSOR BOARD
METER
OPTICAL ASSEMBLY
DC-DC
E4 +15V
E6 COMM. (GND)
E5 -15V
E4 +15 V RED E1
E6 RET +15V BLK E3
E5 -15V GRN E2
E3 REF GATE ORN E4
E9 SIGNAL GATE VIO E5
6 V (TO SOURCE MOTOR CKTS)
E8 AVERAGE PRESSURE BRN E6
E7 RED
E8 BLK
PZ HI BLU
PZ LO (COMM) BLK
MOTOR DRIVE RED
MOTOR RET BLK
SOURCE DRIVE HI ORN/BLK
SOURCE BLK
P1
CHARGER PLUG
ON SWITCH
TEST SWITCH
F1 3A
1.2 Ω
1.2 Ω
BATTERY GC-620
PARTS LIST
QTY REQD | CODE IDENT | PART OR IDENTIFYING NO. | NOMENCLATURE OR DESCRIPTION
UNLESS OTHERWISE SPECIFIED DIMENSIONS ARE IN INCHES TOLERANCES ARE: FRACTIONS ± DECIMALS .XX ± .XXX ± ANGLES ±
CONTRACT NO.
APPROVALS | DATE
DRAWN 11-11-78
CHECKED
APPROVED
MATERIAL
FINISH
NEXT ASSY | USED ON
APPLICATION
DO NOT SCALE DRAWING
ANDROS INC BERKELEY CALIFORNIA
WIRING DIAGRAM
SIZE C | CODE IDENT NO. 50367 | DRAWING NO. 11450 | REV A
SCALE | SHEET | OF

APPENDIX B

PRELIMINARY EVALUATION BY THE BUREAU OF MINES

Andros Portable Methane Detectors
and
Andros Portable Carbon Dioxide Detectors

PRELIMINARY EVALUATION OF ANDROS MODELS 312 AND 322

by

Clarence R. Carpenter
George H. Schnakenberg, Jr.

August-September, 1978

Seven portable instruments were received in the lab from ANDROS, Inc., on August 30, 1978, for evaluation. Four instruments (Model 312) were carbon dioxide detectors, the remaining three (Model 322) were methane detectors. During the morning of August 31, the ZERO and SPAN of each instrument were checked using zero air, 0.95% CO_2, or 2.44% CH_4 as appropriate. Table 1 tabulates the results of this test. The zero on each instrument was adjusted, after conferring with Mr. Abdul Tayeb (of ANDROS), and the instruments were again checked (see table B-2).

On September 20, after the instruments' batteries were charged overnight, the methane units were placed in an Environmental Chamber for testing. The chamber's controls were set to provide a temperature of approximately 20° (68°F) with about 60% relative humidity. A servo system was used to maintain the chambers atmosphere at 1% CH_4 and the atmosphere was continuously monitored by an ANDROS Model 209 Methane Analyzer. A pair of wires was soldered on terminals E-15 and E-2 on each instrument to turn the instrument ON remotely (from outside of the chamber). The instruments were operated (turned ON) for two minutes then the LO range meter indication was recorded. This was done four times over a period of about seven hours (1 day). After the test the batteries were charged overnight. The following day the chamber's atmosphere was maintained at 3% CH_4. During this day, the HI range meter indications were recorded five times over a seven-hour period. The results of these tests are tabulated in Table B-3.

A similar procedure was employed to test the carbon dioxide units. The results of the test on these instruments are tabulated in Table B-4. The relatively high indications observed in these tests indicated the probability of leakage in and around the sensors. Again Mr. Tayeb was consulted. At this time it was decided to return the instruments to the manufacturer for investigation and repair. Prior to shipping, at Mr. Tayeb's suggestion, the AGC voltage (TP-2 to ground) was measured on each instrument (see Table 5).

Additional tests were performed to verify the leakage of the sensors. For these tests, the instrument to be tested was placed in a small chamber. Zero air was plumbed directly to the sensor of the instrument via rubber tubing. A precision gas mixing system provided various concentrations of test gas for the chamber's atmosphere and the atmosphere was continually monitored by an ANDROS 209 (CH_4) or a Beckman 868 (CO_2). See Figure A-1 for the test layout. An external 6 vdc power supply was connected to the I.U.T.* to make the test independent of battery voltage.

The meter indications for various concentrations of CH_4 or CO_2 are tabulated in Table 5.

* Instrument under test.

Table B-1. Initial Check on Instruments

	Carbon Dioxide (%)				Methane (%)		
Instrument: Control No.	1	2	3	4	5	6	7
Serial No.	2	5	4	3	6	7	8
Test Gas							
Zero Air	0.04	0.11	0.04	0.0	0.3	0.5	0.0
0.95% CO_2	0.95	0.62	1.0	0.85	-	-	-
2.44% CH_4	-	-	-	-	2.6	2.4	3.2

Table B-2. Response of Instruments after ZERO Adjustments

	Carbon Dioxide (%)				Methane (%)		
Instrument: Control No.	1	2	3	4	5	6	7
Serial No.	2	5	4	3	6	7	8
Test Gas							
Zero Air	0.0	0.0	0.0	0.0	0.0	0.0	0.0
0.95% CO_2	0.83	0.5	0.99	0.9	-	-	-
2.44% CH_4	-	-	-	-	1.8	2.2	2.4

Table B-3. Response of Instruments in Methane Atmosphere

	Meter Indication (% CH_4)					
Instrument: Control No.	5		6		7	
Serial No.	6		7		8	
Atmosphere						
1% CH_4	3.2	3.0	1.2	1.2	1.9	2.6
	2.7	2.8	1.2	1.3	2.2	2.2
3% CH_4	10.0	9.0	4.5	5.1	8.0	8.0
	10.0	9.5	5.0	5.0	7.5	8.0
	9.5		5.5		8.0	

Table B-4. Response of Instruments in Carbon Dioxide Atmosphere

	Meter Indication (% CO_2)							
Instrument: Control No.	1		2		3		4	
Serial No.	2		5		4		3	
Atmosphere								
0.5% CO_2	0.65	0.6	0.675	0.625	0.625	0.525	0.675	0.625
	0.575	0.55	0.65	0.6	0.53	0.53	0.61	0.59
	0.54	0.55	0.575	0.575	0.525	0.52	0.58	0.59
	0.55		0.6		0.52		0.59	

Table B-5. AGC Voltage

	AGC VOLTAGE (Volts)						
Instrument: Control No.	1	2	3	4	5	6	7
Serial No.	2	5	4	3	6	7	8
TP-2 to Gnd.	4.8	4.62	5.69	4.61	4.56	4.55	4.58

Table B-6. Sensor Leakage Test

Instrument: Control No.	1	2	3	4	5	6	7
Serial No.	2	5	4	3	6	7	8
Atmosphere Concentration (%)	Unable to Test - Zero unstable, fluctuates from "Pegged Left" to "Full Scale"						
0.3 % CO_2		0.18	0.05	0.08			
0.5 "		0.3	0.05	0.12			
0.75 "		0.7	0.06	0.15			
1.0 "		0.95	0.06	0.18			
2.45 "		>1.0	0.1	-			
4.8 "		-	0.2	-			
0.55 % CH_4					1.0	0.25	0.1
0.95 "					1.7	0.25	0.1
2.0 "					4.6	0.25	0.2
2.0 "					3.9*	-	-
3.0 "					6.0*	0.35	0.4
4.0 "					9.0*	0.5	0.45
5.0 "					11.0*	0.6	0.5 0.6*

* HI range

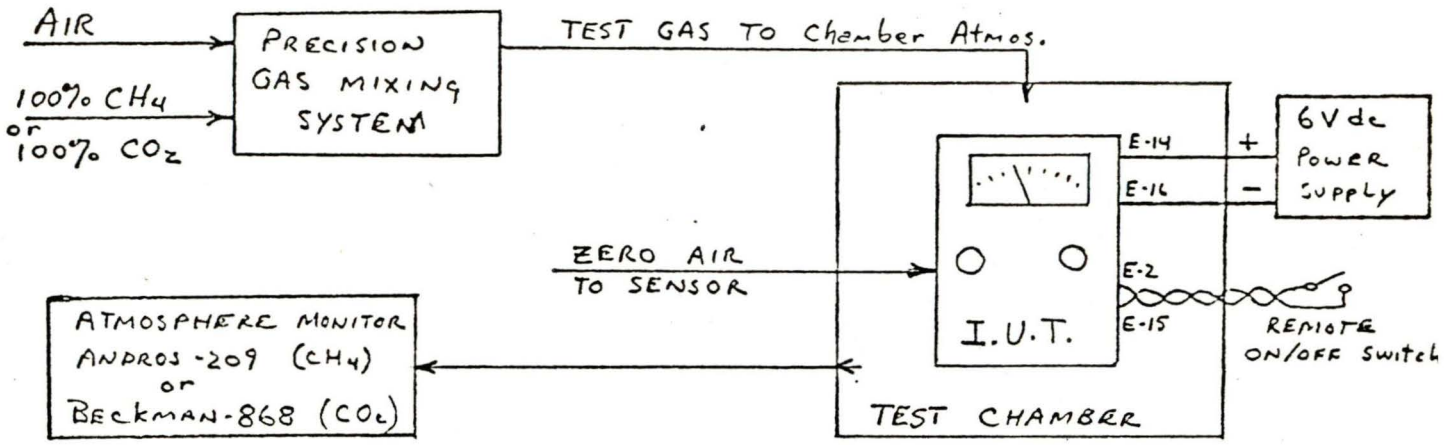

FIGURE B-1 Test Layout - to verify Sensor Leakage

APPENDIX C

FINAL EVALUATION BY THE BUREAU OF MINES

Andros Portable Methane Detectors
and
Andros Portable Carbon Dioxide Detectors

EVALUATION OF ANDROS PORTABLE METHANE DETECTORS AND PORTABLE CARBON DIOXIDE DETECTORS

by

Clarence R. Carpenter
Electronics Technician

George H. Schnakenberg, Jr.
Supervisory Research Physicist

Pittsburgh Research Center
Bureau of Mines
U.S. Department of the Interior
Pittsburgh, Pa. 15213

Introduction

Four portable carbon dioxide detectors (Model 312 - Serial Nos. 2, 3, 4, and 5) and three portable methane detectors (Model 322 - Serial Nos. 6, 7, and 8), manufactured by ANDROS, Inc., were evaluated against the contract (H0377096) performance specifications.

A preliminary evaluation of the instruments during August and September, 1978, showed gas leakage in the optical assemblies. The instruments were returned to the manufacturer for correction of the problem. This leakage caused a difference in the instruments' indicated responses to the test gases when the gases were introduced to the instrument by (1) direct tabulation to the instrument and (2) submersion of the instrument in an atmosphere of the same test gas.

The instruments were returned to us on June 4, 1979, and after perusal of the Instruction Manuals, the instruments were checked for operability during an initial inspection.

The instruments were checked for stability, accuracy over range, effects of temperature change, and sensor leakage during the following seven weeks.

Initial Inspection

Each unit (UUT) was inspected for physical shipping damage immediately after unpacking; no damage was noted. The operability of the UUT's was checked by observing the UUT's meter indication while depressing the "ON" button and challenging the unit with room air (for zero) then 0.95% CO_2/air or 2.44% CH_4/air (for span). The flow rate for each UUT (suction by the internal pump) was also checked with the "ON" button depressed. The meter indication was observed when the "TEST" button was depressed.

In all cases during these tests and all subsequent tests, the meter indication was "read" 30 $\pm$ 2 seconds after the "ON" or "TEST" button was depressed and held.

The indications observed during this test are tabulated in Table C-1.

Table C-1. Initial Meter Indications and Flow Rates

Function	Test Gas	Meter Indication S/N 2	3	4	5	6	7	8
On	Air	.04	.04	.08	<0	<0	<0	<0
	.95% CO_2	.8	1.0	.93	.5	-	-	-
	2.44% CH_4	-	-	-	-	1.9	2.5	2.8
Test	(1)	.39	.6	.625	.38	2.5	>5(2)	2.1
		Flow Rate (cc/min. Suction)						
On	Air	300	200	225	200	275	450	300

(1)"Test Band" CO_2 = 5.25 to 6.75% CO_2

CH_4 = 2 to 3% CH_4 (low range)

(2) Full Scale for CH_4 = 5% (low range)

Stability Test

Between June 5th and July 23rd--approximately seven weeks--the UUT's were checked for repeatability of response to nitrogen (zero gas) and 0.95% CO_2/Air or 2.44% CH_4/Air (span gas).

The UUT pulled samples from gas sample bags which were filled with appropriate cylinder gases. A writing tablet (about 7 ounces) was placed on the sample bag which was laid flat on the bench. This provided just enough positive pressure to inflate the balloon on the calibration-test adaptor (supplied with each instrument) in accordance with the manufacturer's calibration instructions.

The TEST function was also checked each time after the responses were checked.

The UUT's batteries were charged (overnight) twice during this seven-week period--June 11th and July 9th. Prior to the June 11th battery charging, the UUTs' behavior observed was sudden decreases in the response of five of the UUT's to SPAN GAS (all CO_2 units and CH_4 unit S/N 8). The TEST function indication was somewhat confusing--the TEST indications increased (up scale) on four of the units (S/N 2, 5, 6, and 8) but the TEST indications decreased on two of the units (S/N 3 and 4). The TEST function indication on CH_4 unit (S/N 7) was initially

greater than full scale (on low range) and did not change during the entire testing period. Table C-2 tabulates the changes in ZERO and SPAN responses and the TEST function indications just prior to charging the batteries on June 11th and July 9th.

Table C-2. Observed Low Battery Indications

Function Indication	Indication*						
	2	3	4	5	6	7	8
June 11, 1979							
Zero	↑	-	-	-	-	↑	↑
Span	↓	↓	↓	↓	-	↓	↓
Test	↑	↓	↓	↑	↑	-	↑
July 9, 1979							
Zero	-	-	-	↑	-	↑	-
Span	-	-	-	-	↑	↑	-
Test	↓	-	↑	-	↓ then ↑	-	↑

*Indication symbols:

- = no appreciable change
↑ = appreciable increase (up scale) indication
↓ = appreciable decrease (down scale) indication

COMMENT: A separate "battery condition" test would be highly desirable because there is no distinct symptom of a deteriorating battery (charge).

During the period between battery charges (June 12th and July 9th), each unit was tested 15 times (average). Each test consisted of a ZERO check, SPAN check, and a TEST function check. For each check the "ON" or the "TEST" button was depressed for 30 to 35 seconds, for a total "use time" on the batteries of: 3 x 15 x 30 = 1350 seconds to 3 x 15 x 35 = 1575 seconds or 22.5 to 26.25 minutes over the 4-week period. The manufacturer specifies a "total of 50 minutes of continuous operation or 100 individual.....readings between charges," however, no time period between charges is specified. The discrepancy between the number

of "readings" obtained during this test period and the number of readings specified could be due to the self-discharge properties of the lead-acid batteries (GEL-CEL type B). During this test period, the SPAN indications of all the units remained within the manufacturer's specifications (+10% of reading ±2% of full scale). Zero drift was also within the specs. (See Figures C-1 through C-7 for the ZERO, SPAN and TEST indications for S/N's 2 through 8, respectively.)

It should be noted that during the entire test period, S/N 2's SPAN was adjusted twice; these were the only adjustments for all seven instruments. This indicates the close correspondence between ANDROS' test gases and ours, and also is indicative of good mechanical construction of the UUT's, i.e. no changes resulted from possible "rough handling" during shipment.

Accuracy Over Range

A precision gas mixing system was used to produce various concentrations of CO_2 and CH_4 test gases to check the accuracy of each unit's indicated responses. Carbon dioxide was mixed with air to produce concentrations of CO_2 between 0% and 0.95%. Because the CH_4 instruments were designed to indicate concentrations between 0% and 20% (in two ranges), which includes the explosive range of CH_4, the methane was diluted with nitrogen for this test. All mixes were verified by flow rate ratios using a bubble meter (flow rates). The total gas flow from the mixing system was 500 cc/min and was introduced to the UUT via a "T." Excess flow was vented at the "T" through (about) 12 feet of 1/8" i.d. tubing; this provided just enough back-pressure to inflate the balloon on the UUT's input calibration adaptor.

The responses of the instruments are tabulated in Table C-3 (CO_2) and Table C-4 (CH_4).

Table C-3. Accuracy Over Range - CO_2 Instruments

Carbon Dioxide Concentration	Meter Indication (% CO_2)*		
	S/N 2	S/N 3	S/N 5
0.0 (%)	0.00	0.00	0.00
0.1	0.09	0.10	0.12
0.2	0.21	0.20	0.21
0.3	0.30	0.31	0.30
0.4	0.41	0.40	0.40
0.5	0.50	0.49	0.49
0.6	0.58	0.58	0.58
0.7	0.67	0.68	0.66
0.8	0.79	0.79	0.79
0.9	0.90	0.90	0.92
0.95	0.95	0.95	0.95

NOTE: S/N 4 pump failed prior to this test.

* Corrected to .95% indication with .95% test gas.

Table C-4. Accuracy Over Range - CH_4 Instruments

Methane Concentration	Meter Indication (% CH_4) Low Range/High Range		
	S/N 6	S/N 7	S/N 8
0	0 / -	0 / -	0 / -
1	1.0 / 1.0	.99/ 1.0	1.0 / 1.0
2	2.1 / 2.25	1.9 / 2.1	2.0 / 2.1
3	3.3 / 3.3	3.0 / 3.2	3.0 / 3.1
4	4.5 / 4.25	4.1 / 4.1	3.75/ 3.75
5	5.0 / 4.9	5.0 / 5.0	4.9 / 4.75
10	* /10.0	* /10.0	* / 9.0
15	* /11.0**	* /15.0	* /14.9
20	* /11.0**	* /20.0	* /19.9

* Over range (low range is 0 to 5% on the meter).

** Meter indication "limited" at just over 10% on high range.

Temperature Checks

The methane and carbon dioxide instruments were tested for the effects of temperature separately. However, the methodology was the same for each group. Each group was tested inside an environmental chamber for two days. The first day at low temperature, the second day at elevated temperature; humidity was loosely controlled between 70% and 90%. See figure C-8.

Test gases from cylinders were introduced to the UUT's using the same methodology employed during the "accuracy over range" checks, and the flows were maintained at 500 cc/min. The sources of the test gases were the same as used during the "stability" checks.

COMMENT: The instruments exhibited fairly good stability during the "stability" checks; however, the results of the "temperature" checks were somewhat disappointing--especially at the elevated temperature. I reviewed the data for the "stability" checks and noted that there is correlation among the instruments' responses to (in particular) span gas; (i.e. the room temperature during the checks on June 14th was about 4-1/2 °C higher than the temperature on June 13th. The responses of a majority of the UUT's (S/N's 2, 3, 4, 7, and 8) decreased. Barometric pressure may also have an effect on the UUT's responses. Temperature, barometric pressure, and response data are plotted in figure C-9 (CO_2) and figure C-10 (CH_4) for convenience of observation.

Figures C-11 through C-16 are plots of the data obtained during the temperature test for UUT's S/N's 2, 3, and 5 through 8. UUT S/N 4 developed pump/motor problems prior to this series.

Sensor Leakage Test

During the preliminary evaluation of these instruments, it was discovered that the sensors were "leaky." (See report dated September, 1978.) The manufacturer was able to correct this problem as evidenced by the following tests.

The SPAN response of each UUT was checked first by introducing a sample bag of span test gas (0.95% CO_2/air or 2.44% CH_4/air from cylinders). The UUT was then placed inside a plastic bag. The appropriate cylinder gas was then fed into the partially sealed bag and after several minutes, to insure thorough flushing of the bag, the SPAN response of the UUT was checked again. The results of this test, tabulated in Table C-5, indicate that there is no perceptible sensor leakage in any of the instruments.

Table C-5. Sensor Leakage

Test gas	Method of Introduction	Meter Indication (% CO_2 or CH_4)						
		S/N 2	3	4	5	6	7	8
0.95% CO_2	Sample bag	.95	.90	.98	.95	-	-	-
	Submersion	.95	.95	.90	.90	-	-	-
2.44% CH_4	Sample bag	-	-	-	-	2.3	2.3	2.65
	Submersion	-	-	-	-	2.4	2.3	2.6

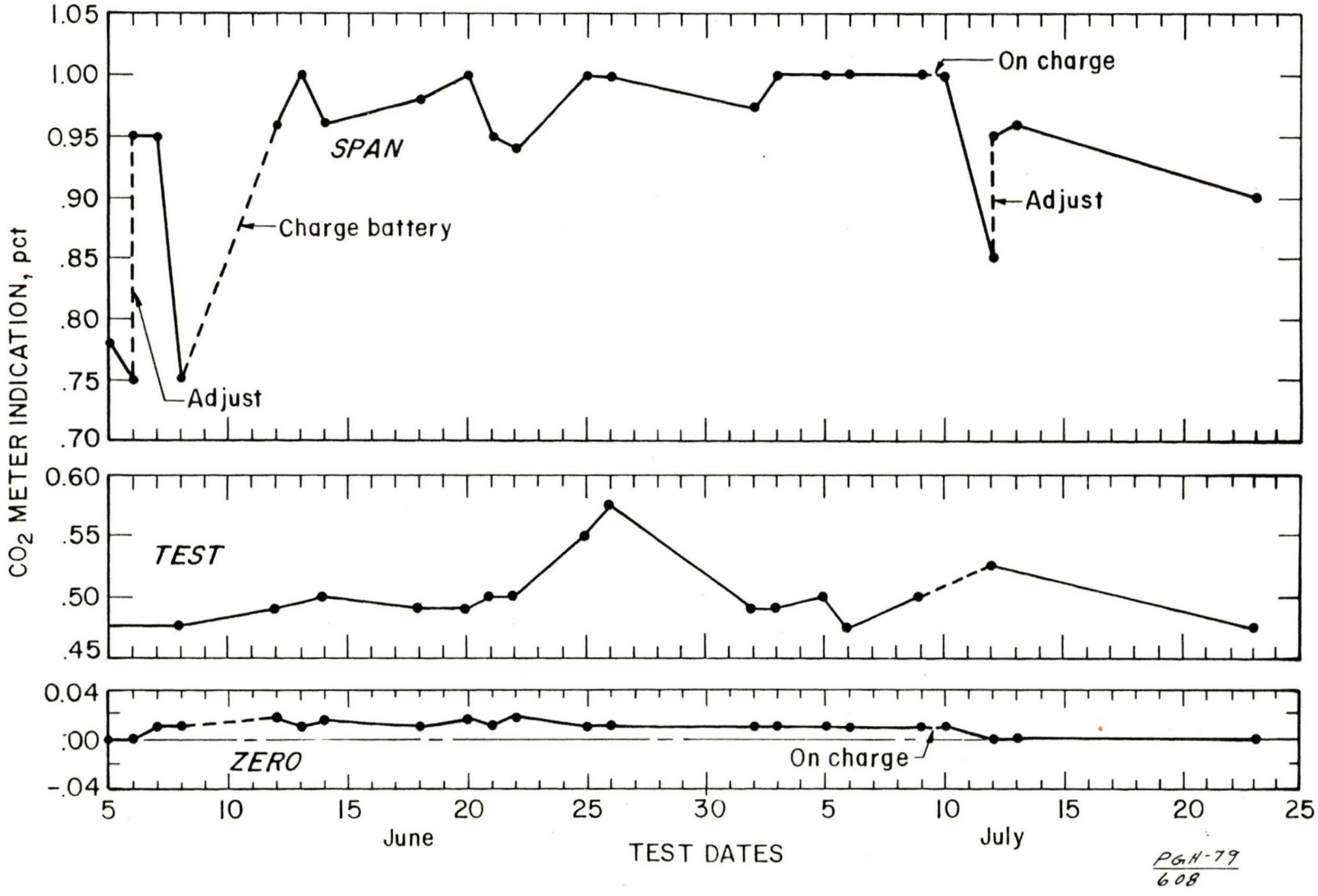

FIGURE C-1. Long-term stability, CO_2 Detector No. 2.

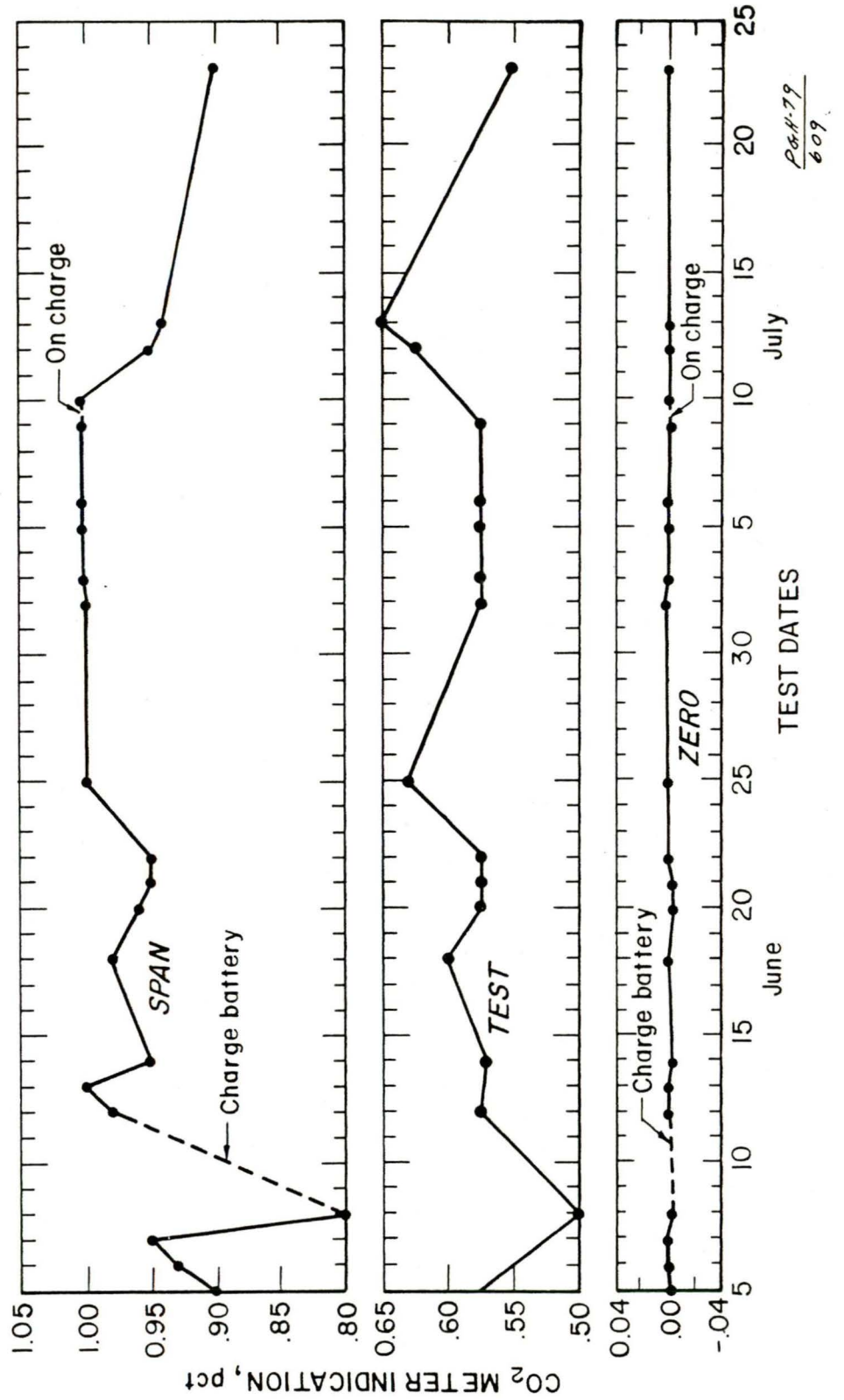

FIGURE C-2. Long-term stability, CO_2 Detector No. 3.

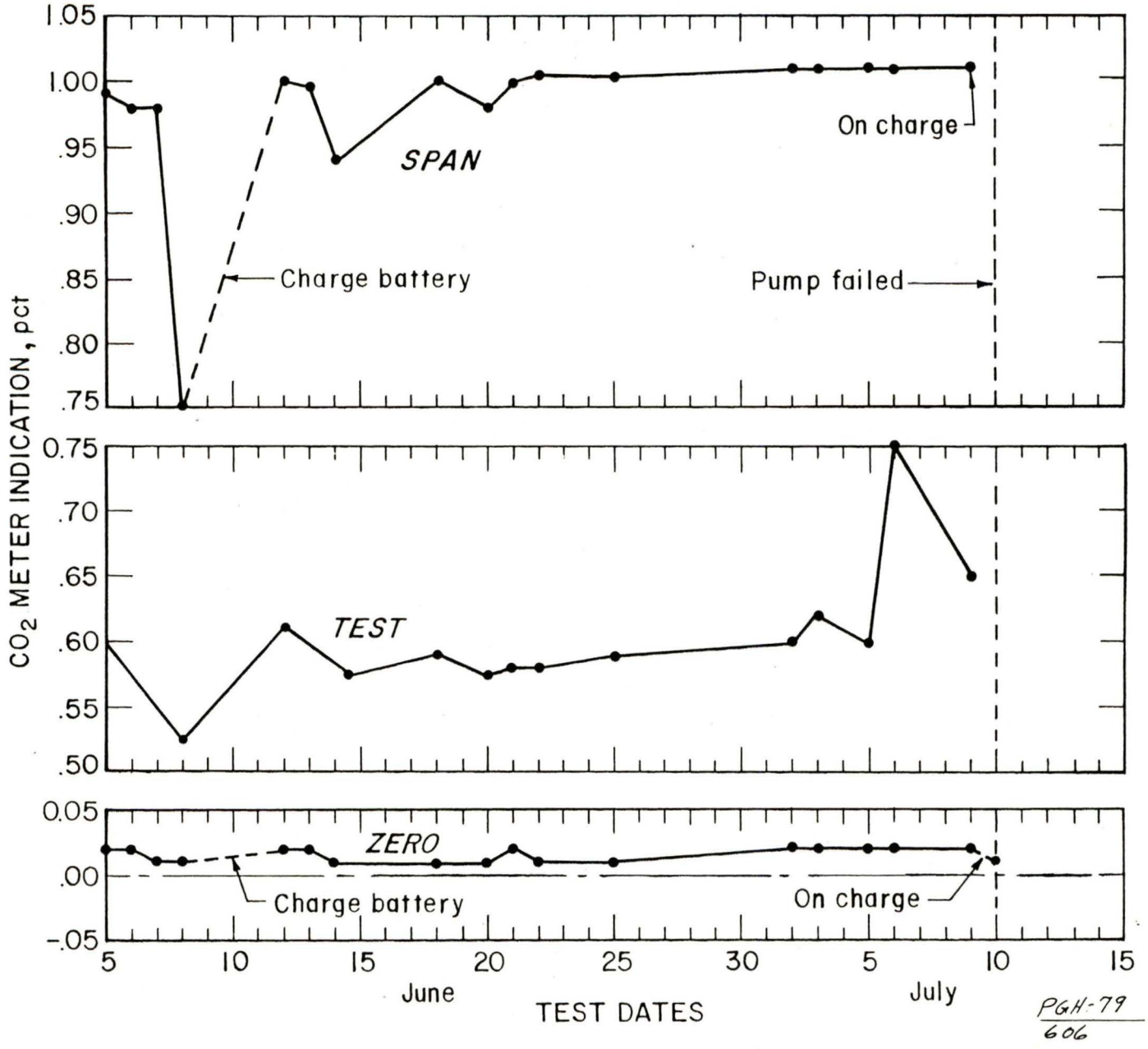

FIGURE C-3. Long-term stability, CO_2 Detector No. 4.

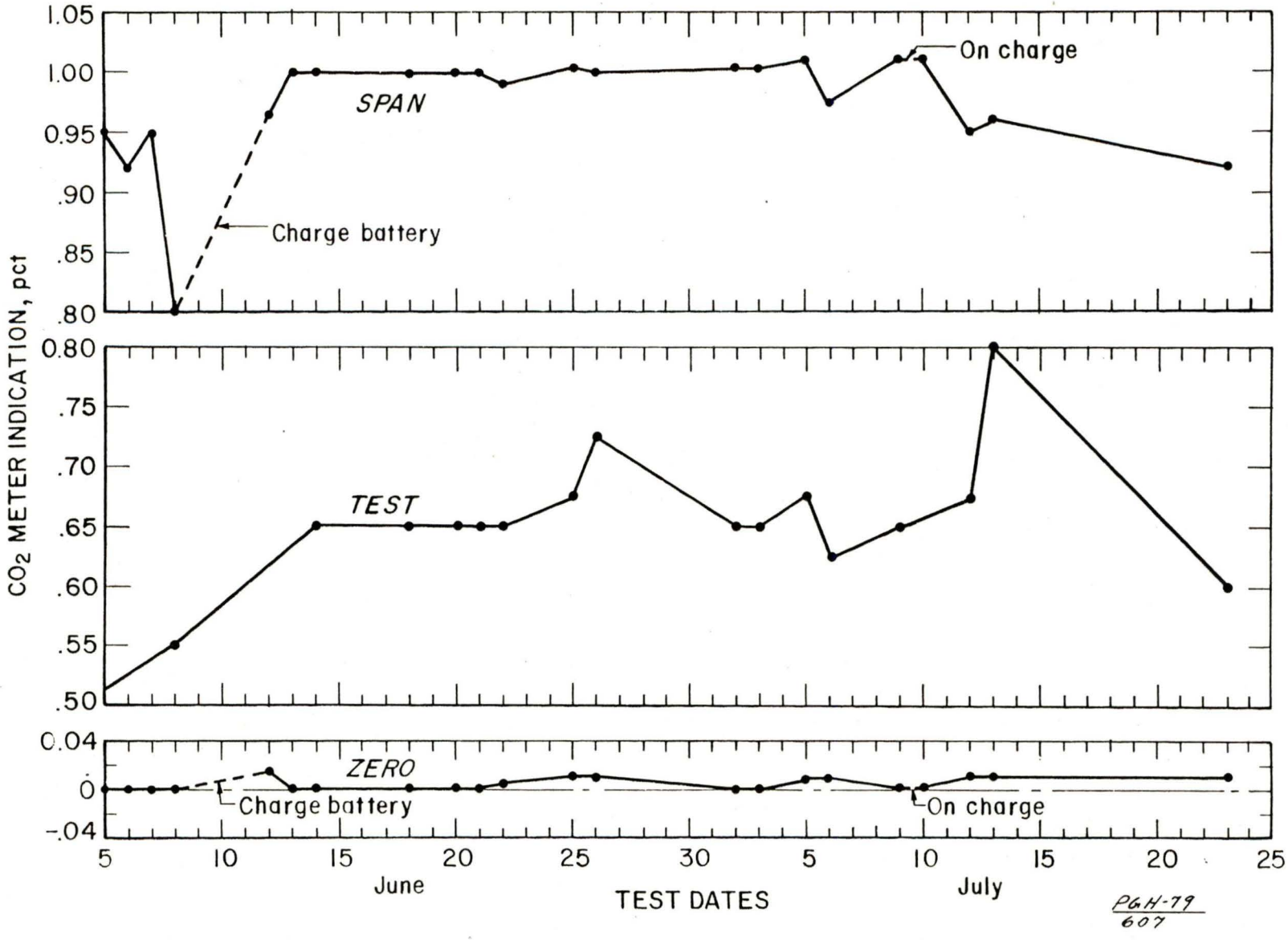

FIGURE C-4. Long-term stability, CO_2 Detector No. 5.

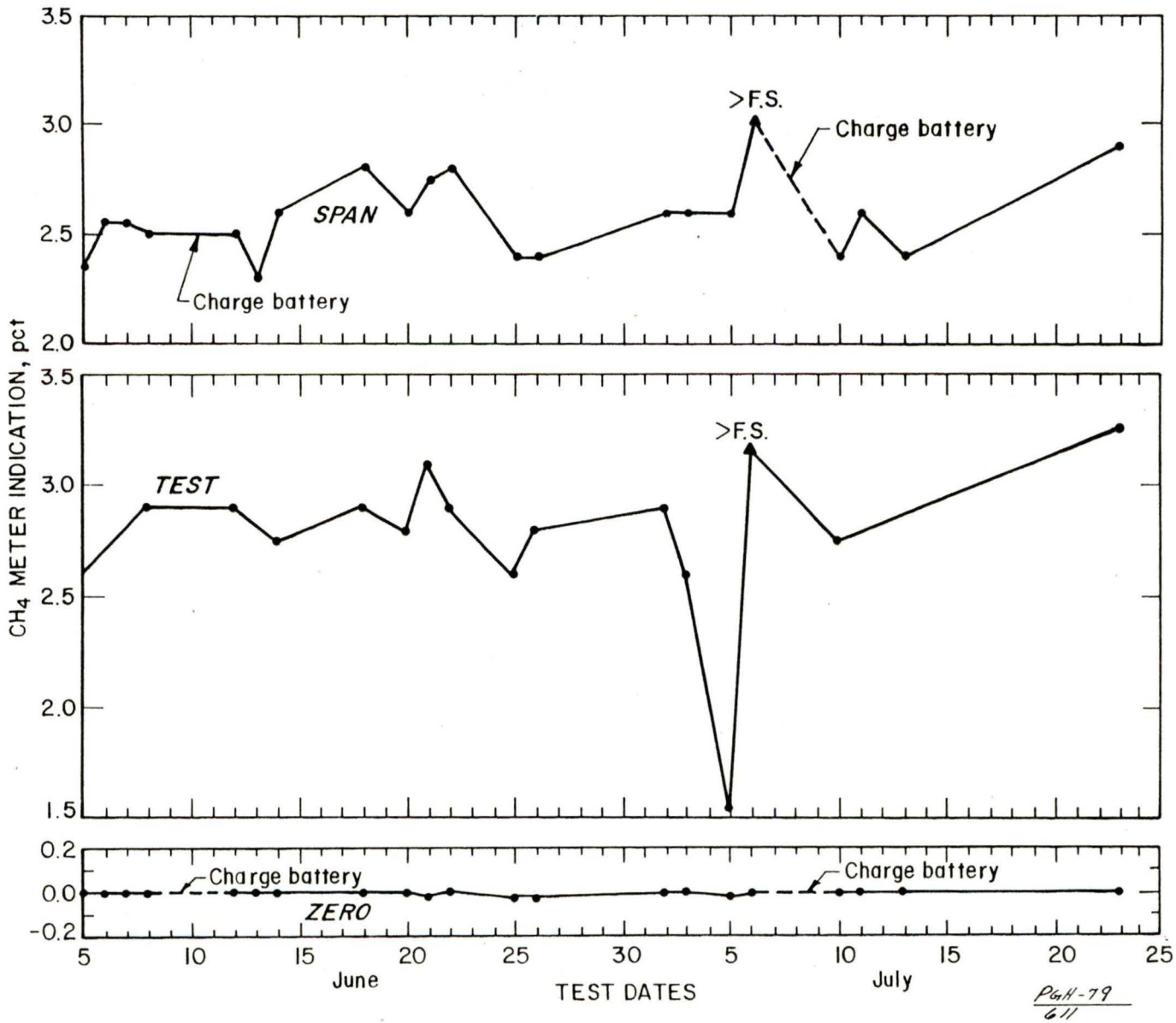

FIGURE C-5. Long-term stability, CH_4 Detector No. 6.

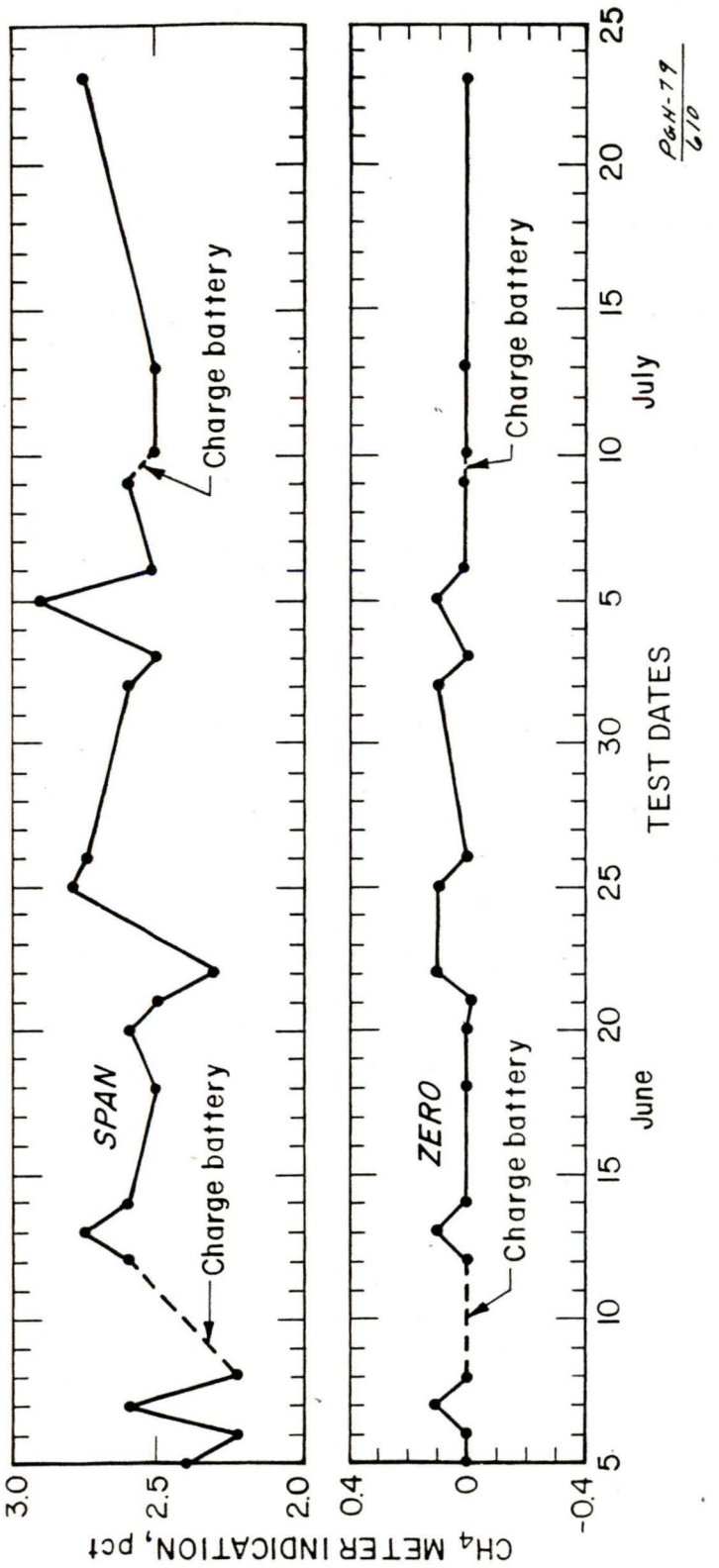

FIGURE C-6. Long-term stability, CH_4 Detector No. 7.

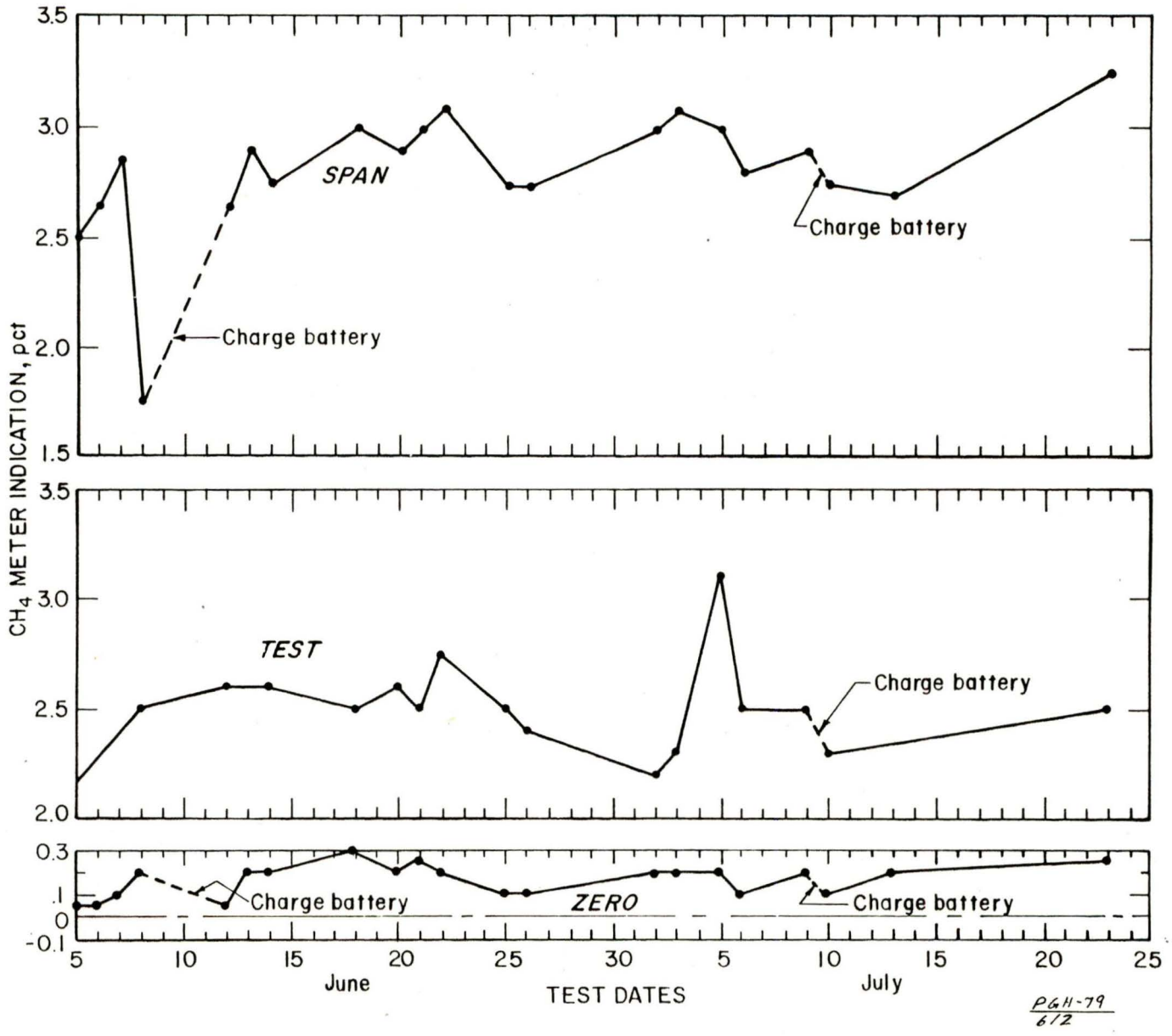

FIGURE C-7. Long-term stability, CH_4 Detector No. 8.

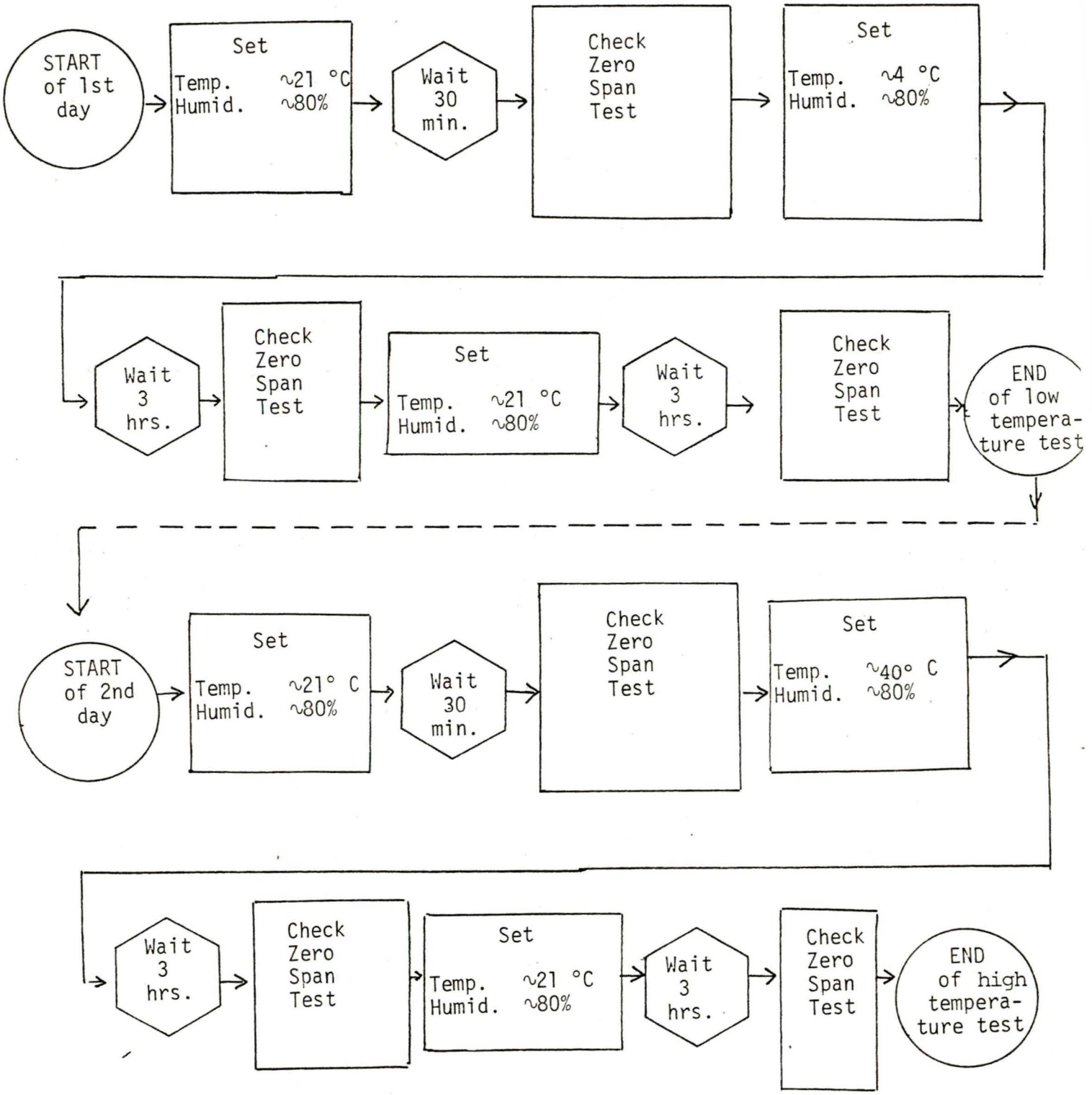

FIGURE C-8. Temperature Tests - Sequencing.

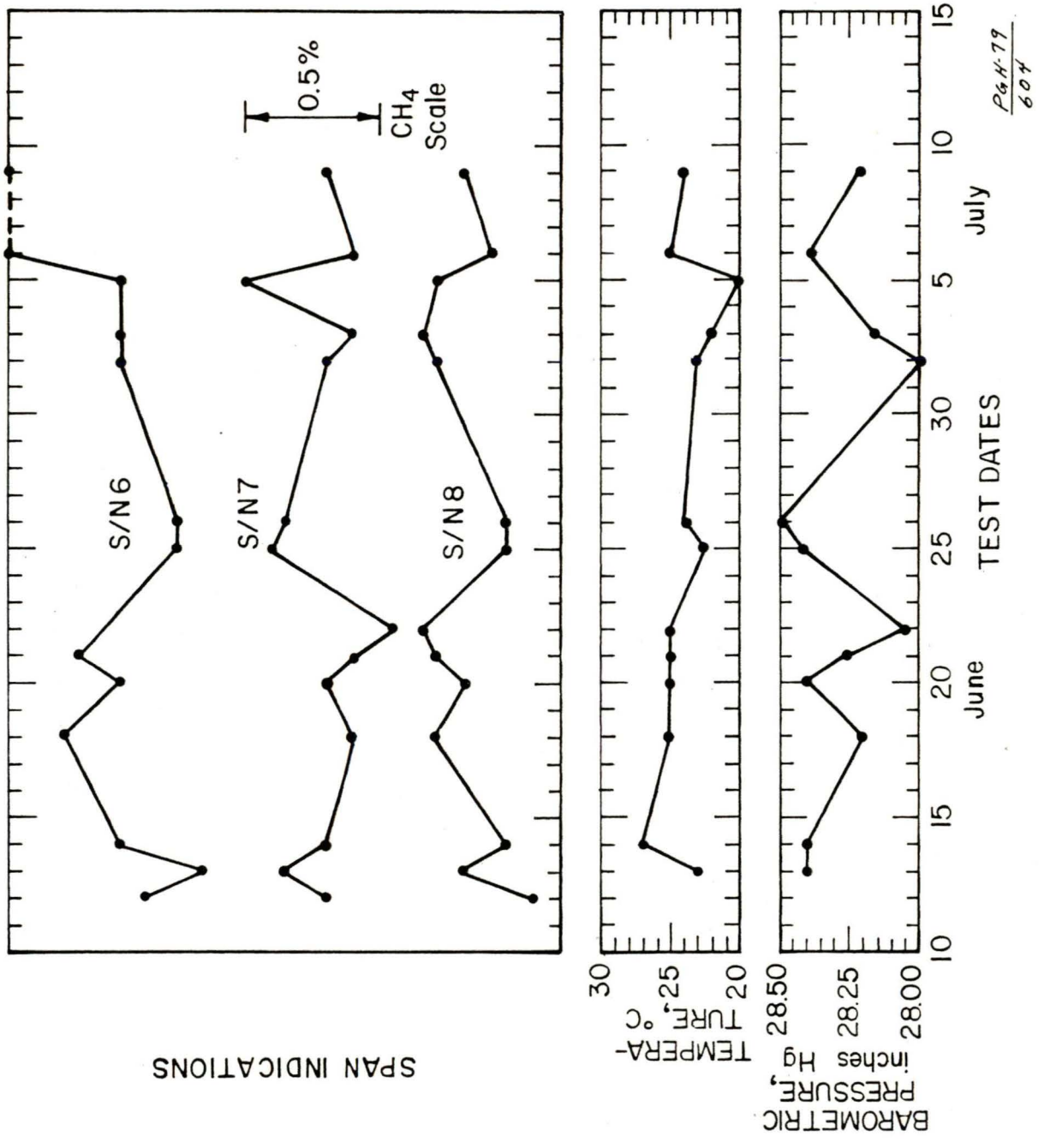

FIGURE C-9. Correlation between ambient temperature, barometric pressure, and deviation of CH_4 detectors' response to span gas.

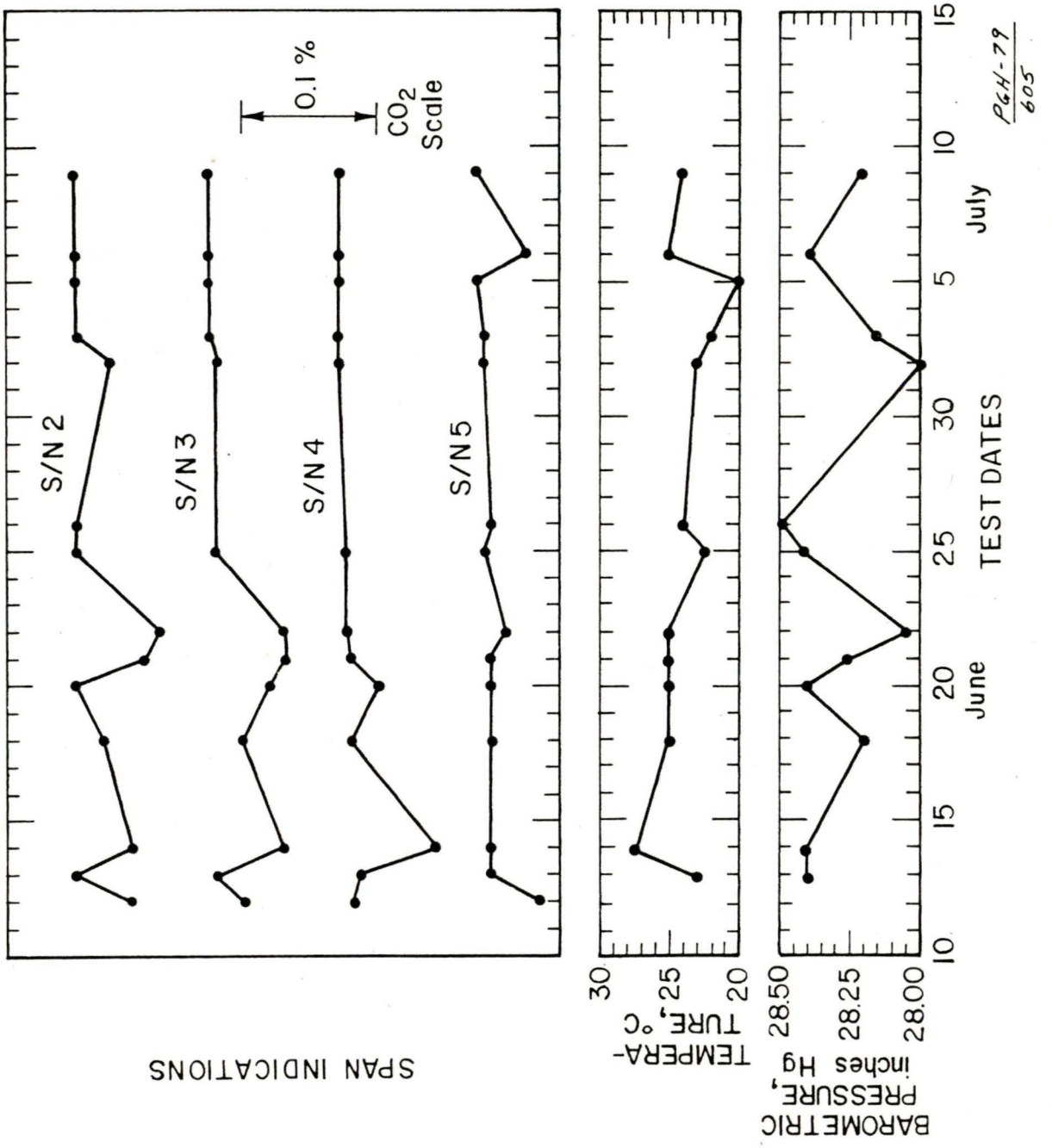

FIGURE C-10. Correlation between ambient temperature, barometric pressure, and deviation of CO_2 detectors' response to span gas.

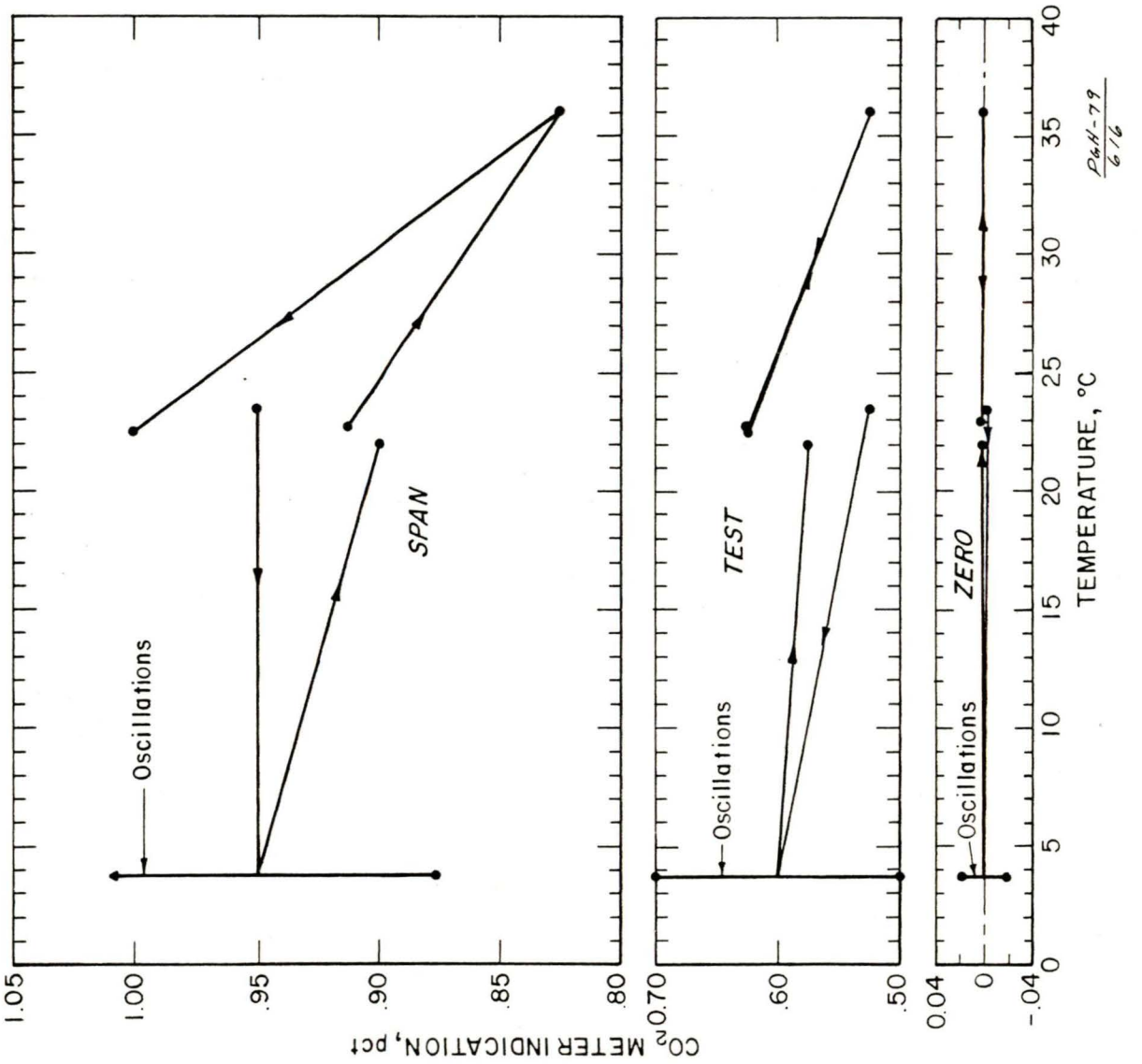

FIGURE C-11. Temperature effects on CO_2 response at zero, to the test function and to span gas; Detector No. 2.

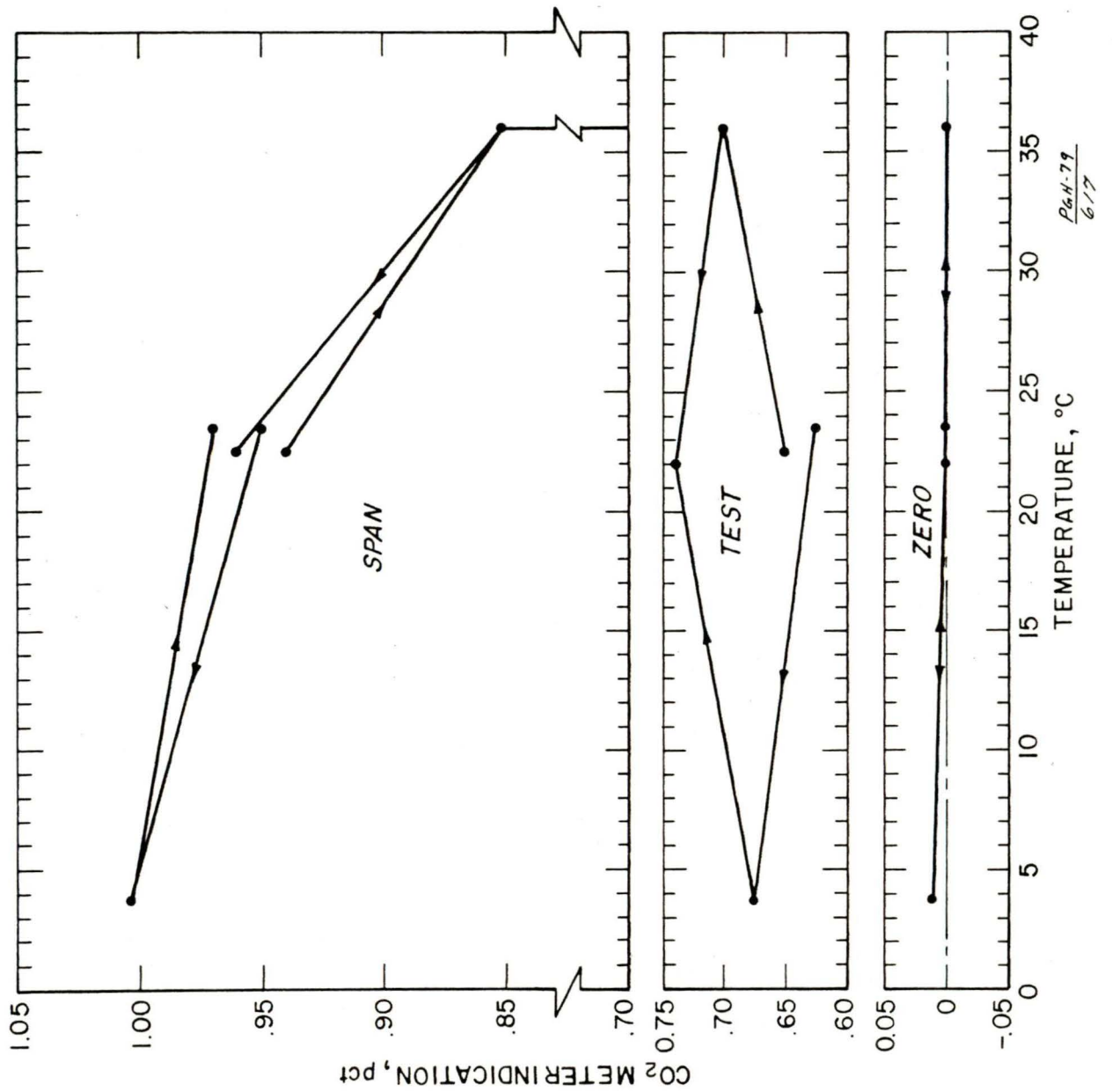

FIGURE C-12. Temperature effects on CO_2 detector response at zero, to the test function and to span gas; Detector No. 3.

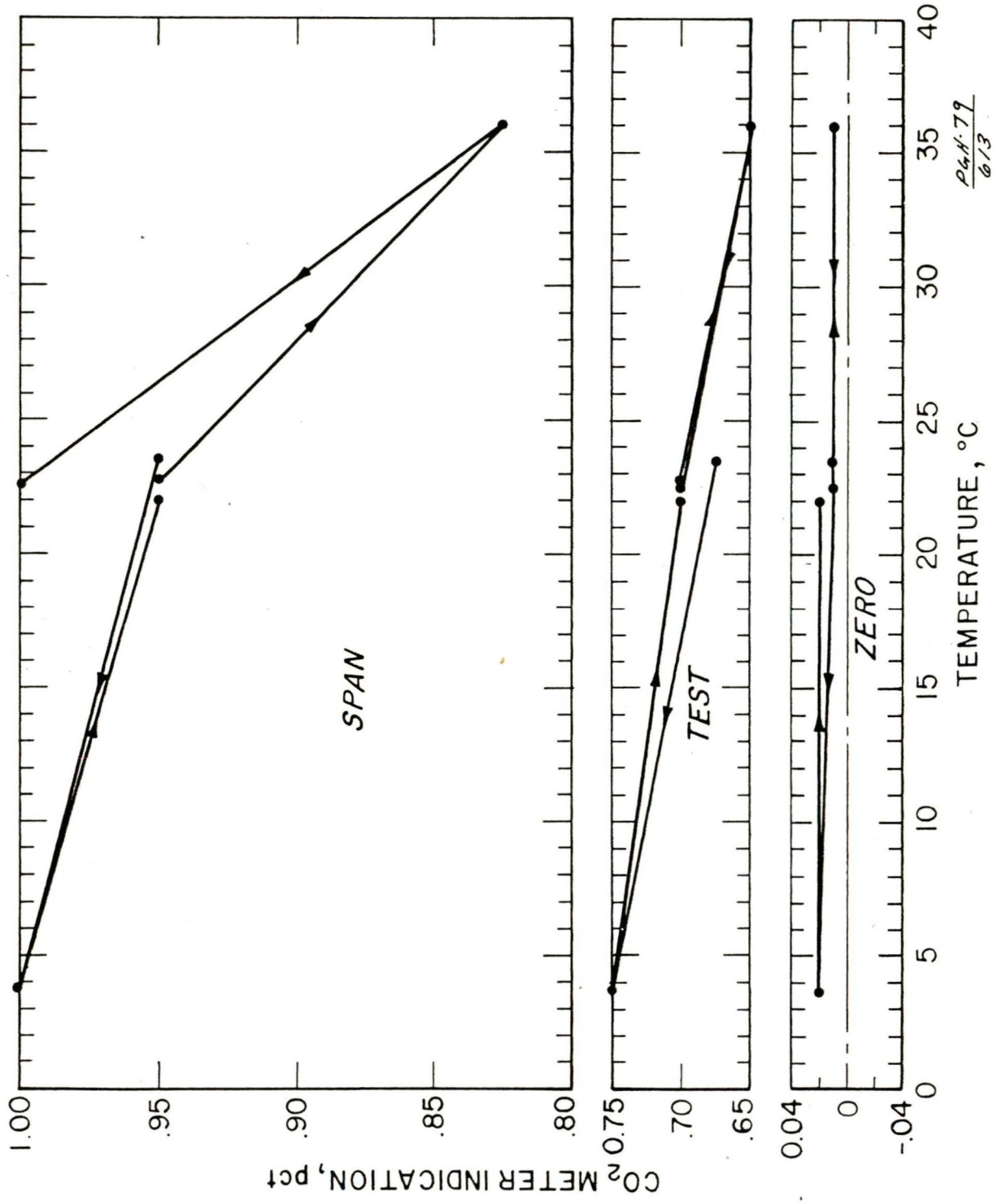

FIGURE C-13. Temperature effects on CO_2 detector response at zero, to the test function and to span gas; Detector No. 5.

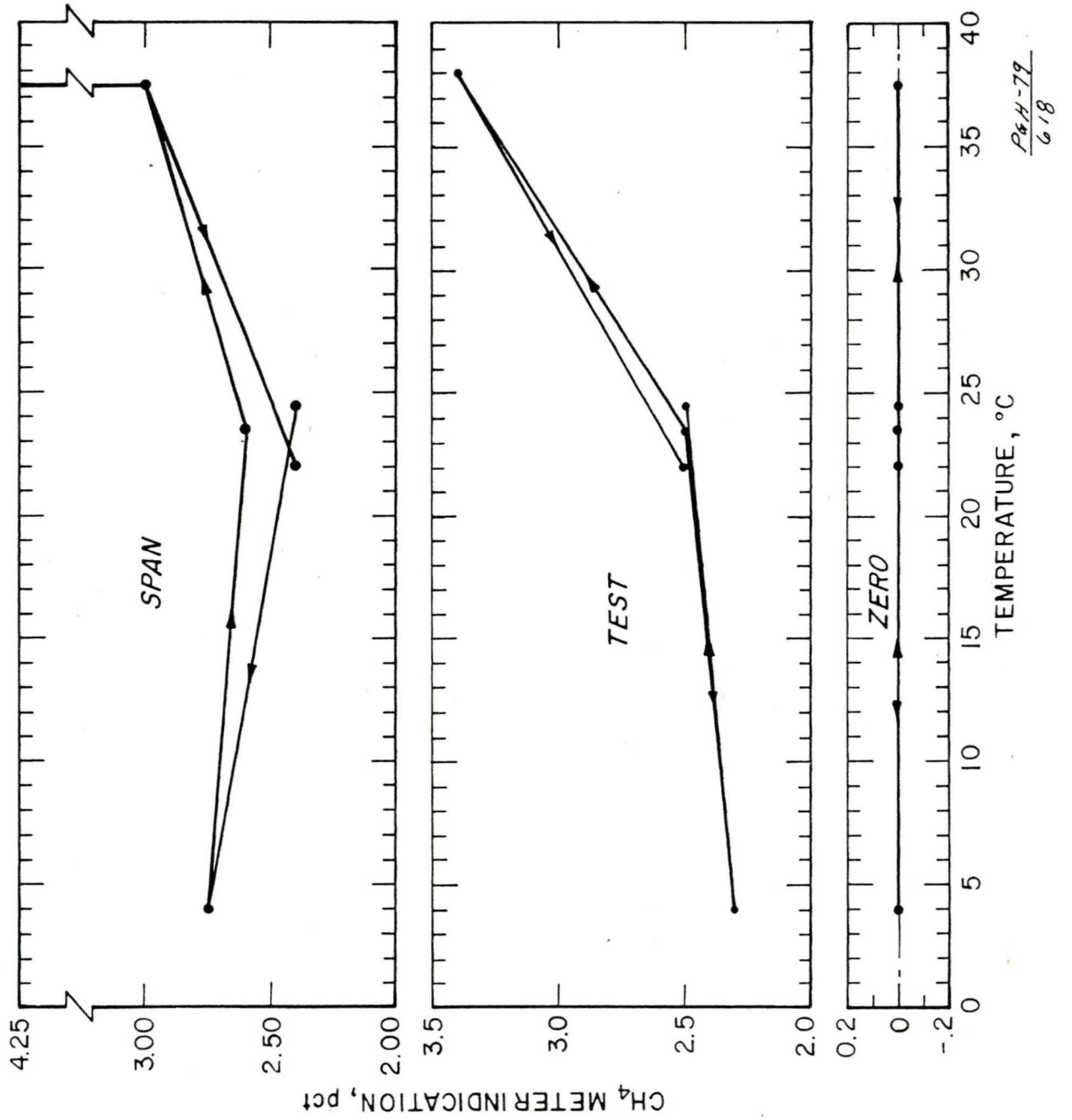

FIGURE C-14. Temperature effects on CH_4 detectors' response at zero, to the test function and to span gas; Detector No. 6.

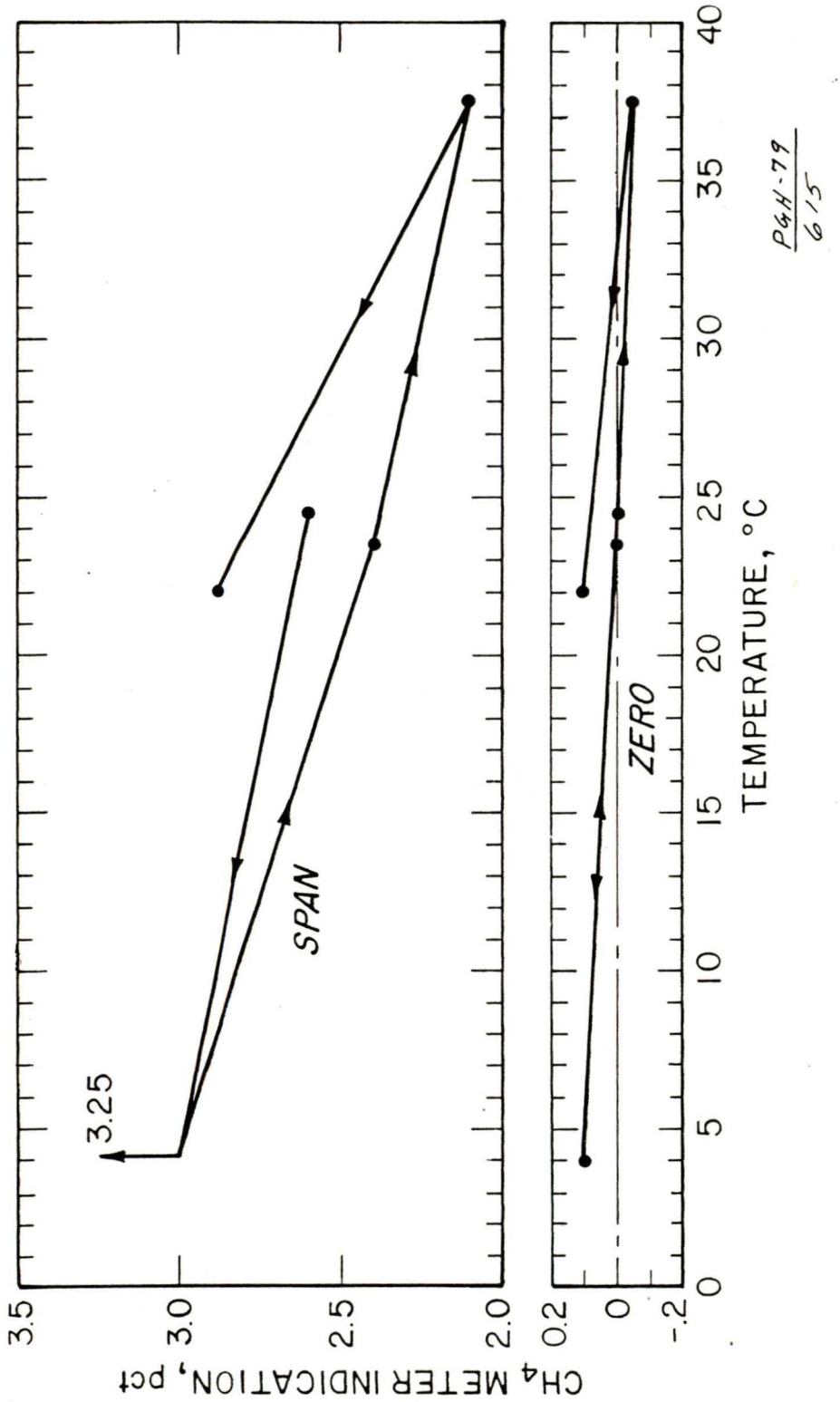

FIGURE C-15. Temperature effects on CH_4 detectors' response at zero, to the test function and to span gas; Detector No. 7.

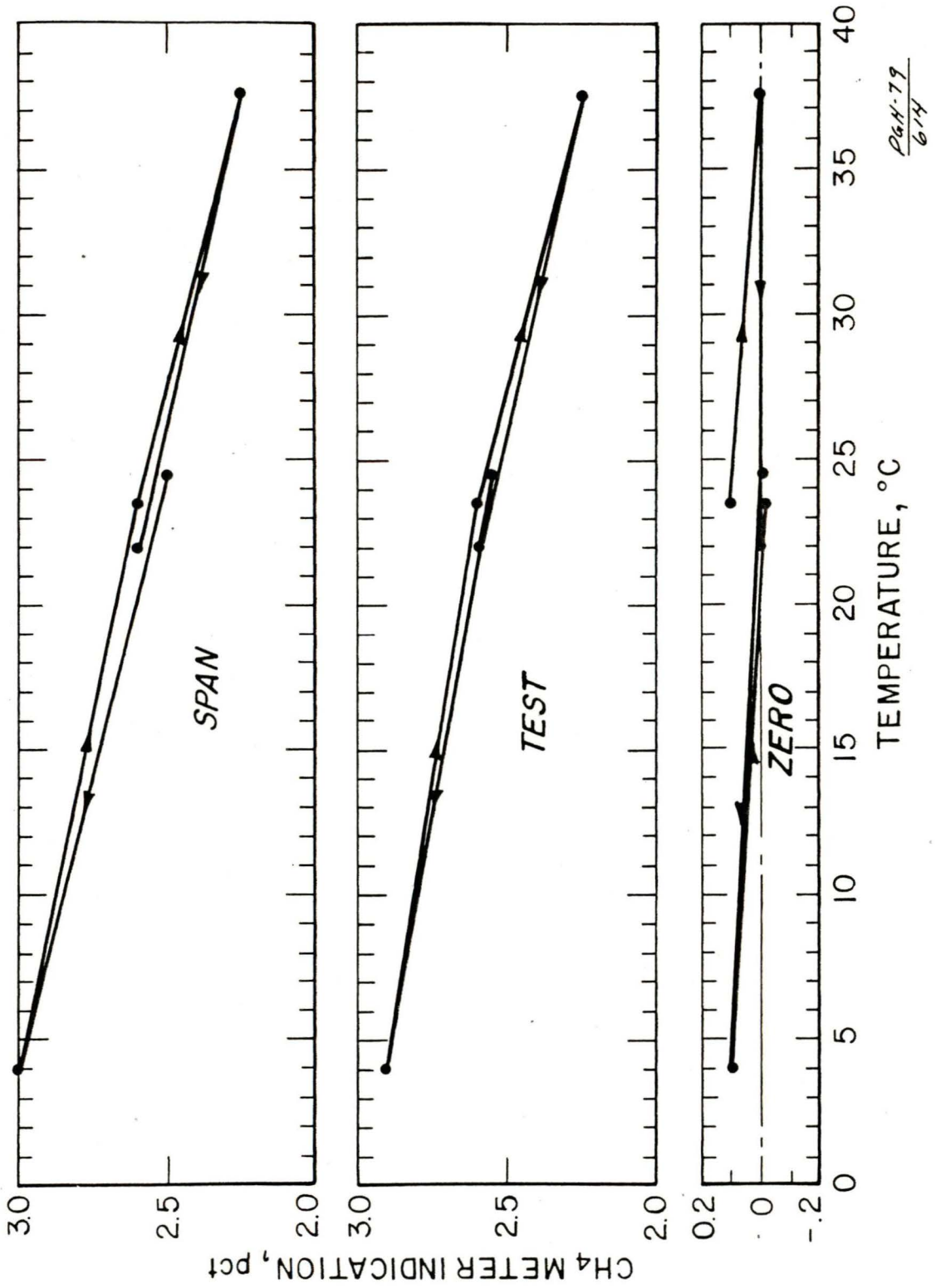

FIGURE C-16. Temperature effects on CH_4 detectors' response at zero, to the test function and to span gas; Detector No. 8.

APPENDIX D

LIST OF ABBREVIATIONS

LIST OF ABBREVIATIONS

CO_2	Carbon Dioxide
CH_4	Methane
NO_2	Nitrogen Dioxide
µm	Micro-meter (micron)
N_2	Nitrogen
°F	Degree Fahrenheit
°C	Degree Celsius
°K	Degree Kelvin
F_1	Signal Frequency One
F_2	Signal Frequency Two
FET	Field Effect Transistor
Fo	Resonant Frequency
F_p	Resonant Frequency of Piezoceramic device
C	Sound Velocity (cm/sec)
A	Neck cross-sectional area (cm^2)
L	Neck Length (cm)
V	Chamber Volume (cm^3)
psi	Pounds Per Square Inch
Q	Figure of Merit Fo/bandwidth
W	Chamber Volume (cm^3)
D	Neck Diameter
R	Resistance (ohms)
PZ	Piezoelectric
IUI	Instrument Under Test

APPENDIX E

SIGNS AND SYMBOLS

SIGNS AND SYMBOLS

+	plus, addition, positive
-	minus, subtraction, negative
$\pm$	plus or minus, positive or negative
$\mp$	minus or plus, negative or positive
÷, /, —	division
x, ·, () ()	multiplication
() [ ]	collection
=	is equal to
$\neq$	is not equal to
$\equiv$	is identical to
$\simeq$	equals approximately, congruent
>	greater than
$\ngtr$	not greater than
$\geq$	greater than or equal to
<	less than
$\nless$	not less than
$\leq$	less than or equal to
::	proportional to
:	ratio
~	similar to
$\propto$	varies as, proportional to
$\rightarrow$	approaches
∞	infinity
$\therefore$	therefore
$\sqrt{}$	square root
$\sqrt[n]{}$	nth root
a^n	nth power of a
log, $\log_{10}$	common logarithm
ln, $\log_e$	natural logarithm
e or ϵ	base of natural logs, 2.718
π	pi, 3.1416
$\angle$	angle
$\perp$	perpendicular to
$\parallel$	parallel to
n	any number
$\lvert n \rvert$	absolute value of n
$\bar{n}$	average value of n
a^{-n}	reciprocal of nth power of a $= [\frac{1}{a^n}]$
n^o	n degrees
n'	n minutes, n feet
n''	n seconds, n inches
f (x)	function of x
Δx	increment of x
dx	differential of x
Σ	summation of
sin	sine
cos	cosine
tan	tangent

GREEK ALPHABET

Alpha	A	α	Iota	I	ι	Rho	P	ρ
Beta	B	β	Kappa	K	κ	Sigma	Σ	σ
Gamma	Γ	γ	Lambda	Λ	λ	Tau	T	τ
Delta	Δ	δ	Mu	M	μ	Upsilon	Υ	υ
Epsilon	E	ϵ	Nu	N	ν	Phi	ϕ	ϕ
Zeta	Z	ζ	Xi	Ξ	ξ	Chi	X	χ
Eta	H	η	Omicron	O	o	Psi	Ψ	ψ
Theta	θ	θ	Pi	Π	π	Omega	Ω	ω